Analysis of dehydrogenase-independent functions of HSD17B10 in humans and animal models

presented by
Dipl.-Biol. Katharina Rauschenberger

Analysis of dehydrogenase-independent functions of HSD17B10 in humans and animal models

Dissertation

submitted to the
Combined Faculties for the Natural Sciences
and for Mathematics
of the Ruperto-Carola University of Heidelberg, Germany

for the degree of

Doctor of Natural Sciences

presented by
Dipl.-Biol. Katharina Rauschenberger
born in Friedrichshafen, Germany

Date of oral examination: 25 February 2011

Analysis of dehydrogenase-independent functions of HSD17B10 in humans and animal models

prepared at the

Institute of Human Genetics, Heidelberg
Division of Developmental Genetics

Referees:
Prof. Dr. rer. nat. Herbert Steinbeisser
Prof. Dr. Dr. med. Johannes Zschocke

The following publication originated from this work:

Rauschenberger K, Scholer K, Sass JO, Sauer S, Djuric Z, Rumig C, Wolf NI, Okun JG, Kolker S, Schwarz H, Fischer C, Grziwa B, Runz H, Numann A, Shafqat N, Kavanagh KL, Hammerling G, Wanders RJ, Shield JP, Wendel U, Stern D, Nawroth P, Hoffmann GF, Bartram CR, Arnold B, Bierhaus A, Oppermann U, Steinbeisser H, Zschocke J (2010)

A non-enzymatic function of 17beta-hydroxysteroid dehydrogenase type 10 is required for mitochondrial integrity and cell survival.

EMBO Mol Med **2**(2)**:** 51-62

Table of contents

1 SUMMARY

Deficiency of the mitochondrial enzyme 2-methyl-3-hydroxybutyryl-CoA dehydrogenase involved in isoleucine metabolism causes an organic aciduria with an atypical progressive neurodegenerative disease course (Zschocke et al, 2000). The symptoms in HSD10 deficiency patients are not correlated with residual dehydrogenase activity of mutated HSD10. LOF and rescue experiments in *Xenopus* embryos showed that a knock-down of HSD10 caused apoptosis. The dehydrogenase activity of HSD10 was not required for cell survival suggesting that HSD10 has additional functions. The pathogenetic basis of HSD10 deficiency has so far remained elusive but the symptoms observed in patients are likely related to defects in general mitochondrial function. Therefore, the effect of HSD10 LOF on mitochondrial structural and functional integrity was investigated. Embryonic *Xenopus* cells displayed severe disruption of mitochondrial morphology and function when translation of HSD10 mRNA was blocked. Similar effects on mitochondria were observed in cells derived from conditional HSD10 knock-out mice and in fibroblasts from patients with a severe clinical phenotype. In *Xenopus* overexpression of two HSD10 mutations, R130C and D86G, associated with severe disease in humans, strongly induced apoptosis in a dominant-negative manner which was not due to the unfolded protein response that is occasionally triggered by overexpression of (mutated) proteins. In contrast, wildtype HSD10 and the Q165H mutation had little effect on apoptosis.

Expression analysis of apoptosis-associated genes in HSD10 depleted cells or cells carrying different HSD10 mutations demonstrated that no specific apoptotic pathway was activated. This indicated that intrinsic as well as extrinsic apoptosis signals contribute to cell death when HSD10 function is perturbed.

Symptoms in patients usually develop after metabolic stress situations. Therefore the stress response behaviour of fibroblasts carrying HSD10 mutations was studied under different stress conditions. In contrast to control cells, fibroblasts from patients were not able to stimulate tRNA transcription upon oxidative stress. Interestingly cells with the R130C mutation could cope with stress just like the Q165H mutation. This was unexpected, since the R130C mutation causes a severe clinical phenotype whereas the Q165H mutation has been found in neurologically normal boys.

In order to understand the mechanisms behind the physiological function of HSD10 a search for its binding partners was performed. In a homology based BLAST in yeast as well as in an IMAC approach putative HSD10-interacting proteins were identified. Unfortunately none of these candidates were directly connected to mitochondrial function or apoptosis. In a previously performed yeast-2-hybrid screen several HSD10 interaction partners had been identified. One of those binding proteins, UXT, was tested for a functional interaction with HSD10 in *Xenopus* embryos. Co-expression of HSD10 and UXT enhanced the induction of apoptosis. The mechanism of this functional interaction remains to be investigated.

HSD10 is a component of the RNAseP complex which is essential for the 5' processing of mitochondrial tRNAs. Therefore I tested the function of RNaseP in HSD10 deficiency in patient fibroblast and in a rescue experiment in HSD10 depleted cells. The rescue experiment, in which wildtype HSD10 function was substituted by the mutations R130C, D86G and Q165H indicated that all mutations still have RNaseP activity. This held also true for patient fibroblasts where no tRNA precursor accumulation or inhibition of mitochondrial translation was detected. Experiments with cells that are depleted of mitochondrial DNA and hence do not require mitochondrial transcription or mtRNaseP function revealed that these cells still become apoptotic upon HSD10 knock-down. Therefore, the apoptosis phenotype upon HSD10 LOF is not dependent on RNaseP function. Taken together, these experiments indicate that clinical symptoms in HSD10 deficiency are not fully explained by an impairment of RNaseP function.

2 ZUSAMMENFASSUNG

Ein Mangel des mitochondrialen Enzyms 2-Methyl-3-Hydroxybutyryl-CoA-Dehydrogenase, das eine Rolle im Isoleucin Metabolismus spielt, ist die Ursache einer organischen Azidurie mit einem atypischen progressiven neurodegenerativen Verlauf (Zschocke et al, 2000). Die Symptome des HSD10-Mangels sind nicht mit der Dehydrogenase Restaktivität der mutierten HSD10 Proteine korreliert. LOF und Rettungsexperimente in *Xenopus* zeigten, dass ein knock-down von HSD10 Apoptose verursacht. Die Dehydrogenase Aktivität von HSD10 ist nicht ausschlaggebend für das Überleben der Zelle, was darauf hindeutet, dass HSD10 über zusätzliche Funktionen verfügt. Die pathogenetische Grundlage des HSD10-Mangels ist bisher unbekannt, aber den Symptomen der Patienten liegt wahrscheinlich eine allgemeine Störung der Mitochondrienfunktion zu Grunde. Daher wurde der Effekt eines HSD10 LOF auf die mitochondriale Struktur und Funktion untersucht. *Xenopus* Zellen, in denen die Translation von HSD10 mRNA blockiert war, wiesen eine schwere Störung der mitochondrialen Morphologie und Funktion auf. Ähnliche Effekte auf die Mitochondrien wurden in Zellen von konditionalen HSD10 knock-out Mäusen und in Fibroblasten von Patienten mit schwerem klinischen Phänotyp beobachtet.

In *Xenopus* hatte die Überexpression der beiden mit einem schweren Krankheitsverlauf assoziieren HSD10 Mutationen, R130C und D86G, einen dominant-negativen Effekt auf den Anstieg der Apoptose, was nicht mit der „unfolded protein response", die gelegentlich durch die Überexpression von (mutierten) Proteinen ausgelöst wird, zusammenhing. Im Gegensatz dazu hatten wildtyp HSD10 und die Mutation Q165H wenig Einfluss auf die Apoptose. Expressionsanalysen von Apoptose-assoziierten Genen in HSD10 depletierten Zellen oder in Zellen mit HSD10 Mutationen zeigten, dass kein spezifischer Apoptoseweg aktiviert wurde. Intrinsische wie auch extrinsische Signale führen zum Zelltod, wenn die HSD10 Funktion gestört ist.

In der Regel entwickeln Patienten Symptome nach metabolischen Stresssituationen. Deshalb wurde das Verhalten von Fibroblasten mit HSD10 Mutationen unter verschiedenen Stressbedingungen untersucht. Im Unterschied zu Kontrollzellen waren Fibroblasten von Patienten nicht in der Lage die Transkription von mitochondrialen tRNAs zu stimulieren. Interessanterweise konnten Zellen mit der R130C Mutation Stress ebenso gut bewältigen wie die Mutation Q165H. Dies war unerwartet, da die R130C Mutation einen schweren klinischen Phänotyp verursacht, während die Mutation Q165H in neurologisch normalen Jungen gefunden wurde.

Um die Mechanismen der physiologischen Funktion von HSD10 zu verstehen wurde nach Bindungspartnern des Proteins gesucht. In einem BLAST in Hefe sowie in einem IMAC Ansatz wurden potentielle Interaktionspartner von HSD10 identifiziert. Leider hatte keiner dieser Kandidaten eine direkte Verbindung zu Mitochondrien oder Apoptose. In einem yeast-2-hybrid Screen waren einige Interaktionspartner identifiziert worden. Eines dieser Proteine, UXT, wurde auf eine funktionelle Interaktion mit HSD10 in *Xenopus* getestet. Co-Expression von HSD10 und UXT verstärkt die Induktion von Apoptose. Der Mechanismus dieser funktionellen Interaktion ist bisher nicht bekannt.

HSD10 ist eine Komponente des RNAseP Komplexes, der die 5’ Prozessierung von mitochondrialen tRNAs durchführt. Deshalb wurde die Rolle der RNaseP Funktion im HSD10-Mangel an Fibroblasten von Patienten und in einem Rettungsexperiment in HSD10 depletierten Zellen getestet. Das Rettungsexperiment, in dem die wildtyp HSD10 Funktion durch die Mutationen R130C, D86G und Q165H ersetzt wurde, deutete darauf hin, dass alle Mutationen RNaseP Aktivität haben. Dies galt ebenfalls für Patienten Fibroblasten. Zellen, die keine mitochondriale DNA enthalten und somit die mtRNaseP Funktion nicht benötigen, reagieren dennoch mit Apoptose auf einen HSD10 knock-down. Der Apoptose-Phänotyp im HSD10 LOF ist demnach nicht abhängig von der RNaseP Funktion von HSD10. Diese Experimente zeigen, dass die Symptome des HSD10-Mangels nicht vollständig durch eine Beeinträchtigung der RNaseP erklärt werden können.

3 INTRODUCTION

3.1. 17β-hydroxysteroid-dehydrogenase type 10 – an evolutionary conserved multifunctional protein

HSD10 was first identified as an enzyme involved in the oxidation of branched chain fatty acids in the rat liver and as such it was named SCHMAD (short chain L-3-hydroxy-2-methylacyl-CoA dehydrogenase; Luo et al, 1995). Later on it was found in bovine mitochondria and it was given an additional name: HADH2 (L-3-hydroxyacyl-CoA dehydrogenase type II; Kobayashi et al, 1996). Yan et al. discovered HSD10 in a yeast-2-hybrid screen for binding partners of the amyloid-β peptide (Yan et al, 1997) and named it ERAB (endoplasmic reticulum-associated amyloid β-peptide binding protein), since they found it located in the endoplasmic reticulum which later turned out to be an artefact. Afterwards HSD10 received several more names like ABAD (amyloid β-binding alcohol dehydrogenase; Yan et al, 1999), SCHAD (short chain 3-hydroxyacyl-CoA dehydrogenase; He et al, 1999), MHBD (2-methyl-3-hydroxybutyryl-CoA dehydrogenase; Zschocke et al, 2000) and 17βHSD10 (17β-hydroxysteroid dehydrogenase type 10; He et al, 2001). To sort out all these different names, HSD17B10 and HSD10 were chosen to be the official designations for the gene and the gene product, respectively (OMIM 300256; Korman & Yang, 2007).

HSD17B10 is located on the short arm of the X-chromosome (Xp11.2) and is composed of six exons stretched over approximately 3 kb (fig. 1; Yang et al, 2005a). Exons 1-3 form the NAD-binding domain at the amino terminus. The C-terminal domain, which binds the substrate and catalyses the enzymatic reaction, consists of exons 4-6 (He et al, 1998).

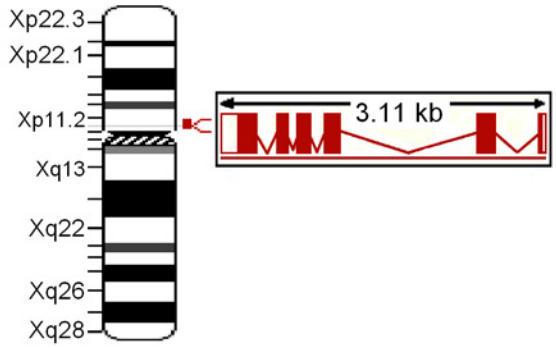

Figure 1 Localisation of HSD17B10 on the X-chromosome (adapted from Yang et al, 2005a). HSD17B10 is located on Xp11.2 and is composed of six exons stretched over approximately 3 kb.

The HSD10 protein consists of 261 amino acids and has a molecular mass of about 27 kD. It forms homotetramers with a molecular mass of 108 kD *in vivo*. The expression of HSD10 occurs ubiquitously in all tissues (He et al, 2000a; He et al, 2001; He et al, 2003) but predominantly in liver, heart and brain (Yan et al, 1997; He et al, 2003). The expression of HSD10 is regulated by C/EBPβ (CCAAT enhancer binding factor β) and several isoforms of C/EBPβ (Rotinen et al, 2010). The promoter of HSD17B10 contains a CCAAT box at -30/-19 and two binding sites for C/EBPs.

Due to alternative splicing sites in the mRNA there are several isoforms of HSD10 (Yang et al, 2007). The splicing signal at exon 5 is rather weak and can be skipped in favour of

an alternative splicing site. This results either in the omission of approximately 55 nucleotides at the end of exon 5 and the beginning of exon 6 processed to form the isoform 2 or the choice of an alternative splicing site occasionally results in the exclusion of the entire exon 5. Isoform 2 (NM_001037811) is stable and found in normal human brain tissue. Exon skipping leads to a frame shift and the formation of a premature stop codon. Hence, isoform 3 is unstable since it is probably submitted to nonsense-mediated decay. Correct splicing of HSD10 is crucial for maintenance of normal brain function.

Subcellularly, HSD10 is located in the mitochondrial matrix proven by several different methods like confocal and electron microscopy (Yan et al, 1999; He et al, 1999; He et al, 2002), subcellular fractionation (Luo et al, 1995) and immuno histology (Frackowiak et al, 2001). Computational analysis of the amino acid sequence of HSD10 revealed a putative mitochondrial localisation signal, ERLVGQ, at the N-terminus of the protein (Sambamurti & Lahiri, 1998). Eleven N-terminal amino acids form a positively charged amphiphilic α helix that is sufficient but not required for mitochondrial import (He et al, 2001). HSD10 might have one or more additional mitochondrial localisation signals, although an internal or C-terminal targeting signal was not found in the protein sequence.

HSD10 is the only 17β-hydroxysteroid dehydrogenase located in mitochondria. Within the 17β-HSDs, HSD10 belongs to the family of SDR (short chain dehydrogenases/ reductases). It can catalyse NADH-dependent redox reactions of many different substrates including branched short chain acyl-CoAs, fatty acids, linear alcohols, amino acid catabolites as well as steroids (Kobayashi et al, 1996; Furuta et al, 1997; Yan et al, 1997; He et al, 1998; He et al, 1999; Yang et al, 2005a). The alcohol dehydrogenase activity of HSD10 is marginal (Yan et al, 1999; He et al, 2000b).

3.2. Function of HSD10 in fatty acid metabolism and isoleucine breakdown

HSD10 oxidises specifically the L-form of L-3-hydroxyacyl-CoAs to 3-ketoacyl-CoAs but does not turn over the D-isomere. This reaction is one of the steps in isoleucine breakdown before the products acetyl-CoA and propionyl-CoA are generated (fig. 2). In its function as MHBD (2-methyl-3-hydroxybutyryl-CoA dehydrogenase), HSD10 catalyses the NADH-dependent oxidation of 2-methyl-3-hydroxybutyryl-CoA, an intermediate product of the isoleucine metabolism, to 2-methyl-acetoacetyl-CoA (Luo et al, 1995; fig. 2). The degradation of branched chain amino acids like isoleucine primarily takes place in organs like kidneys, skeletal and heart muscle. β-oxidation is also a source of ketone bodies that can provide energy for the brain if glucose levels are low (Eaton et al, 1996; Rinaldo et al, 2002). Although HSD10 does not play an essential role in ketone metabolism under physiological conditions, Yan et al, 2000a and 2005, suggest that it can assist the mitochondrial β-hydroxybutyrat-dehydrogenase, which is normally responsible for the oxidation of β-hydroxybutyrat, in cellular stress situations.

HSD10 deficiency clinically manifests in an accumulation of the metabolites 2-methyl-3-hydroxybutyryl-CoA and tiglylglycin in urinary organic acid assays. So far it is not known to what extent the other enzymatic functions of HSD10 play a role in human metabolism.

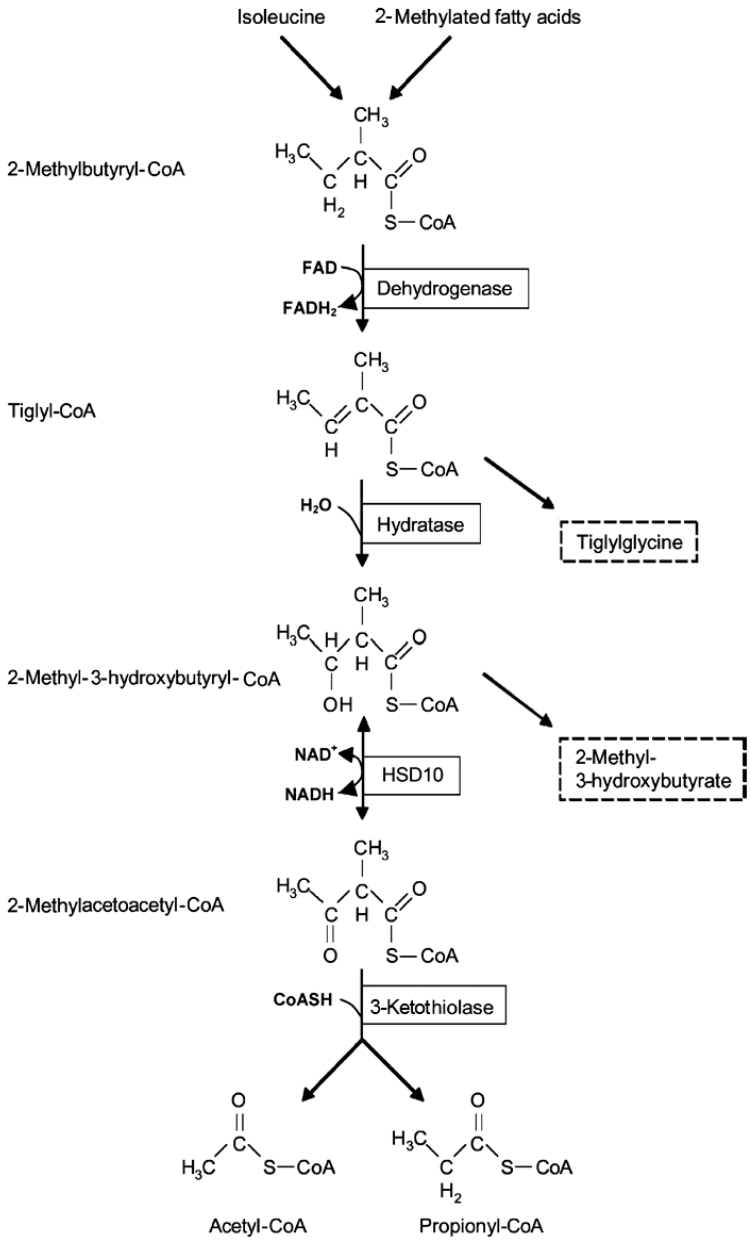

Figure 2 HSD10 in the β-oxidation of short chain methylated acyl-CoAs (adapted from Zschocke et al, 2000). The essential amino acid isoleucine becomes metabolised in several steps which are catalysed by different enzymes, one of them being HSD10. End products are acetyl-CoA and propionyl-CoA which are important initial substances for other metabolic pathways that are involved in the generation of cellular energy.

3.3. HSD10 in steroid metabolism

HSD10 has been suggested to play a role in sex steroid hormone metabolism as well as in the metabolism and synthesis of neuroactive steroids.

In the former function it is relevant for the biosynthesis and inactivation of steroid hormones (Yang et al, 2005b) like androgen, estrogen and progesterone. More specifically, it oxidises 17β-estradiol to estrone and thereby inactivates it in the placenta and ovaries (He et al, 1999; He et al, 2000a) and probably in testis (Ivell et al, 2003). HSD10 is abundantly expressed in Leydig cells which might protect these cells from the effect of estrogens. Furthermore, it oxidises 3-α-adiol to the physiologically active androgen 5α-dihydrotestosteron *in vitro* (He et al, 2000a; He et al, 2001; He et al, 2003).

It has been proposed that HSD10 exerts its role in neuroactive steroid metabolism in the brain e.g. by catalysing the oxidation of allopregnanolone to 5α-DHP (5α-dihydroprogesterone) and of 3α,5α-THDOC (3α,5α- allotetrahydrodeoxycorticosterone) to DHDOC (5α-dihydrodeoxycorticosterone; fig. 3). Allopregnanolone and 3α,5α-THDOC increase receptor opening frequency and duration and thus are positive modulators of $GABA_A$ receptors (gamma-aminobutyric acid type A receptors, Lambert & Grover, 1995), that become inactivated by HSD10 *in vitro*. Therefore, the level of these neurosteroids in the brain influences neuronal excitability and HSD10 plays a role in the maintenance of normal function of GABAergic neurons (He et al, 2005a; He et al, 2005b). In addition, 5α-DHP can modulate gene expression.

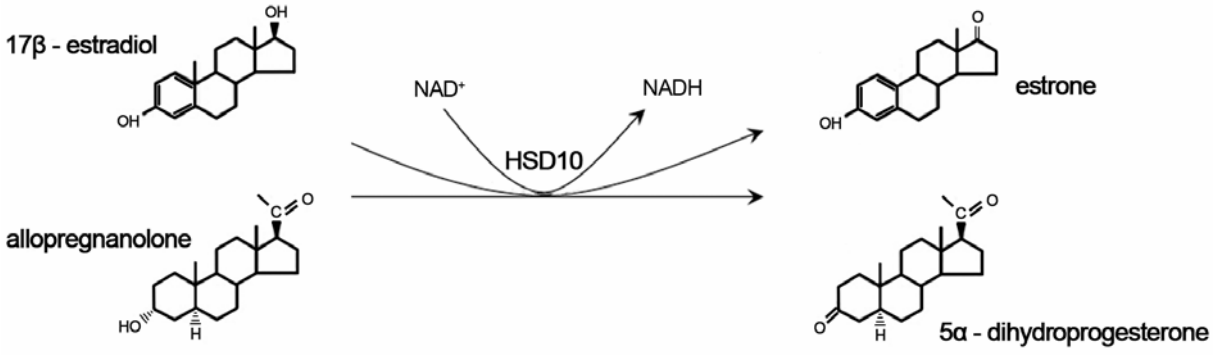

Figure 3 Reactions catalysed by HSD10 in steroid metabolism (modified from Yang et al, 2007). 17β-estradiol and allopregnanolone are inactivated irreversibly with the concomitant reduction of NAD^+.

3.4. HSD10 deficiency in humans

Missense mutations in the HSD17B10 gene cause a congenital neurodegenerative disease called HSD10 deficiency (Zschocke et al, 2000; Ensenauer et al, 2002; Olpin et al, 2002). Biochemically HSD10 deficiency manifests in the accumulation of the metabolites 2-methyl-3-hydroxybutyryl-CoA and tiglylglycin in urinary organic acid assays.

HSD17B10 is located on the X-chromosome and although it has been reported to escape X-inactivation recent publications indicate that it becomes normally X-inactivated (Garcia-Villoria et al, 2010). Boys suffer from a more severe progressive clinical disease course than girls (Ofman et al, 2003; Ensenauer et al, 2002). Heterozygous girls show a variety of non-progressive symptoms ranging from normal cognitive function to psychomotor retardation (Ensenauer et al, 2002; Perez-Cerda et al, 2005; Garcia-Villoria et al, 2009).

HSD10 deficiency has been identified in 15 patients (12 male) from 12 families so far (Ensenauer et al, 2002; Olpin et al, 2002; Sutton et al, 2003; Poll-The et al, 2004; Sass Sass et al, 2004; Perez-Cerda et al, 2005). The following missense mutations (table 1) have been found to be the underlying disease cause:

mutation	amino acid exchange
c.257A>G	D86G
c.364C>G	L122V
c.388C>T	R130C
c.495A>C	Q165H
c.628C>T	P210S
c.740A>G	N247S
c.745G>C	E249Q

Table 1 Mutations causing HSD10 deficiency.

In order to gain insight into the pathogenesis of neurodegeneration in HSD10 deficiency and to obtain further information on the biological role of HSD10, three of these mutations that cause significantly distinguishable clinical pictures were investigated. The R130C mutation causes the classical disease presentation; the D86G mutation is associated with a very severe clinical phenotype and patients with the Q165H mutation display normal neurological development. Patients usually develop clinical symptoms after times of increased metabolic stress like infections or vaccinations.

Boys with the R130C mutation usually show a progressive neurodegenerative disease course starting from year 1 or 2 that can lead to death within few years. Besides the progressive loss of motor and mental skills including a progressive loss of sight, the patients often develop epilepsy that is difficult to treat (Zschocke et al, 2000; Poll-The et al, 2004; Sass et al, 2004; Ensenauer et al, 2002; Olpin et al, 2002; Sutton et al, 2003 and Ofman et al, 2003).

A recently described male patient with the D86G mutation showed severe neurological abnormalities and little psychomotor development in the first months of life (Rauschenberger et al, 2010). At the age of 6 months the patient showed truncal hypotonia with increased muscle tone of arms and legs, gross motor dyskinesia and athetosis, smacking of the lips, absent head control and a horizontal nystagmus with absence of focusing. Clinical chemical studies revealed intermittently elevated lactate up to 5 mM (norm < 2.1) with increased lactate/pyruvate ratios compatible with a disturbance in oxidative phosphorylation. HSD10 activity in fibroblasts was only partially reduced to 30-70 % of normal (0.72 nmol/min/mg protein, norm 1.04±0.50 and 2.8 nmol/min/mg protein, norm 7.3±1.2). Repeated electroencephalography was normal despite several epileptic seizures in the last month of life. Magnetic resonance tomography of the brain yielded no abnormality. Echocardiography revealed a progressive hypertrophic cardiomyopathy. Cardiac function and cardiomegaly deteriorated rapidly and the boy died at age 7 months of progressive heart failure.

The Q165H mutation was identified in three boys (brothers and cousin) of one family. One child has been entirely normal from birth onwards, whereas in another boy early infancy was marked by poor feeding and failure to gain weight necessitating investigation aged 8 months. In all three boys a urine organic acid screen revealed metabolites ascribed to 2-methyl-3-hydroxy-butyryl-CoA dehydrogenase deficiency. Enzyme studies identified a profoundly low HSD10 activity of 0.2 nmol/min/mg (norm 7.3±1.2). Cognitive and motor development has been entirely normal up to the present age of 9 years. Magnetic resonance imaging confirmed normal brain structure and echocardiography was unremarkable.

Clinical and enzymatic findings in patients with HSD10 deficiency indicated that symptoms are not due to the accumulation of toxic metabolites in the isoleucine pathway. A deficiency of the enzyme catalysing the last step in the breakdown of isoleucine (3-ketothiolase) causes the same metabolites in urinary organic acid assays but a very different clinical picture not including progressive neurodegeneration but rather the classical symptoms of an organic aciduria. Also, an isoleucine restrictive diet, that avoids the accumulation of potentially toxic metabolites failed to improve the condition of patients.

Observations in these patients indicated that the development and severity of symptoms is unusual for an organic aciduria and unrelated to residual enzyme activity but the pathogenetic basis of HSD10 deficiency had so far remained elusive.

In order to characterise the mutations found in patients, they were cloned and expressed in bacteria. Recombinant proteins were purified and used to determine the 3D structure of HSD10 as well as kinetic constants with different substrates (fig. 4).

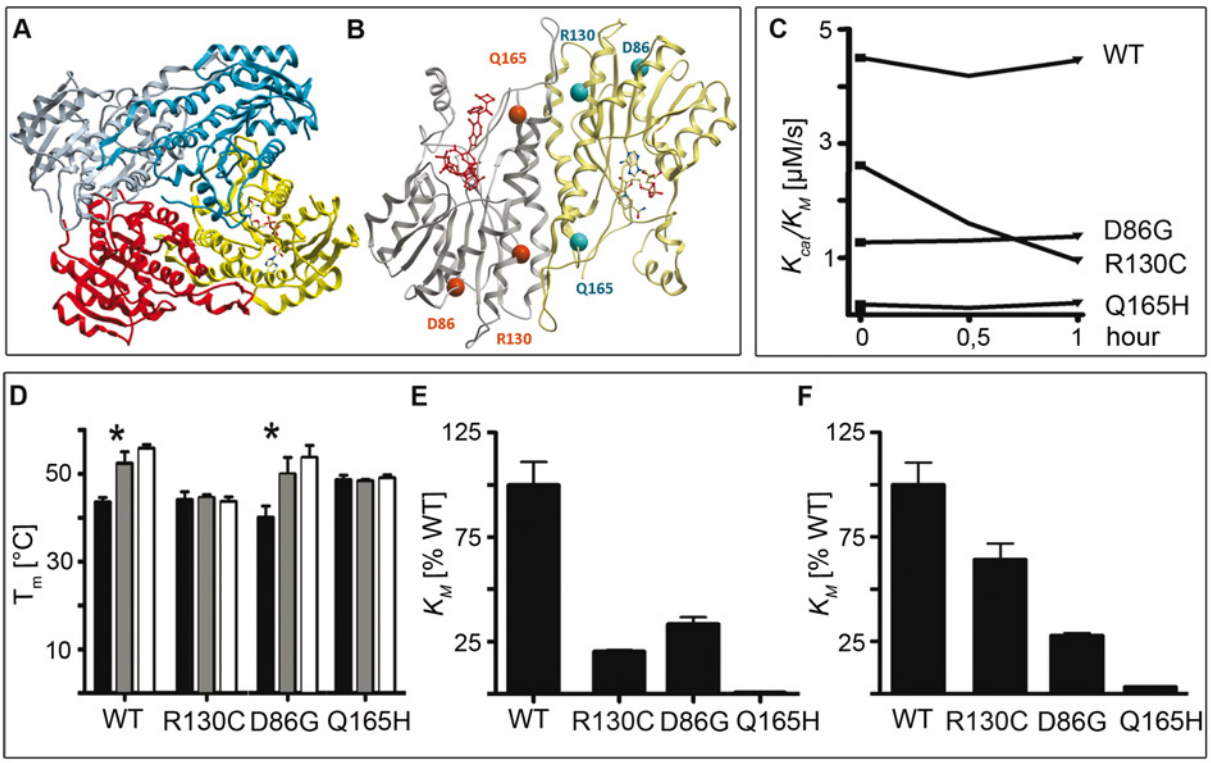

Figure 4 Crystal structure, stability and activity of the HSD10 homotetramer from HSD10 patients (adapted from Rauschenberger et al, 2010). **(A, B)** Crystal structure of HSD10. **(A)** Diagram of the homotetramer with bound cofactors to each monomer. **(B)** Diagram of a dimer with the location of the mutations. The location of the active centre is marked by the substrate in red. **(C)** Enzyme activity of HSD10 over time. K_{cat}/K_M of HSD10 wildtype and mutations measured in a 30 min interval; substrate 2-methyl-3-hydroxybutyryl-CoA. **(D)** Stability of HSD10 wildtype and mutations. Mean value of T_m determined by DSF (differential scanning fluorimetry)-experiments and standard deviation are shown. Black column: no cofactor/substrate, gray column: cofactor NAD^+, white column: cofactor NADH (* indicates significant cofactor binding). **(E)** Enzyme activity of HSD10 with hydroxybutyryl-CoA as substrate (wildtype enzyme is taken as 100 %). **(F)** K_{cat}/K_M of HSD10 mutations with 2-methyl-3-hydroxybutyryl-CoA as substrate in relativity to the wildtype enzyme. K_M: Michaelis-Menten-constant, K_{cat}: turnover number.

Residual dehydrogenase activities of 64 % and 28 % were measured for mutations R130C and D86G, respectively, which both cause a severe phenotype in patients. However, mutation R130C was unstable at room temperature and steadily lost enzymatic activity (fig. 4C). This mutation might interfere with the oligomerization of the HSD10 tetramer (Kissinger et al, 2004) and thus influence its stability. Cofactor binding of NAD^+ or NADH, as reflected by increased thermal stability (fig. 4D), was observed for both, wildtype and D86G. In contrast, mutation Q165H located at the active centre of the enzyme showed neither residual activity nor cofactor binding in our experimental settings. Inability of the mutation Q165H to bind the cofactor indicates that regardless of the substrate, no enzymatic reaction requiring NADH or NAD^+ (all known reactions) will be sufficiently catalysed by this mutant protein. Surprisingly, this mutation was found in patients with normal neurological development.

The lack of correlation between residual enzyme activity and disease severity indicates that the pathogenesis of HSD10 deficiency is mediated by an as yet unknown non-dehydrogenase function of HSD10.

3.5. Implication of HSD10 in Parkinson's, Alzheimer's and other clinical symptoms

HSD10 has been suggested to be involved in several other clinical conditions apart from HSD10 deficiency, like mental retardation, cancer, Parkinson's and Alzheimer's.

An apparently silent mutation in the HSD17B10 gene that affects splicing efficiency has been linked to mental retardation, choreoathetosis and abnormal behaviour (Reyniers et al, 1999; Lenski et al, 2007). This mutation reduces the amount of HSD10 protein and shifts the ratio of alternatively spliced transcripts. Microduplications of HSD17B10 and the resulting increase in protein level have also been found to be associated with mental retardation (Froyen et al, 2008).

Moreover, HSD10 seems to play a role in some forms of cancer. It has been suggested that a high level of HSD10 might be protective against gynecological cancers (Yang et al, 2005b) but on the other hand there is also evidence that malignant prostatic epithelial cells have elevated HSD10 levels which might promote cancer growth (He et al, 2003).

Furthermore, Tieu et al, 2004, found a reduced level of HSD10 in dopaminergic neurons of Parkinson's patients. Parkinson's is a neurodegenerative disease that is accompanied by the loss of dopaminergic neurons in the substantia nigra pars compacta. Complex I activity of the respiratory chain is impaired in brains of Parkinson's patients (Dauer & Przedborski, 2003). This leads to a disturbance in energy generation and necessitates the usage of alternative energy sources like ketone bodies and D-β-hydroxybutyrat (Kashiwaya et al, 2000; Tieu et al, 2003). A mouse model of Parkinson's has been established using the neurotoxin MPTP (1-methyl-4-phenyl-1,2,3,6-tetrahydropyridin), which blocks complex I (Nicklas et al, 1987) and reproduces typical symptoms of Parkinson's in mice (Langston et al, 1983) including the downregulation of HSD10 (Tieu et al, 2004). In this mouse model, Tieu et al. found that a simultaneous overexpression of HSD10 has a protective effect on neurons regarding the mitochondrial inhibition caused by MPTP. HSD10 improves mitochondrial respiration and ATP production by complex I. In addition, they showed by subcellular fractionation that HSD10 is re-distributed from the mitochondrial matrix to the membrane under oxidative stress caused by inhibition of complex I.

One of the names HSD10 has been given due to its history of identification is ABAD (amyloid β-peptide-binding alcohol dehydrogenase). HSD10 was detected in a yeast-2-hybrid screen as one of the binding partners of amyloid β, a neurotoxic peptide implicated in Alzheimer's (Yan et al, 1997). Alzheimer's is characterised by dementia due to progressive nerve cell death in the brain. Aberrant amyloid β production and its deposition in so-called senile plaques plays an important but not yet fully understood role in the pathomechanism of Alzheimer's.

Binding of amyloid β abolishes the enzyme activity of HSD10 since it blocks its cofactor binding site (Yan et al, 1999; Oppermann et al, 1999; Lustbader et al, 2004; Kissinger et

al, 2004). It also leads to the production of lipid peroxidating aldehydes like hydroxynonenal and malondialdehyd *in vivo* (Yan et al, 1999). Lipid peroxidation has later been shown not to be the reason for amyloid β induced cell death in neurons of Alzheimer's patients (Salim et al, 2000). HSD10 and amyloid β interact directly in neuronal mitochondria of Alzheimer's patients as well as in mice double transgenic for HSD10 and a mutant form of human APP (Tg mAPP/ABAD; Lustbader et al, 2004). Affected brain regions in Alzheimer's patients express elevated levels of HSD10 (Yan et al, 1997; Yan et al, 2000a; Yang & He, 2001; Lustbader et al, 2004; He et al, 2005b). Co-transfection of HSD10 and amyloid β in cultured cells results in an increase in cytotoxicity, more specifically in apoptosis, that cannot be seen with HSD10 or amyloid β alone (Yan et al, 1999).

There is evidence that the energy metabolism in the brains of Alzheimer's patients is disturbed. Complex IV activity is diminished in the central and peripheral nervous system (Kish et al, 1992; Mutisya et al, 1994; Parker et al, 1994; Maurer et al, 2000; Bosetti et al, 2002). In mice transgenic for HSD10 and a mutant form of human APP (Tg mAPP/ABAD) it was shown that complex IV activity in neurons and the cerebral glucose metabolism are decreased (Yan et al, 1999; Yan & Stern, 2005; Takuma et al, 2005). In addition, elevated levels of free radicals and hydrogen peroxide were found in these neurons. A caspase-3-like activity as well as cytochrome c release and DNA fragmentation were strongly increased in neurons from Tg mAPP/ABAD mice leading to a significant decrease in cell viability. These double transgenic mice are phenotypically unremarkable but they display a reduced learning ability (Lustbader et al, 2004; Takuma et al, 2005).

Amyloid β seems to act on mitochondria since it has been shown to cause increased permeability of the outer mitochondrial membrane induced by pro-apoptotic Bax and subsequently mitochondrial swelling and caspase activation (Giovanni et al, 2000; Zhang et al, 2002). Thus, Alzheimer's appears to be associated with a mitochondrial dysfunction which may be mediated by the interaction of amyloid β and HSD10 leading to oxidative stress and apoptotic cell death.

3.6. HSD10 – cytoprotective or cytotoxic?

The expression and localisation of HSD10 is dependent on cellular stress. HSD10 expression is upregulated in stress situations like hypoxia-ischemia, nutritional stress and the presence of amyloid plaques (Yan et al, 2000a; Yan et al, 2000b; Yan & Stern, 2005). Under normal physiological conditions HSD10 is localised in the mitochondrial matrix and is re-distributed to the membrane under stress (Tieu et al, 2004).

On one hand, a cytotoxic role in Alzheimer's was implied for HSD10 as it appears to mediate the cytotoxic effect of amyloid β (Yan et al, 1997).

On the other hand, a protective effect of overexpressed HSD10 under conditions of oxidative stress was found in the setting of acute brain damage (Yan et al, 2000a) and in a mouse model of Parkinson's (Tieu et al, 2004). In addition, HSD10 can maintain cellular energy homeostasis by oxidising ketone bodies to D-3-hydroxybutyrate in nutritional stress situations (Yan et al, 2000a; Yan et al, 2000b). Overexpressed HSD10 also had a protective effect on neurons in mice after strokes induced by transient middle cerebral artery occlusion. These publications do not present any functional data that would suggest a mechanism for the protective function of HSD10.

Furthermore, an anti-apoptotic function was suggested for HSD10 in mitochondria. HSD10 binds CypD (cyclophilin D; Ren, 2008), a peptidylprolyl isomerase F localised in the mitochondrial matrix that is recruited to the inner membrane under oxidative stress in order to form the MPTP (mitochondrial permeability transition pore; Connern & Halestrap, 1994). Addition of cyclosporin A, an immune suppressor, inhibits the formation of the MPTP. It binds to CypD and thereby blocks its participation in pore formation. Binding of HSD10 and CypD in the mitochondrial matrix might have the same effect as cyclosporin A and inhibit the translocation of CypD and thus the formation of the MPTP (fig. 5). Therefore, HSD10 might have a protective, anti-apoptotic function in the mitochondrial matrix (Yan & Stern, 2005).

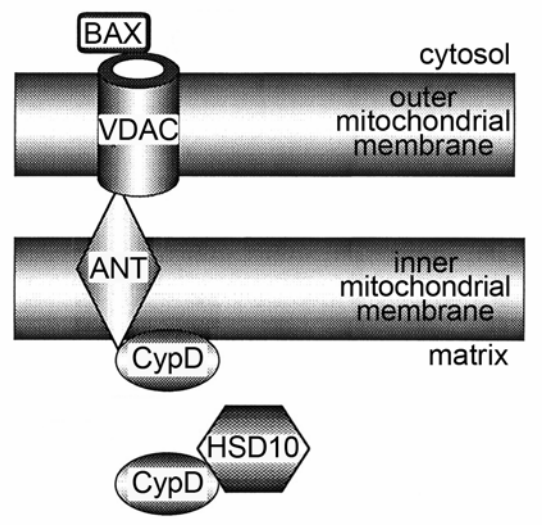

Figure 5 Constitution of the MPTP and its inhibition by the interaction between CypD and HSD10 (adapted from Szewczyk & Wojtczak, 2002). CypD is a protein of the mitochondrial matrix that can translocate to the membrane where it is one of the components of the MPTP (mitochondrial permeability transition pore). Binding of HSD10 and CypD in the mitochondrial matrix might block the function of CypD in the initiation of apoptosis. VDAC: voltage dependent anion channel, ANT: adenine nucleotide transporter.

3.7. Intrinsic and extrinsic regulation of apoptosis

The progressive neurodegeneration observed in HSD10 deficiency seems to be associated with apoptotic cell death caused or accompanied by mitochondrial dysfunction.

Apoptosis is controlled by many different signals. These signals can either originate extracellularly as extrinsic inducers like hormones or the lack of growth factors, or they can arise intracellularly triggered by intrinsic factors like any disturbance of cellular homeostasis e.g. a high concentration of intracellular calcium or anorganic phosphate, DNA damage or oxidative stress accompanied by high levels of ROS (reactive oxygen species; Strasser et al, 1995). In addition, lack of adenine nucleotides and an alkaline pH lead to apoptosis.

Extrinsic and intrinsic inducers can act pro- or anti-apoptotic. Despite of their diverse origin these signals eventually activate a common cell death machinery. Once a certain threshold is crossed apoptotic cells develop characteristic features like chromatin condensation and margination at the nuclear membrane, cell shrinkage and detachment, blebbing of the plasma membrane, cleavage of DNA and finally the fragmentation of the cell into so-called apoptotic bodies.

The extrinsic apoptotic pathway is mediated by death receptors of the TNFR (tumour necrosis factor receptor) family (fig. 6). Those receptors consist of an extracellular ligand binding domain and an intracellular death domain (Banner et al, 1993; Smith et al, 1994; Krammer, 2000). Ligand binding causes trimerization of the TNFR and the binding of death proteins to the intracellular death domain. Adaptor molecules like FADD (Fas associated death domain protein) link the transmembrane receptor to caspase-8 and thereby activate it. This sets the caspase cascade in motion that executes the irreversible morphological changes of apoptosis in the cell. Caspases are pro-apoptotic mediators that exist in an inactive precursor form and are activated in a caspase cascade by proteolytical cleavage. There are initiator caspases including procaspases-2, -8, -9 and -10 and executioner caspases including procaspases-3, -6, and -7. The initiator caspase-8 is specifically activated via the extrinsic pathway and activates the executioner procaspase-3 (Peter & Krammer, 2003).

Mitochondria play an important role in apoptosis (fig. 6) since they can intrinsically induce apoptosis (Orrenius, 2004). Mitochondria of an apoptotic cell swell due to MMP (mitochondrial membrane permeabilization) including the formation of membrane pores like MACs (mitochondrial apoptosis-induced channels) or MPTPs (mitochondrial permeability transition pores). This latter pore forms in the inner and outer membrane and consists of an ANT (adenine nucleotide transporter) in the inner membrane and a VDAC (voltage dependent anion channel) in the outer membrane (fig. 5; Zoratti & Szabo, 1995; Halestrap & Brenner, 2003). Another component of the MPTP is Bax, a pro-apoptotic molecule of the Bcl-2 family. It is a cytosolic protein that binds to the VDAC in response to apoptotic signals. Binding of CypD (cyclophilin D) to ANT facilitates a calcium induced conformational change in the specific adenine nucleotide transporter to an unspecific pore. Formation of the MPTP makes the membrane permeable and causes mitochondrial swelling supported either by additional channels in the outer membrane formed by members of the Bcl family (Bax, Bad, Bak, Bid) or by disintegration of the outer membrane (Gross et al, 1999). Additionally, the mitochondrial membrane potential

is disturbed and thus ATP production is impossible. Proteins of the intermembrane space like cytochrome c, AIF (apoptosis inducing factor) and Smac (second mitochondria-derived activator of caspase) leak from mitochondria into the cytosol. Released cytochrome c binds Apaf-1 (apoptotic-protease-activating factor 1) which in turn proteolytically activates caspase-9 and thus initiates the caspase cascade. SMACs bind and thereby deactivate IAPs (inhibitors of apoptosis proteins) which normally suppress the activity of caspases. Procaspase-9 is specific for the intrinsic induction of apoptosis and both, procaspase-8 and -9, activate the executioner procaspase-3 (Green & Kroemer, 1998; Green, 1998; Green & Reed, 1998; Susin et al, 1999; Kroemer & Reed, 2000; Green & Kroemer, 2004). AIF released from mitochondria enters the nucleus and mediates the condensation and fragmentation of DNA.

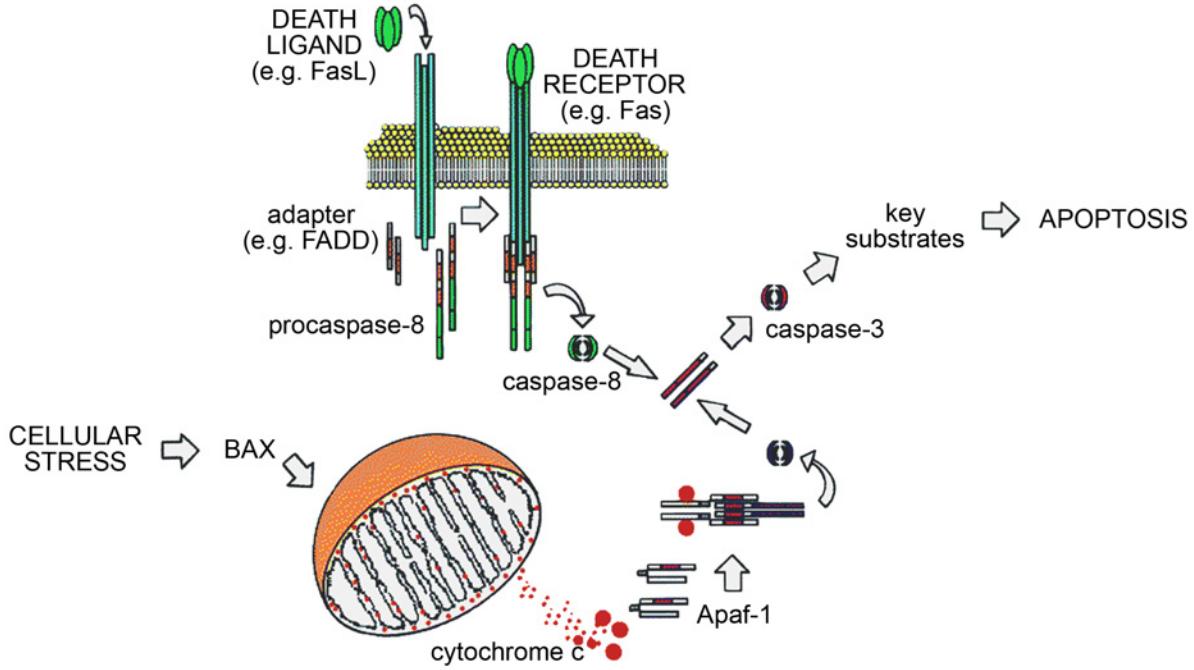

Figure 6 Overview of intrinsic and extrinsic induction of apoptosis (from Green, 1998). Both pathways converge on the activation of effector caspases (like caspase-3, -6 and -7) and the cleavage of key substrates like lamin and DNA.

Apoptosis is a strictly regulated process with several different mechanisms of regulation at the protein level. As described above, proteolytic cleavage activates caspases but also posttranslational modifications such as phosphorylation and the subcellular re-distribution of proteins like BAX and cytochrome c contribute to the regulation of apoptosis. On the other hand, apoptosis is also regulated transcriptionally through a number of transcription factors including p53, myc, NF-κB, FOXO, HOX and Snail (Bates & Vousden, 1999; Gilley et al, 2003; Dudgeon, 2009). For example, apoptosis caused by cellular stress upon DNA damage is regulated by transcription factors of the p53 and AP-1 family. HOX and Snail proteins modulate developmental apoptosis and NF-κB and FOXO family members are regulators of apoptosis mediated by proinflammatory cytokines or growth factors. Additionally, members of the Bcl-2 family have been shown to be

transcriptionally regulated by the zinc finger protein WT1 (Loeb, 2006) and by p53 (Bates & Vousden, 1999).

These transcription factors activate the expression of pro-apoptotic Bcl-2 family members, caspases, death receptors and their ligands and downregulate the transcription of the anti-apoptotic Bcl-2 family and IAPs (inhibitors of apoptosis proteins). Hence, the intrinsic apoptotic pathway is transcriptionally regulated via the pro- and anti-apoptotic Bcl-2 family members and the extrinsic pathway by the means of death receptors and IAPs, respectively.

3.8. HSD10 function in the model organisms *Drosophila* and mouse

A complete knock-out of HSD10 is embryonic lethal in *Drosophila* as well as in mice (Rumig, 2006; Torroja et al, 1998).

The homolog of HSD10 in *Drosophila*, Scully, exerts the same enzymatic functions as human HSD10 (Shafqat et al, 2003) but it is a cytosolic enzyme rather than mitochondrially localised. The N-terminal sequence of human HSD10 forms a positively charged amphiphilic α helix that can act as a mitochondrial localisation signal, but there might be at least one additional mitochondrial importing signal (He et al, 2001). *Drosophila* HSD10 is missing six of these amino acids at the N-terminus compared to human or *Xenopus* HSD10 which possibly causes the cytosolic distribution. The remaining protein sequence exhibits 69 % identity with the human sequence. A knock-down of HSD10 in *Drosophila* results in early embryonic lethality. Thus, four different mutations have been introduced by EMS (ethyl methanesulphonate) and x ray in *Drosophila* larvae (Torroja et al, 1998). Two of these (scu^{174} and scu^{S152}) are point mutations that cause the amino acid exchanges L33Q and F120I in two well-conserved residues. One mutation (scu^{3127}) is a 254 base pair deletion that introduces a frame shift after 86 amino acids and removes the catalytic centre. The fourth mutation (scu^{4058}) is a deletion of two base pairs that results in a frame shift after 205 amino acids. The catalytic centre in this mutation is intact. All of these mutations are early embryonic lethal. Mutants with the scu^{3127} mutation are viable during embryonic development but die as third instar larvae. Scully is expressed at a very low level in unfertilized eggs and increases during embryonic development. Mature gonads show a particularly high expression of Scully. Mutant pupal testes are reduced in size whereat the degree of reduction is: scu^{174} > scu^{4058} > scu^{S152} > scu^{3127}. In mosaic analysis, scu^{3127} again showed the mildest phenotype although this mutation introduces a large deletion with a frame shift after only 86 amino acids and abolishes the catalytic centre.

Cells in mutant flies exhibit large multilayered accumulations of membraneous material and a high amount of clear cytoplasmic vesicles of lipid nature. Nucleoli are not as compact as in control flies and contain many cavities. Mitochondria are fewer and smaller and comprise fewer and swollen cristae. Torroja et al. argued that these cellular changes are due to a defect in the β-oxidation of fatty acids like those observed in human pathologies (Torroja et al, 1998; Eaton et al, 1996; Torroja et al, 1998 Wanders et al, 1999; Rinaldo et al, 2002).

Homozygous knock-out mice are not viable and die at a very early developmental stage (Rumig, 2006). To study the function of HSD10 *in vivo* several conditional knock-out lines have been established.

The so-called ERAB/neo line is generated by crossing animals that still contain the neomycin resistance gene in the 5' UTR together with exon 1 of HSD10 within the loxP sites with Cre deleter mice. It has been shown before that the insertion of a neomycin resistance gene in introns may cause the disruption of normal gene expression. This crossing yields males with a decreased HSD10 expression in all organs except the spleen. These animals are phenotypically unremarkable until the age of 11-14 weeks when they start to develop physical changes like a scrubby fur and a progressive movement disorder that results in complete immobilisation and breathing difficulties. They die or are dispatched between week 15-24. Internally those animals display a highly enlarged bladder and abnormal bleeding in the gut. Bloodflow is decreased and bleeding through the tail vein is not possible. The lymph nodes, thymus and most of all the spleen are reduced in size but not altered in their structure. Only the testes are remarkably changed and have a highly decreased number of mature spermatids that probably causes the observed subfertility of these male mice. Spleen, kidneys, bowel, testes, liver, thymus and the cerebrum show highly increased levels of apoptosis. Symptoms in these ERAB/neo mice are distantly comparable to the clinical phenotype observed in HSD10 deficiency patients. Therefore, the urinary organic acids were tested for metabolites indicative of a disturbed isoleucine metabolism but no elevated organic acids were detected.

A conditional knock-out in endothelial cells and hematopoetic stem cells was generated by the Cre recombinase under the control of the Tie2 promoter. Tie2 is a receptor tyrosine kinase expressed predominantly in vascular endothelium. Those ERAB/Tie2 animals exhibit almost the same phenotype as the ERAB/neo line but the onset of symptoms does not take place until week 20-22 and those animals deteriorate faster. In addition, they suffer from convulsions and die or are put to death around week 26. Heterozygous as well as homozygous females are unremarkable.

An additional conditional knock-out was established in T-cells by a Cre recombinase under the control of the Ick promoter. The resulting homozygous ERAB/Ick males and females are phenotypically unremarkable and fertile but show an increased thymus cell number. Thymus cells were used to investigate apoptosis *in vivo* in a HSD10 knock-out situation. Either the intrinsic or the extrinsic apoptotic pathway was induced chemically in these cells and HSD10 knock-out thymus cells were much more sensitive to the intrinsic induction of apoptosis than control cells. Thus, HSD10 had a protective effect on mitochondrially mediated apoptosis in thymus cells.

Another conditional knock-out in noradrenergic neurons was generated with a Cre recombinase under the control of the DBH promoter (dopamine β-hydroxylase). These mice are viable and fertile but die around week 26.

3.9. HSD10 in the development of *Xenopus laevis*

The clinical phenotype observed in patients and the respective residual enzyme activity of mutant HSD10 suggests a dehydrogenase-independent function in embryonic development for HSD10 corroborated by the early embryonic lethality in the knock-out mouse (Rumig, 2006) and *Drosophila* (Torroja et al, 1998).

One of the best model organisms for developmental studies is *Xenopus laevis*. Eggs can be easily manipulated and selective targeting of manipulation is possible in *Xenopus* embryos because the dorsal/ventral and the left/right axes can be determined already at the 4-cell stage due to pigmentation differences of the animal blastomeres in so-called "Kleins". Fate maps are available (Bauer et al, 1994) that enable the tracing of each blastomere in the early embryo to the adult frog. Thus, a very localised and exclusive manipulation of distinct body regions is possible.

In *Xenopus* a complete knock-out of HSD10 is not embryonic lethal in contrast to mice and *Drosophila* since HSD10 is also provided maternally and the Morpholino oligonucleotide-mediated knock-down is only carried out in specific regions of the body. Zygotic transcription of *Xenopus* HSD10 (NCBI Locus BC077977) starts at neurula stages and takes place in ventral parts of the somites, the neural tube, the pronephros and the eyes (Rauschenberger et al, 2010).

Knock-down of HSD10 leads to a reduction of brain tissue and eyes that does not affect the a/p (anterior/posterior) patterning of the brain shown by the spatial expression patterns of the forebrain marker BF1 and the fore-/midbrain marker otx2 (Rauschenberger, 2007). Apoptosis was enhanced in injected tissue. The phenotype caused by HSD10 knock-down as well as the elevated level of apoptosis can be rescued by human HSD10 wildtype protein. The mutated HSD10 proteins found in human patients, however, showed remarkable differences in their ability to rescue the apoptotic phenotype. The Q165H mutation, which has less than 3 % residual enzymatic activity but was identified in three neurologically normal boys, partially rescued HSD10 Mo^{ATG}-induced apoptosis. In contrast, injection of the mutations R130C and in particular D86G failed to rescue, and instead further enhanced apoptosis. D86G has considerable residual enzyme activity despite being associated with a very severe clinical phenotype. The inability of the R130C and D86G mutants to rescue apoptosis was not due to protein mis-localisation. In *Xenopus* A6 cells wildtype and all mutated proteins co-localised with mitochondria. Thus, apoptosis after HSD10 loss-of-function is not dependent on the dehydrogenase activity of HSD10, arguing for a non-enzymatic function of this protein which is required in mitochondria.

Furthermore, a knock-down of HSD10 in *Xenopus* leads to a severe reduction in blood vessel formation (Rauschenberger, 2007; Guerra, 2010).

3.10. Interaction partners of HSD10

As described above HSD10 can bind to amyloid β *in vitro* and *in vivo* in brains of Alzheimer's patients.

Also mentioned above, is the physical interaction between HSD10 and CypD (cyclophilin D) in the mitochondrial matrix (Ren, 2008) that might prevent CypD from translocation to the membrane and formation of the MPTP.

In addition, HSD10 binds to the estrogen receptor α which is not only present in the nucleus and cytosol but also in mitochondria (Jazbutyte et al, 2009). The mitochondrial genome contains ERE (estrogen response elements) that are regulated by the ligand-receptor-complex and they postulate that the estrogen receptor α plays a role in the regulation of estrogen levels by modulating HSD10 activity. Estrogen is essential for cellular integrity since it reduces oxidative stress and this maintains mitochondrial structure and function and inhibits apoptosis.

In a yeast-2-hybrid screen, where HSD10 was used as bait and a HeLa cDNA library as prey, two potential interaction partners were identified: PCBP1 and UXT (unpublished data). PCBP1 (PolyC binding protein 1) binds to mRNAs that contain a DICE (differentiation control element) in the cytoplasm and thereby represses their translation, e.g. the endogenous L1 cell adhesion molecule mRNA, which contains two DICE motifs in the 3' untranslated region. Upon phosphorylation it releases the mRNAs for translation and migrates to the nucleus where it is a transcription factor for target genes like eIF4E (eukaryotic translation initiation factor 4E; Lynch et al, 2005) and GDF15 (growth differentiation factor 15; Huo et al, 2009). It also binds caper-α and plays a role in splicing. UXT (ubiquitously expressed transcript) is implicated in several cellular functions. One of them is the promotion of the NFκB (nuclear factor kappa-light-chain-enhancer of activated B cells) enhanceosome in the nucleus and as such it plays a role in mitochondrial aggregation and apoptosis.

Moreover, HSD10 functions in a complex called RNaseP which is involved in the processing of human mitochondrial tRNAs (Holzmann et al, 2008).

3.11. HSD10 as a component of human mitochondrial RNaseP

Mitochondria contain their own circular genome (Nass & Nass, 1963a; Nass & Nass, 1963b) in 2-10 copies per mitochondrion (Wiesner et al, 1992) and consequently in 100-10000 copies per cell depending on the cell type. mtDNA is inherited uniparentally from the mother in most organisms. It is particularly vulnerable to oxidative damage due to its vicinity to the respiratory chain that generates ROS and this leads to a rapid mutation rate of mtDNA (Brown et al, 1979). In humans the double stranded mtDNA consists of around 16.6 kb. The so-called heavy strand (H-strand) contains more guanine than the cytosine rich strand called light strand (L-strand). In total, 13 proteins of the respiratory chain are encoded in mitochondria but the majority of mitochondrial proteins is coded for by nuclear DNA and imported (Shoffner, 1995; Neupert, 1997). In addition, 22 tRNAs (transfer RNAs) and two rRNAs (ribosomal RNAs) are mitochondrially encoded. mtDNA has no introns and no non-coding sequences between the genes (Anderson et al, 1981;

Wallace et al, 1992; Zeviani et al, 1998). The displacement loop (D-loop) is the only non-coding section of the mitochondrial genome and encloses the origin of replication of the H-strand (O_H) and the promoters for L- and H-strand transcription (P_L and P_H ; fig. 7). Replication starts at the O_H and continues until it reaches the O_L that folds a stem-loop structure and initiates replication of the L-strand that proceeds back using the H-strand as a template. This makes mtDNA replication a bi-directional and asynchronous process (Clayton, 1982). Transcription of mtDNA starts from both promoters, proceeds along the mtDNA circle and creates a long polycistronic RNA. By cutting out interjacent tRNAs from the polycistronic transcript according to the "tRNA punctuation model of RNA processing in human mitochondria" rRNAs and mRNAs are liberated, polyadenylated and subsequently translated (Ojala et al, 1980; Ojala et al, 1981). The genetic code in human mitochondria is different from the one in the nucleus (Wallace, 1982), e.g. AUA codes for methionine and not isoleucine (Anderson et al, 1981; Montoya et al, 1981).

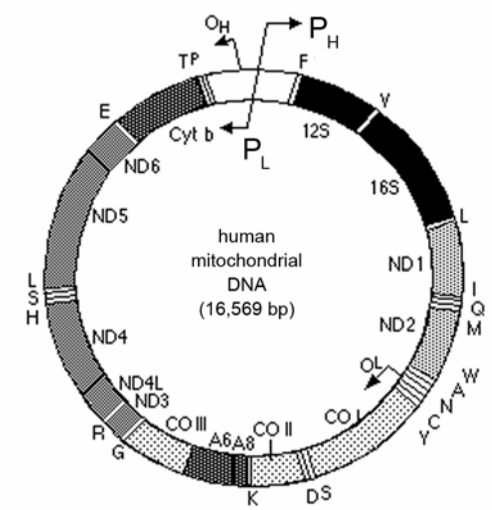

Figure 7 Circular and double stranded human mitochondrial DNA (modified from Holland & Huffine, 2001). It encodes 13 proteins of the respiratory chain, 2 rRNAs and 22 tRNAs. The abbreviated amino acid names show the position of the respective tRNA genes. The replication origins of the outer heavy and inner light strand are indicated with O_H and O_L, respectively. P_H and P_L are the transcription initiation sites. ND: NADH dehydrogenase, CO: cytochrome c oxidase.

Mitochondrial tRNAs are transcribed as immature precursors in long polycistronic transcripts, in which they fold into their secondary structure (fig. 8). They are excised at the 3' end by tRNaseZ and the 5' end by an enzyme complex called RNaseP (ribonuclease P; Robertson et al, 1972). Cleavage by RNaseP precedes 3' end maturation by RNaseZ in many systems including human mitochondria (Levinger et al, 2001; Levinger et al, 2004). Once the tRNAs are cut from the polycistronic transcript they are post-transcriptionally modified e.g. by methylation and the addition of CAA at the 3' terminus.

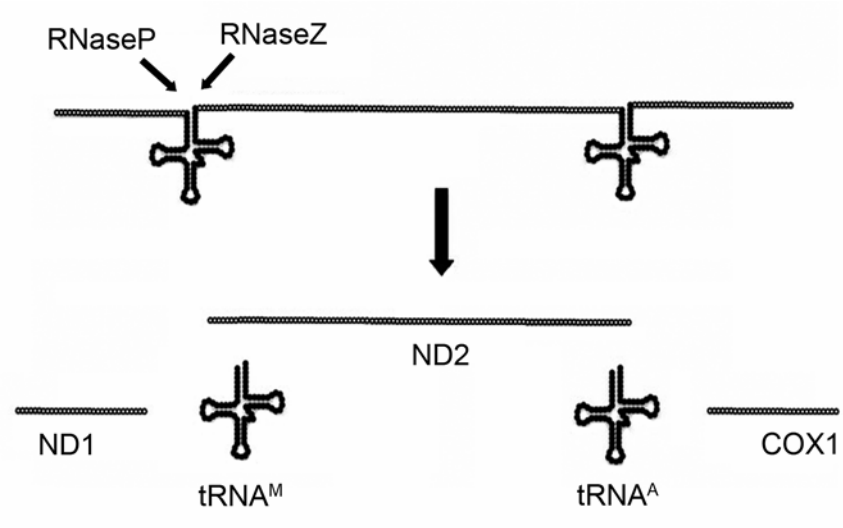

Figure 8 Schematic presentation of mitochondrial tRNA processing (modified from Hurto, 2011). Mitochondrial tRNAs are cleaved from the long polycistronic transcript first at the 3' end by RNaseZ followed by an incision at the 5' end by RNaseP. Arrows mark the cleavage position. According to the "tRNA punctuation model of RNA processing in human mitochondria" the excision of interjacent tRNAs (e.g. $tRNA^M$ and $tRNA^A$) yields mature rRNAs and mRNAs (e.g. ND1, ND2 and COX1). ND1 and ND2: NADH dehydrogenase subunit 1 and 2, COX1: cytochrome c oxidase subunit 1.

Recently, HSD10 has been shown to be a component of the human mitochondrial RNaseP complex (Holzmann et al, 2008). Until the components of this complex were identified, all RNaseP enzymes that have been characterised so far in various species consisted of a RNA moiety plus one or more proteins (reviewed in Hartmann & Hartmann, 2003; Willkomm & Hartmann, 2007). The RNAs have a similar core structure and seem to be capable of mediating cleavage of the 5' leader sequence of tRNAs even in the absence of protein (Guerrier-Takada et al, 1983). Thus, tRNA 5' maturation in addition to ribosomal protein synthesis was considered to be the only cellular process catalysed by a ribozyme universally persistent since the hypothetical prebiotic RNA world. In contrast, RNaseP from human mitochondria (mtRNaseP) has been shown to be a RNA free, protein-only enzyme (Holzmann et al, 2008). Its components were identified from mitochondrial extract in five different two-step purification procedures. RNaseP was partially purified in these preparations and the protein composition of the different purifications was compared for proteins they have in common and yielded the "partial purification overlap proteome". These analyses rendered three proteins that functionally reconstituted mtRNaseP *in vitro* without any RNA contribution: MRPP1, MRPP2 (HSD10) and MRPP3 (mitochondrial Ribonuclease P proteins 1-3).

Excision of mitochondrial tRNAs at the 3' and 5' end from the long polycistronic transcript and subsequent modification, the addition of CAA at the 3' terminus and aminoacetylation yields mature tRNAs. Classical tRNAs fold into a cloverleaf secondary structure and a L-shaped tertiary structure whereas human mitochondrial tRNAs can deviate structurally from this cloverleaf (Helm et al, 2000; fig. 9). The classical cloverleaf tRNAs like human mitochondrial $tRNA^V$, $tRNA^I$ and $tRNA^M$ consist of a very conserved number of nucleotides in their respective domains (Sprinzl et al, 1998).

Possible variations include the absence of the entire D-loop and an extended anticodon stem in $tRNA^S$ or absent nucleotides that are highly conserved in classical tRNAs suggesting that the formation of the tertiary L-shape does not occur (fig. 9).

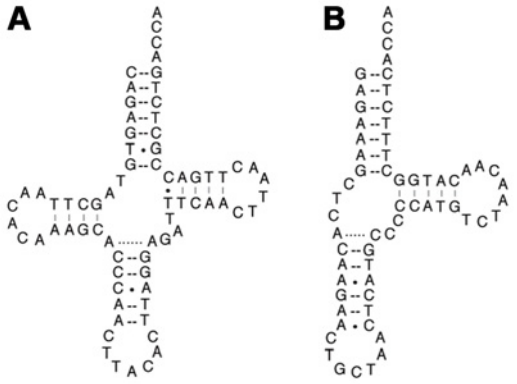

Figure 9 Structure of human mitochondrial tRNAs (from http://mamit-trna.u-strasbg.fr/mutations.asp?idAA=22). **(A)** Classical cloverleaf $tRNA^V$. Classical tRNAs consist of an acceptor stem (7 bp), connector (2 nt), D-stem and -loop (variable, 3-4 bp and 8-10 nt), second connector (1 nt), anticodon stem (5 bp), anticodon loop (7 nt), variable region, T-stem and -loop (variable, typically 5 bp and 7 nt). **(B)** Structurally different $tRNA^S$. This tRNA with an absent D-loop is the most extreme example of deviate tRNA structures in human mitochondria. bp: base pairs, nt: nucleotides.

Mutations in mitochondrial tRNAs cause a disturbance of mitochondrial translation that elicits many different clinical syndromes including MERRF (myoclonic epilepsy and ragged red muscle fibers; Finnila et al, 2001), mitochondrial myopathy (Swalwell et al, 2006), CPEO (chronic progressive external ophtalmoplegia; Spagnolo et al, 2001), progressive respiratory failure (Bruno et al, 2003), MELAS (mitochondrial encephalomyopathy, lactis acidose, stroke-like episodes; Tzen et al, 2003) and ADPD (Alzheimer's disease and Parkinson's disease; Wallace et al, 1992).

Mutation of one of the components of RNaseP inhibits the correct processing of polycistronic mitochondrial transcripts and thereby also disrupts mitochondrial translation. Therefore, the function of HSD10 in mitochondrial tRNA processing might be the underlying reason for the clinical phenotype in HSD10 deficiency patients.

3.12. Purpose of this study

HSD10 is implicated in two neurodegenerative disorders, Alzheimer's and HSD10 deficiency, but the pathogenetic basis has so far remained elusive. This study should contribute to understand the role of HSD10 for cellular integrity and also help to find the underlying cause for the clinical picture observed in HSD10 deficiency patients by characterising the different mutations.

Several lines of evidence suggest that HSD10 has other functions in addition to the known enzymatic dehydrogenase activity.

1. The clinical symptoms in HSD10 deficiency patients are not correlated with residual enzymatic dehydrogenase activity of mutated HSD10 and experiments in *Xenopus* embryos revealed that dehydrogenase activity of HSD10 was not required for cell survival (Rauschenberger et al, 2010).
2. The symptoms observed in HSD10 deficiency patients rather resemble a mitochondriopathy (Finsterer, 2004) than an organic aciduria and are likely related to defects in general mitochondrial function.
3. Recently it was demonstrated that HSD10 is a component of the human mitochondrial RNaseP which is essential for the processing of mitochondrial tRNAs.

The aim of this work is to investigate the role of wildtype and mutated HSD10 in mitochondria under physiological and stress conditions. In order to elucidate the components and mechanisms that link HSD10 to mitochondrial function proteins which interact physically and functionally with HSD10 will be identified.

Furthermore it will be tested whether impaired RNAseP function can be detected in patients carrying mutations in the HSD17B10 gene.

Taken together, these experiments are designed to help to characterise the so far unknown non-dehydrogenase function that HSD10 obviously has in the maintenance of cellular integrity and that is impaired in HSD10 deficiency and maybe in other neurodegenerative diseases.

4 RESULTS

4.1. Localisation and amount of HSD10 in human cells under various conditions

To ensure that the phenotype observed in HSD10 deficiency patients is not simply due to mis-direction of intracellular protein transport or impaired mitochondrial localisation of mutated HSD10, patient fibroblasts and HEK293 cells were used to show the intracellular localisation under physiological and cellular stress conditions. Furthermore, the amount of mitochondria and HSD10 protein and mRNA in patient fibroblasts was determined to exclude differences in protein level or mitochondrial content as a cause for the observed disease phenotype.

4.1.1. Mitochondrial localisation of HSD10 in HSD10 deficiency patient fibroblasts

HSD10 contains a mitochondrial targeting signal at its N-terminus (He et al, 2001) and was shown to be localised in mitochondria in human cells (Yan et al, 1999) and *Xenopus*. *Drosophila* HSD10 has some differences in the N-terminal sequence and possibly therefore shows a cytosolic localisation pattern (Torroja et al, 1998). To investigate if the mutations interfere with the normal localisation pattern, HSD10 of patient fibroblasts was co-stained together with the mitochondrial marker porin (fig. 10).

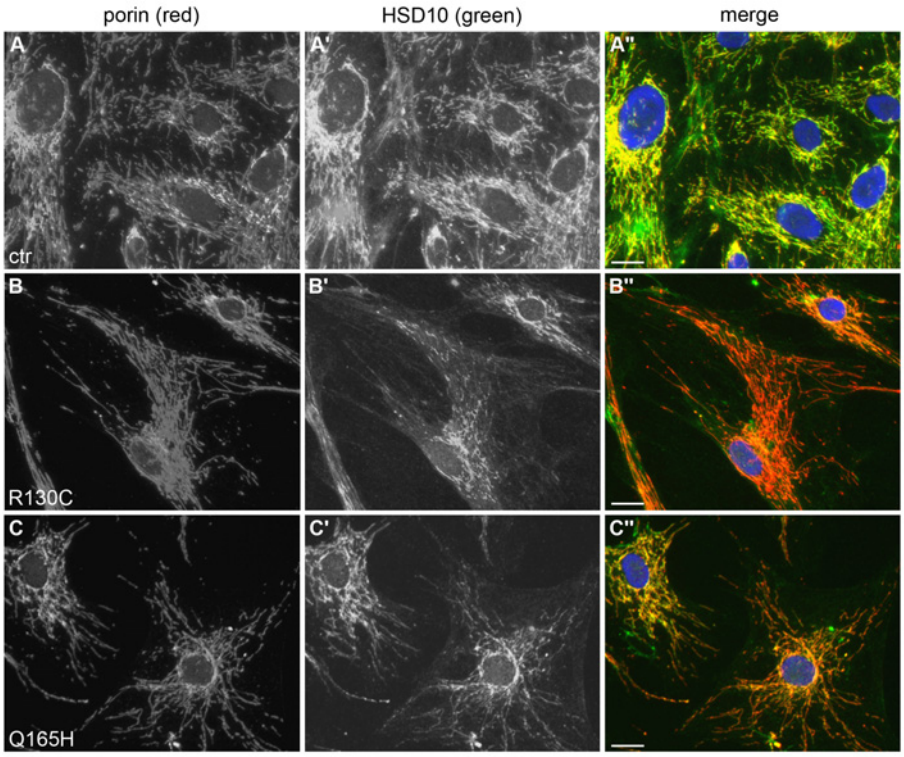

Figure 10 Localisation of HSD10 in HSD10 deficiency patient fibroblasts. Fibroblasts were cultivated on chamber slides and proteins were detected using mouse monoclonal anti-HSD10 antibody (1:100) and rabbit polyclonal anti-porin (1:500). After incubation with secondary antibodies (anti-mouse Alexa 488, 1:500, and anti-rabbit Alexa 594, 1:1000) the cells were counterstained with DAPI nuclear stain and mounted in Fluorescence Mounting Media. Scale bars: 10 µm. **(A-C)** Mitochondrial porin staining in control cells, R130C and Q165H. **(A'-C')** HSD10 staining in control cells, R130C and Q165H and merged images of both stainings **(A''-C'')**.

Mitochondria form a dynamic reticular network throughout the cell which is regulated by frequent fission and fusion events (Okamoto & Shaw, 2005). The fluorescent signal of HSD10 and porin appears as a fibrous network within the cytosol (fig. 10; A-C and A'-C'). Merged images show clear co-localisation of the mitochondrial marker porin and HSD10 in wildtype and mutant fibroblasts (fig. 10; A''-C''). A small fraction of HSD10 might not be mitochondrially localised but distributed in the cytosol. All proteins show a similar cellular distribution pattern. Since the fluorescent signal is captured under comparable conditions for each sample a semi-quantitative conclusion can be drawn about the abundance of mitochondria and HSD10 in patient fibroblasts. The amount and structure of the mitochondrial network does not seem to be altered in mutant fibroblasts in comparison to wildtype. In contrast, the level of HSD10 is reduced in fibroblasts carrying the Q165H mutation and significantly reduced in R130C fibroblasts, respectively. This finding is in agreement with the aforementioned instability of the R130C mutation, but the Q165H mutation has been shown to be stable (fig. 4).

Wildtype and mutant HSD10 is localised mitochondrially with the possibility of a small cytosolic contingent. This semi-quantitative approach suggests, that the mitochondrial content and its structure are unchanged in patient fibroblasts and that the protein level in R130C fibroblasts is reduced.

Unfortunately, fibroblasts carrying the D86G mutation are not available for cell culture based studies since they are viable but grew very slowly. Due to this slow growth rate they were only used for a few experiments like immune fluorescence staining and electron microscopy. While investigating the cellular morphology of patient fibroblasts, some differences in nuclear morphology of fibroblasts carrying the D86G mutation became apparent compared to control cells.

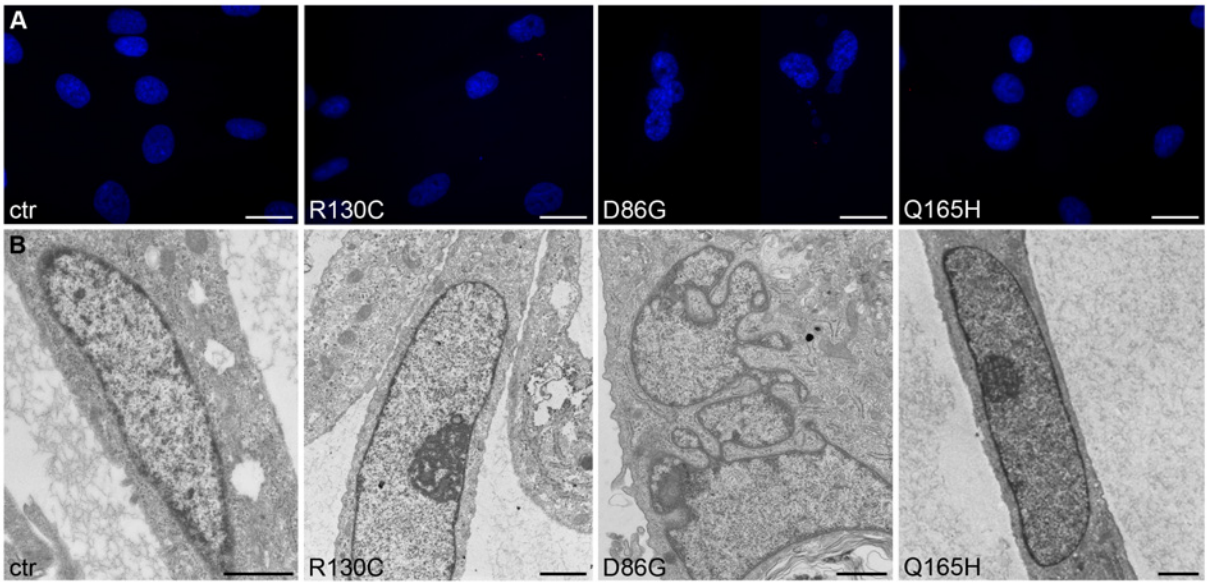

Figure 11 Cell morphology of patient fibroblasts. (A) Fluorescent nuclear staining of patient fibroblasts using 0.8 µg Hoechst nuclear stain per ml medium. Scale bars: 20 µm. **(B)** Fibroblasts were sectioned for electron microscopy. Scale bars: 1 µm.

A nuclear staining with Hoechst revealed regular and round nuclei in control cells and in fibroblasts with the R130C and Q165H mutation (fig. 11A). In contrast, fibroblasts carrying the D86G mutation display multiple nuclei per cell or strongly fragmented nuclei. Electron microscopic pictures affirmed this observation by showing fragmented and constricted nuclei with the D86G mutation and a regular elongated nuclear shape in control cells and the R130C and Q165H mutation (fig. 11B). The slow growth rate and multiple nuclei per cell suggest that the D86G mutation causes defects in cell division. Additionally, the observed fragmentation of nuclei could be a sign for nuclear fragmentation during apoptosis.

4.1.2. Mitochondrial and HSD10 content in HSD10 deficiency patient fibroblasts

To further investigate the semi-quantitative conclusions from the co-immunostainings using antibodies against HSD10 and porin (fig. 10) and to quantitatively exclude differences in protein amount or a reduction of mitochondrial content as a cause for the observed disease phenotype, the relative amount of two mitochondrial markers and of HSD10 was measured in patient fibroblasts. mRNA and protein levels of TOMM20 (translocase of outer mitochondrial membrane 20) and Grp75 (75 kD glucose regulated protein also known as mortalin) were determined. Those two proteins served as mitochondrial marker at which the former is a transporter protein of the outer mitochondrial membrane and the latter is a heat shock protein located in the mitochondrial matrix. Together they were used to determine the amount of mitochondria on the basis of TOMM20 mRNA (fig. 12A) and Grp75 protein levels (fig. 12B) in mutant fibroblasts relative to control cells. Additionally, HSD10 mRNA and protein levels were measured in comparison to control fibroblasts.

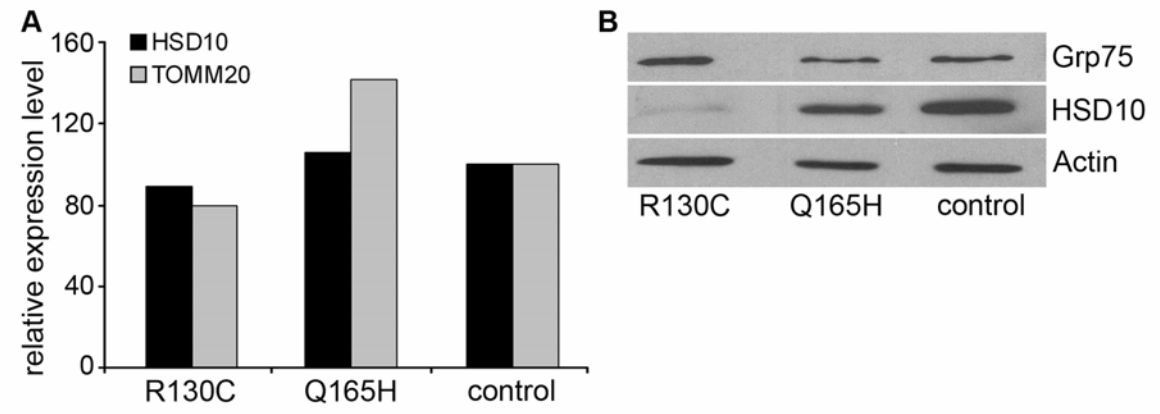

Figure 12 Content of mitochondrial material and HSD10 in fibroblasts from HSD10 deficiency patients. (A) Total RNA isolated from fibroblasts was transcribed into cDNA and subjected to qRT-PCR with primers for HSD10 and TOMM20. qRT-PCR was normalised against GAPDH and relative expression levels were calculated using a standard curve. **(B)** For detection of HSD10 and Grp75 protein levels cells were lysed and analysed by SDS-PAGE and Western Blot using anti-Grp75 (1:5000), anti-HSD10 (1:500) and anti-β actin (1:5000) antibodies.

Comparison of the relative expression levels of HSD10 mRNA in patient fibroblasts shows that the amount of HSD10 transcripts is almost equal in the cells analysed (fig. 12A). In agreement with the finding that the R130C mutation is unstable, and in line with the immunostaining of R130C fibroblasts (fig. 10), less HSD10 protein can be detected in fibroblasts carrying this mutation (fig. 12B). The amount of HSD10 in fibroblasts carrying the Q165H mutation also seems to be slightly reduced compared to control cells although this mutation does not alter the stability of the protein (fig. 4). Again this is consistent with the semi-quantitative finding of the immunostaining of Q165H fibroblasts. The content of mitochondrial material is not significantly reduced in patient fibroblasts judged by the amount of mitochondrial marker Grp75 protein (fig. 12B) and TOMM20 mRNA (fig. 12A).

Wildtype and mutant HSD10 mRNA is almost equal in patient and control fibroblasts but HSD10 protein is significantly decreased in R130C and slightly decreased in Q165H cells. Mitochondrial material is not reduced in patients.

4.1.3. HSD10 translocates from the mitochondrial matrix to the membrane under oxidative stress

The localisation of HSD10 is dependent on cellular stress and a protective function for HSD10 in cells under oxidative stress has been postulated (Tieu et al, 2004). To investigate the exact intracellular localisation of HSD10 under physiological or stress conditions cells were treated with rotenone or left untreated. Rotenone is a chemical that induces oxidative stress by interfering with the electron transport chain in mitochondria. Specifically, it inhibits the transfer of electrons from iron-sulfur centres in complex I to ubiquinone and thereby prevents the formation of ATP.

Mitochondria were isolated from untreated cells or cells stressed with rotenone and the membrane fraction was analysed separated from the matrix as to their content of HSD10 protein in comparison to a reference protein (Grp75) that is localised in the mitochondrial matrix and does not change its distribution upon stress (fig. 13). The analysis of the behaviour of HSD10 under stress was thought to help and characterise or even reveal differences between mutant proteins.

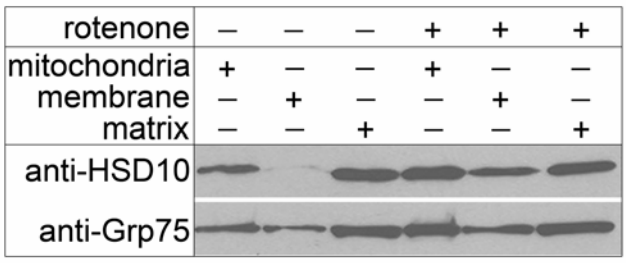

Figure 13 Translocation of HSD10 from the mitochondrial matrix to the membrane under oxidative stress. HEK293 cells were treated with 50 µM rotenone overnight or were left untreated. Mitochondria were isolated and separated into membrane and matrix fractions which were subsequently analysed by SDS-PAGE and Western Blot using anti-Grp75 (1:1000) and anti-HSD10 (1:500) antibodies.

A small amount of Grp75 can be found in the isolated membrane fraction although Grp75 is localised in the mitochondrial matrix and does not change its position under stress. This is probably due to incomplete separation of the two compartments by this kind of differential centrifugation. However, in unstressed cells HSD10 can only be detected in the mitochondrial matrix fraction (fig. 13). In contrast to the localisation in the mitochondrial matrix under these physiological conditions, HSD10 shifts to the membrane under oxidative stress induced by rotenone treatment.

It had been planned to use this experimental procedure for the identification of differences between wildtype and mutant HSD10 when applied to patient fibroblasts. Although mutant proteins are imported into mitochondria they could have reduced ability to translocate to the membrane under stress. Unfortunately, it was not possible to carry out this kind of subcellular fractionation using mutant fibroblasts due to technical problems.

To analyse this in greater detail including the localisation of mutant proteins an immunogold staining of electron microscopy sections would be useful but unfortunately the commercially available antibody against HSD10 did not detect its antigen on these sections.

Hence, this experiment merely confirmed the previously published result that under physiological conditions wildtype HSD10 is localised in the matrix and translocates to the mitochondrial membrane under oxidative stress (Tieu et al, 2004).

4.2. Mitochondrial morphology and function after HSD10 loss-of-function

Since HSD10 is located in the mitochondrial matrix and patients with HSD10 deficiency show signs of mitochondrial dysfunction such as elevated lactate concentrations, the mitochondrial morphology was analysed by Mitotracker staining and electron microscopy in fibroblasts derived from patients. Furthermore, mitochondria in a knock-down and knock-out situation were investigated in the *Xenopus* and mouse animal model, respectively.

4.2.1. Mutations D86G and R130C cause severe disruption of mitochondrial morphology

In order to investigate the impact of mutant HSD10 on mitochondria, mitochondria of fibroblasts derived from HSD10 deficiency patients were visualised by Mitotracker staining (fig. 14A) and subsequently analysed by electron microscopy (fig. 14B).

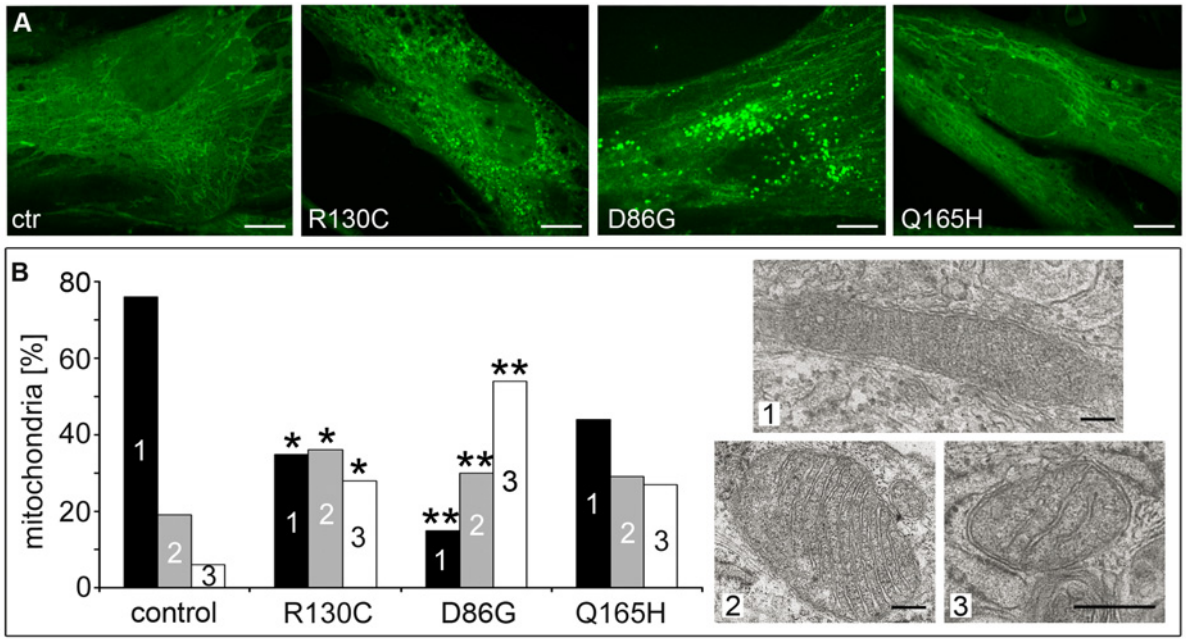

Figure 14 Mitochondrial morphology in patient fibroblasts. (A) 300 nM Mitotracker Green FM were used on cells fixed with 3.7 % formaldehyde on coverslips and mitochondria were visualised by fluorescent microscopy. Scale bars: 10 µm. **(B)** Fibroblasts were sectioned for electron microscopy. Pictures of 10-43 random systematically chosen visual fields were taken in a magnification of 11.5×10^3, scale bars: 100 nm. Mitochondria were classified into 3 groups (1 – dense, dark; 2 – loosely packed; 3 – depleted cristae). Counted visual fields were 22 (control), 11 (R130C), 43 (D86G) and 10 (Q165H) and total numbers of evaluated mitochondria were 281 (control), 203 (R130C), 1,017 (D86G) and 86 (Q165H). ** indicates significance at $p < 0.0001$, * gives significance at $p = 0.0366$ - 0.0857 adjusted for multiple comparisons within the experiment compared to control fibroblasts.

Although the mitochondrial network stained with porin antibody was not altered in fibroblasts with mutated HSD10 compared to control cells (fig. 10) the Mitotracker staining revealed differences in the mitochondrial organisation of mutant fibroblasts (fig. 14). Wildtype cells and fibroblasts carrying the Q165H mutation comprise a filamentous network-like structure of mitochondria. Cells with the R130C and D86G mutations show punctate and fragmented mitochondrial organisation (fig. 14A).

Mitochondria consist of an outer membrane and an inner membrane which folds into membrane staples, so-called cristae. Electron microscopy showed that the majority of mitochondria in control cells have wildtype morphology with dark mitochondria densely packed with cristae (fig. 14B). Fibroblasts carrying the Q165H mutation maintain wildtype morphology of almost half of the mitochondria, 30 % display an intermediate phenotype with loosely packed and/or swollen cristae and 27 % show depletion of cristae and appear "empty". In contrast, in cells carrying the D86G and R130C mutation 65-85 % of the mitochondria display an aberrant phenotype (group 2 and 3). Mitochondria classified as group 3 are not only morphologically distinct but on average also smaller than wildtype mitochondria.

These findings show that mutations D86G and R130C cause severe disruption of mitochondrial morphology.

4.2.2. Mitochondrial disintegration after conditional HSD17B10 knock-out in mice

Since a knock-out of HSD17B10 in mice results in early embryonic lethality at gastrula stages (B. Arnold, unpublished data), a conditional HSD17B10 knock-out mouse line was established. HSD17B10 was eliminated in noradrenergic neurons by mating mice carrying a floxed allele of HSD17B10 with a DBH-Cre line. This conditional knock-out eliminates HSD10 in noradrenergic neurons of the CNS (central nervous system) as well as the PNS (peripheral nervous system). Noradrenergic neurons in the CNS are for example located in the LC (locus coeruleus) and in the PNS in the SCG (superior cervical ganglia) and the inferior cervical ganglia (stellate ganglia).

The LC is part of the reticular formation in the hindbrain which is probably responsible for the control of orientation and attention. It is also involved in mediation of many of the sympathetic effects during stress responses by increasing noradrenaline secretion which in turn alters cognitive function, increases motivation and inhibits the parasympathetic tone.

The SCG (superior cervical ganglia) lie posterior to the internal carotid artery, opposite of the second and third cervical vertebrae. They contain neurons that play a role in the sympathetic innervation to the face. Stellate ganglia are found at the level of the seventh cervical vertebrae, anterior to the neck of the first rib. They arise from a fusion of the inferior cervical and the first thoracic ganglia. Stellate ganglia are sympathetic ganglia that render the inferior cardiac nerve, and offsets to blood vessels.

To analyse the morphology of mitochondria in a HSD10 knock-out situation brains from DBH-Cre conditional knock-out mice were cut in Vibratome sections to pinpoint the small region of the LC which is more pigmented than the surrounding tissue (fig. 15A). Its light blue colour is due to melanin enclosed in the noradrenergic nerve cell bodies. The LC is located in the brain stem in the lateral floor of the fourth ventricle in the dorsal wall of the rostral pons. This region was then sectioned for electron microscopy and evaluated by means of mitochondrial morphology (fig. 15B and C).

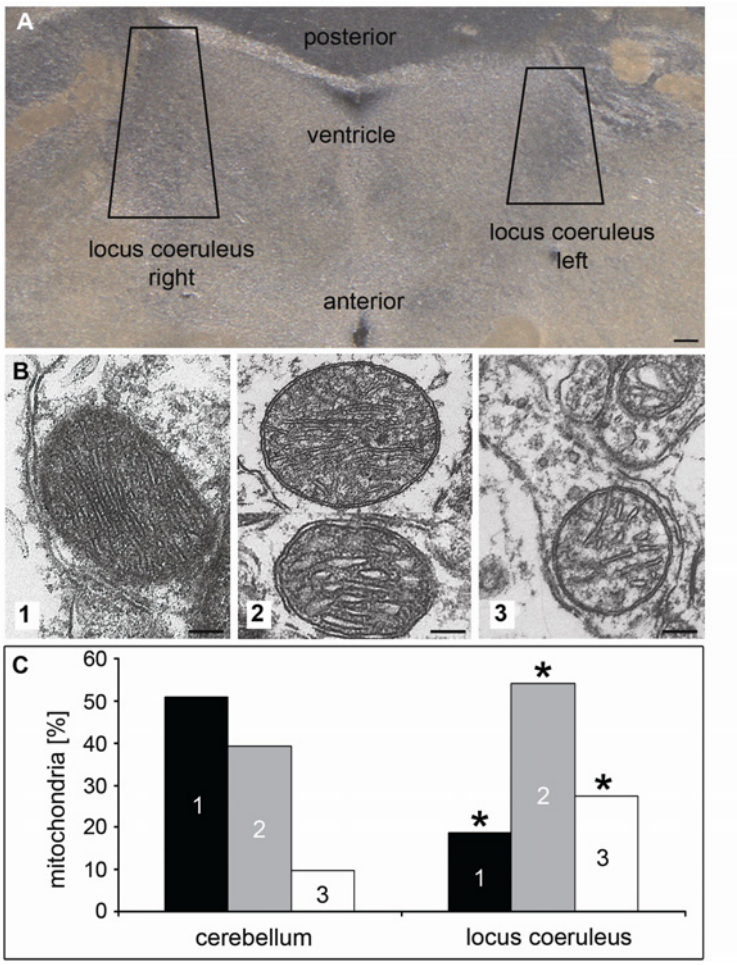

Figure 15 Mitochondrial morphology in brains of mice with a conditional knock-out in noradrenergic neurons (DBH-Cre). (A) Brains from knock-out mice were Vibratome sectioned (50 µm) and the loci coerulei were dissected and prepared for electron microscopy. Scale bar: 100 µm. **(B)** Pictures of 33 random systematically chosen visual fields were taken in a magnification of 11.5×10^3, scale bars: 100 nm. Mitochondria were classified into 3 groups (1 – dense, dark; 2 – loosely packed/swollen cristae; 3 – depleted cristae). The total number of evaluated mitochondria was 10,167 (cerebellum) and 2,446 (locus coeruleus). **(C)** Classified mitochondria in percent. Sections of the cerebellum, which lacks noradrenergic neurons, served as a control. * indicates significance ($p < 0.0001$) of differences to the cerebellum.

In the loci coerulei of DBH-Cre HSD10 deficient mice, almost 30 % of the mitochondria show depletion of cristae and appear "empty", more than 50 % of the mitochondria are loosely packed and have swollen cristae, while normal morphology (dense, dark) is only found in 20 % (fig. 15C). In the cerebellum of the same mice, which lack noradrenergic

neurons, 50 % of the mitochondria have wildtype morphology, 40 % display the intermediate phenotype and only 10 % appear "empty" and without cristae.

To analyse the morphology of the mitochondria in a HSD10 knock-out situation in the PNS, ganglia from these HSD17B10 DBH-Cre conditional knock-out mice were isolated.

SCG and stellate ganglia were isolated, cryosectioned and sectioned for electron microscopy to analyse the ganglia tissue as well as the mitochondria morphologically after HSD10 knock-out (fig. 16).

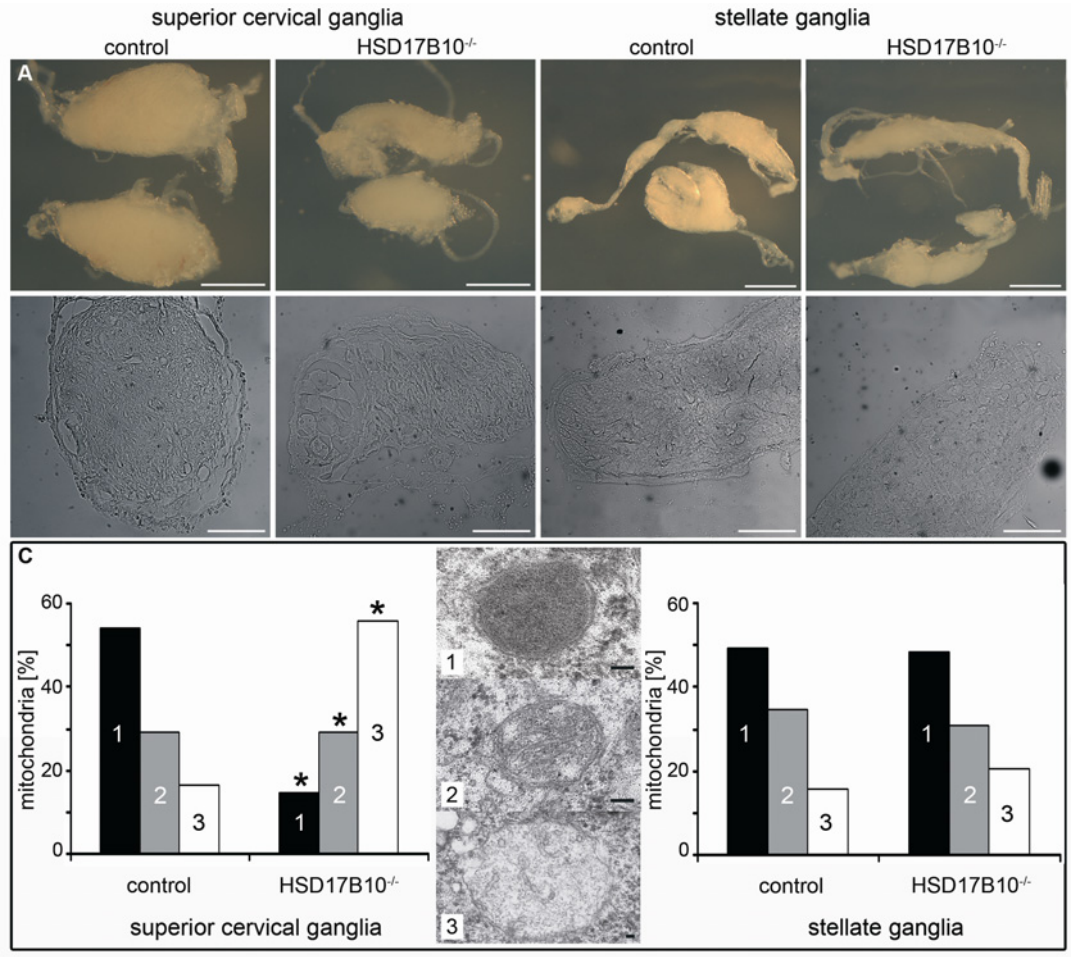

Figure 16 Morphology of ganglia derived from mice with a conditional knock-out in noradrenergic neurons (DBH-Cre). (A) Isolated ganglia, scale bars: 500 µm. **(B)** Cryosectioned ganglia. Sections are 15 µm, scale bars: 150 µm. **(C)** Pictures of 4 to 13 random systematically chosen visual fields were taken in a magnification of 11.5×10^3, scale bars: 100 nm. Mitochondria were classified into 3 groups (1 – dense, dark; 2 – loosely packed/swollen cristae; 3 – depleted cristae). The total number of evaluated mitochondria was 840 (SCG control), 335 (SCG HSD10$^{-/-}$) and 196 (stellate ganglia control) and 666 (stellate ganglia HSD10$^{-/-}$), respectively. * indicates significance ($p < 0.0001$) of differences to control ganglia.

Ganglia from knock-out mice are already distinguishable by eye right after isolation because they are smaller and look porose compared to control ganglia (fig. 16A). Also

when cryosectioned the morphological differences are obvious at least in the SCG of HSD17B10$^{-/-}$ mice. Those ganglia exhibit large fissures within the tissue (fig. 16B).

A similar picture of mitochondrial morphology as in the CNS (fig. 15) is observed in the PNS (peripheral nervous system) in SCG but not in stellate ganglia. Mitochondria are morphologically severely altered in superior cervical ganglia isolated from DBH-Cre conditional knock-out mice (fig. 16C). More than 85 % of mitochondria show an aberrant phenotype (group 2 and 3), while normal morphology (dense, dark) is only found in 15 %. In addition, mitochondria of the groups 2 and 3 are significantly larger than wildtype mitochondria, whereas the aberrant phenotype in patient fibroblasts is accompanied by a smaller size of these mitochondria. This effect of a HSD10 knock-out on mitochondrial morphology cannot be observed in stellate ganglia. In these ganglia almost 50 % of the mitochondria have wildtype morphology, around 30 % display the intermediate phenotype and only 15-20 % appear "empty" and without cristae in both the control animals and mice with the DBH-Cre conditional knock-out.

In general, cells that show this altered mitochondrial morphology also exhibit nuclei and nuclear budding containing large amounts of condensed chromatin which suggests that these cells are apoptotic.

The EM analysis of two independent primary cell types (neurons of the CNS and PNS) from HSD17B10 DBH-Cre conditional knock-out mice thus confirmed in a genetic system that HSD10 is required for mitochondrial structural integrity in the CNS and the PNS. The same morphological changes in mitochondria are observed in fibroblasts from patients and in neurons from conditional knock-out mice indicating that they are cell type independent.

4.2.3. HSD10 knock-down in Xenopus impairs mitochondrial integrity

In order to study the effect of HSD10 loss-of-function on mitochondrial morphology in early vertebrate embryos *Xenopus* was used as an experimental model. In *Xenopus* embryos, translation of mRNAs can be specifically blocked by Mo (Morpholino) antisense oligonucleotides. MoHSD10^{ATG} targets the coding region of HSD10 and specifically suppresses HSD10 translation in *Xenopus* embryos (Rauschenberger et al, 2010).

Antisense MoHSD10^{ATG} was microinjected into the prospective ectoderm and the injected region (animal cap) was explanted and cultured. Explanted animal caps differentiate into a homogeneous tissue, the so-called atypical epidermis. After 2 days in culture, when control embryos had reached tailbud stage, the animal caps were sectioned for electron microscopy.

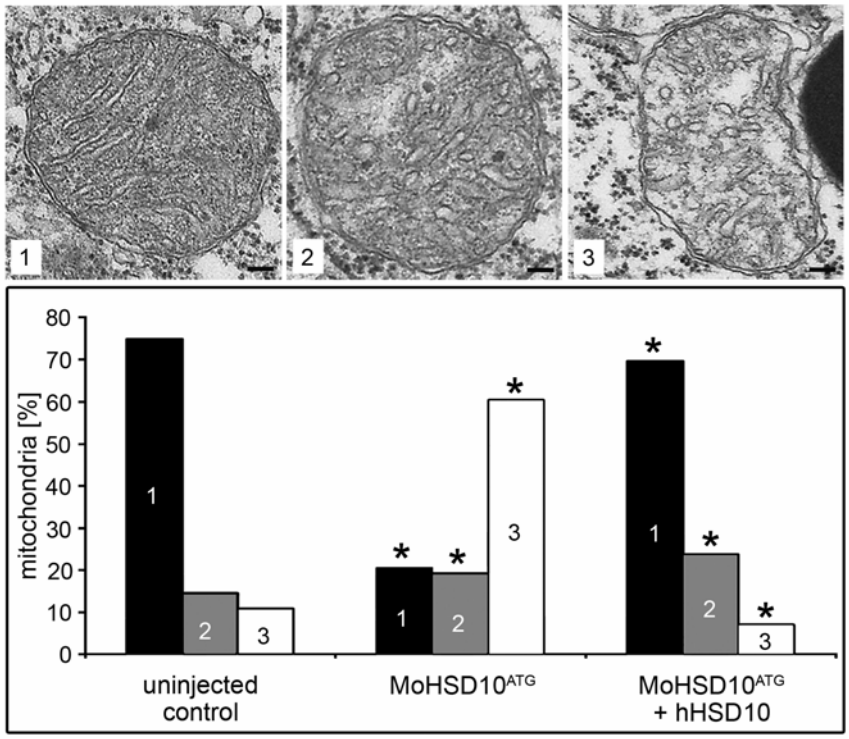

Figure 17 Mitochondrial morphology in *Xenopus* animal caps after knock-down of HSD10. Animal caps were dissected from *Xenopus* embryos injected with 20 ng MoHSD10^{ATG} alone or 20 ng MoHSD10^{ATG} together with 150 pg hHSD10 (pT-Rex-DEST30) and sectioned for electron microscopy. Pictures of 24 random systematically chosen visual fields were taken in a magnification of 6.6×10^3, scale bars: 100 nm. Mitochondria were classified into 3 groups (1 – dense, dark; 2 – loosely packed; 3 – depleted cristae). * indicates significance at $p < 0.0001$ compared to uninjected control animal caps. Total numbers of evaluated mitochondria per sample were 1,193 (control), 653 (MoHSD10^{ATG}) and 945 (MoHSD10^{ATG}+hHSD10).

Electron microscopic analysis revealed that the morphology of mitochondria in animal cap explants is changed after HSD10 knock-down (fig. 17). 80 % of mitochondria show a severe reduction of cristae and a generally irregular shape (group 2 and 3). This phenotype is rarely observed in uninjected samples (25 %) or in tissue in which the MoHSD10^{ATG} is injected together with a human HSD10 expression construct (30 %).

This experiment demonstrates by loss-of-function analysis that HSD10 is required for structural integrity of mitochondria in early vertebrate embryos.

Having shown by loss-of-function analysis that HSD10 is required for structural integrity of mitochondria in various systems, the next question was whether HSD10 knock-down also impaired mitochondrial function. Antisense MoHSD10^{ATG} was microinjected into the prospective ectoderm and the injected region (animal cap) was explanted and cultured. After 2 days in culture, when control embryos had reached tailbud stage, pyruvate turnover was measured as a parameter of mitochondrial function.

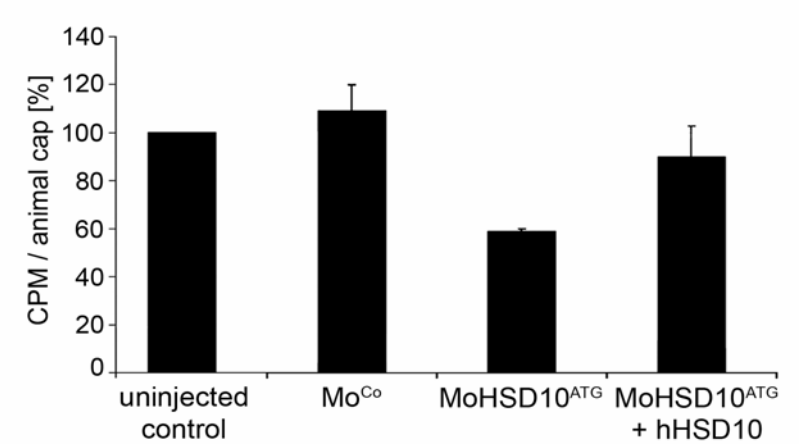

Figure 18 Mitochondrial function in *Xenopus* animal caps after knock-down of HSD10. Animal caps were dissected from *Xenopus* embryos injected with 20 ng control Mo^{Co} or $MoHSD10^{ATG}$ alone or 20 ng $MoHSD10^{ATG}$ together with 150 pg hHSD10 (pT-Rex-DEST30) and the turnover of 1-C14 pyruvate was measured. CPM (Counts per minute) are shown in relation to uninjected control (100 %) and the standard error for two independent experiments is given.

$MoHSD10^{ATG}$-injected samples display a 40 % reduction in pyruvate turnover compared to the uninjected or Mo^{Co} injected tissue (fig. 18). Impaired mitochondrial function is specific because co-injection of a human HSD10 expression construct which is not targeted by the $MoHSD10^{ATG}$ rescues pyruvate turnover almost to the level of uninjected controls.

This loss-of-function analysis shows that HSD10 is required for functional integrity of mitochondria.

4.3. Induction of apoptosis after HSD10 gain- and loss-of-function

It has been shown previously that HSD10 loss-of-function elicits an increase in apoptosis (Rauschenberger et al, 2010). TUNEL staining of *Xenopus* embryos which received the MoHSD10^{ATG} only into the right side of the body showed enhanced apoptosis on the injected side. Induction of apoptosis after siRNA-mediated knock-down of HSD10 was confirmed in human SHSY5Y cells and also in dendritic cells from mice with a conditional knock-out in endothelial cells and haematopoietic stem cells (Tie2-Cre).

The increase in apoptosis rate in *Xenopus* embryos caused by HSD10 knock-down can be rescued by human HSD10 wildtype. The mutated HSD10 proteins found in human patients, however, show remarkable differences in their ability to rescue the apoptotic phenotype. The Q165H mutation, which has less than 3 % residual enzymatic activity but was identified in three neurologically normal boys, partially rescued MoHSD10^{ATG}-induced apoptosis. In contrast, the mutations R130C and in particular D86G failed to rescue, and instead further enhanced apoptosis. Both mutations have considerable residual enzyme activity despite being associated with a very severe clinical phenotype.

These experiments demonstrated that loss of HSD10 results in induction of apoptosis independent of the cell type and organism. The rescue experiments furthermore showed that apoptosis after HSD10 loss-of-function is not dependent on the enzymatic dehydrogenase activity of HSD10, arguing for a non-enzymatic function of this protein which is required in mitochondria.

4.3.1. HSD10 gain-of-function in Xenopus induces apoptosis

Since co-injection of the R130C and D86G mutation together with MoHSD10^{ATG} into *Xenopus* embryos enhanced the induction of apoptosis even further than the knock-down of HSD10 alone, the effect of these mutations on the apoptosis rate was investigated (fig. 19). Expression plasmids carrying the three different mutations were microinjected into the right body half of *Xenopus* embryos. After two days (stage NF 33/34) these embryos were TUNEL stained and scored for apoptosis on each body half (fig. 19A). The left side was used as an internal control and the amount of apoptotic spots on the right (injected) side was normalised against the left (uninjected) control side (fig. 19B).

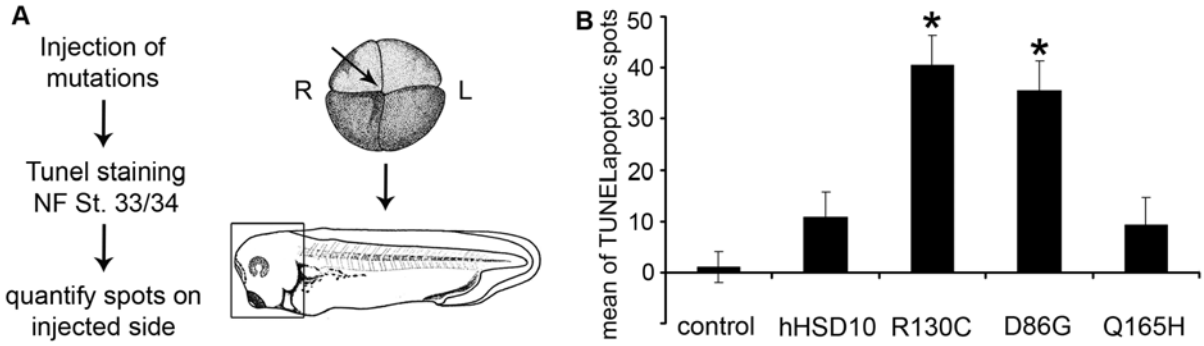

Figure 19 Quantitative analysis of the effect of wildtype and mutant HSD10 on the apoptosis rate. (A) Experimental scheme. Embryos were injected with 150 pg DNA in 5 nl (pT-Rex-DEST30 containing cDNA coding for HSD10 WT or the mutations R130C, D86G, Q165H). **(B)** Quantification of TUNEL staining on the right (injected) side of tailbud stage embryos (stage NF 33/34) normalised against the left (control) side. The standard error for 3 individual experiments (n = 42–51 embryos) is shown. Significant differences between control and injected embryos were calculated using the student t-test. * indicates significance at $p \leq 0.0001$.

Embryos injected with human wildtype HSD10 show a mild increase in apoptosis on the injected side (fig. 19B). In contrast, when injected with the mutations R130C and D86G, induction of apoptosis is very much enhanced compared to the uninjected internal control side. Overexpression of the Q165H mutation does not result in such a severe increase but only in a mild induction of apoptosis comparable to the effect of human wildtype HSD10.

This gain-of-function experiment shows that not only the loss-of-function of HSD10 but also the overexpression leads to a mild induction of apoptosis. The two severe mutations R130C and D86G strongly induce apoptosis and seem to have a dominant-negative effect on the initiation of apoptosis.

4.3.2. Apoptosis induced by HSD10 gain-of-function is not due to the unfolded protein response

The ER (endoplasmic reticulum) orchestrates the synthesis and processing of nearly all proteins in eukaryotic cells. Soluble and membrane proteins are delivered to the ER as linear polypeptides that acquire their secondary structure and posttranslational modifications in the ER lumen. Overexpression or mutation of proteins can induce accumulation of unfolded or misfolded proteins which causes ER stress and initiates the UPR (unfolded protein response). Mitochondria can also activate a UPR. UPR coordinates the interplay of processing and degrading unfolded proteins and activates both adaptive and apoptotic pathways.

To check if the apparent dominant-negative effect of the R130C and D86G mutations on induction of apoptosis is due to their overexpression and accumulation in the ER and a subsequent activation of the UPR eventually leading to apoptosis, the upregulation of one mediator of the UPR, CHOP, was determined (fig. 20). CHOP (C/EBP homologous protein,

also known as growth arrest- and DNA damage-inducible gene 153, GADD153) is a transcription factor that is upregulated in the UPR of ER and mitochondria.

Expression constructs coding for HSD10 wildtype or the three different mutations were microinjected into the prospective ectoderm and the injected region (animal cap) was explanted and cultured. When control embryos had reached stage NF 31 positive control animal caps were treated with TM (tunicamycin). TM is a mixture of homologous nucleoside antibiotics that inhibits the enzyme GPT (GlcNAc phosphotransferase), which catalyses the first step of glycoprotein synthesis. By blocking the synthesis of all N-linked glycoproteins tunicamycin induces the UPR in the ER and is used as a positive control for CHOP upregulation. After two days in culture (stage NF 33/34) animal caps were used to measure CHOP levels as an indicator for UPR after overexpression of mutant and wildtype HSD10.

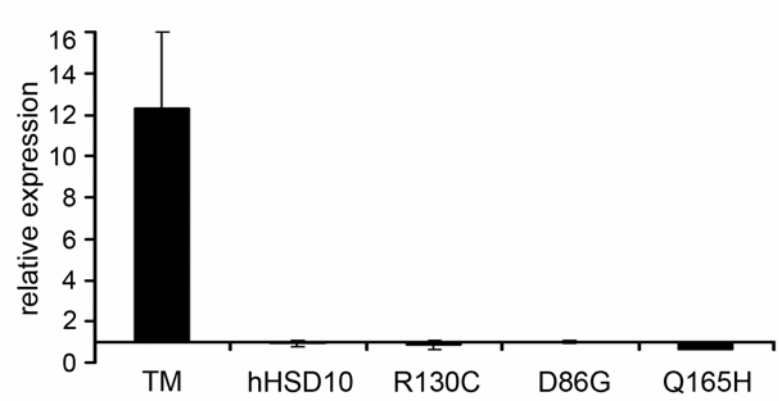

Figure 20 Upregulation of CHOP after overexpression of HSD10 wildtype and mutations. *Xenopus* embryos were injected with 5 nl in each blastomere at the 4-cell-stage containing 150 pg DNA (pT-Rex-DEST30 HSD10 WT or the mutations R130C, D86G, Q165H) and animal caps were dissected. Animal caps treated with 2.5 µg/ml TM (tunicamycin) from stage NF 31 were used as a positive control. Total RNA was isolated at stage NF 33/34 and transcribed into cDNA which was then subjected to qRT-PCR with primers for CHOP and ODC (Ornithine decarboxylase). qRT-PCR was normalised against ODC and relative expression levels compared to uninjected and untreated animal caps were calculated using a standard curve. The standard error for two independent experiments is given.

Neither the overexpression of HSD10 wildtype nor the three mutations cause an upregulation of CHOP (fig. 20). Only tunicamycin treated *Xenopus* embryos show an upregulation of CHOP mRNA.

Therefore, the UPR of the ER or mitochondria is not induced by overexpression of HSD10 wildtype or mutations in *Xenopus* embryos and thus is not the elicitor of apoptosis after HSD10 injection.

4.3.3. Analysis of the apoptotic pathway induced by HSD10 loss-of-function

Apoptosis is controlled by many different signals. These signals can either originate extracellularly as extrinsic inducers like hormones or the lack of growth factors or they can arise intracellularly triggered by intrinsic factors like stress, increased calcium levels or DNA damage. Extrinsic and intrinsic inducers can act pro- or anti-apoptotic. Despite of their diverse origin these signals eventually activate a common cell death machinery. For example, both, extrinsically activated procaspase-8 and intrinsically activated procaspase-9 proteolytically cleave and thereby set off the executioner procaspase-3.

The Human Apoptosis PCR Array by RealTimePrimers.com is a primer library that contains 88 primer sets directed against apoptosis genes. This array was used as a means to help to determine whether the mitochondrial phenotype observed upon HSD10 loss-of-function is the source or a consequence of the induction of apoptosis by profiling the changes that occur in human cells upon HSD10 knock-down (fig. 21) or mutation (fig. 22). Since both pathways include mediators that are specifically activated in the intrinsic or the extrinsic induction of apoptosis, the pattern of genes that are upregulated upon HSD10 knock-down should reveal which apoptotic pathway is initiated by HSD10 loss-of-function.

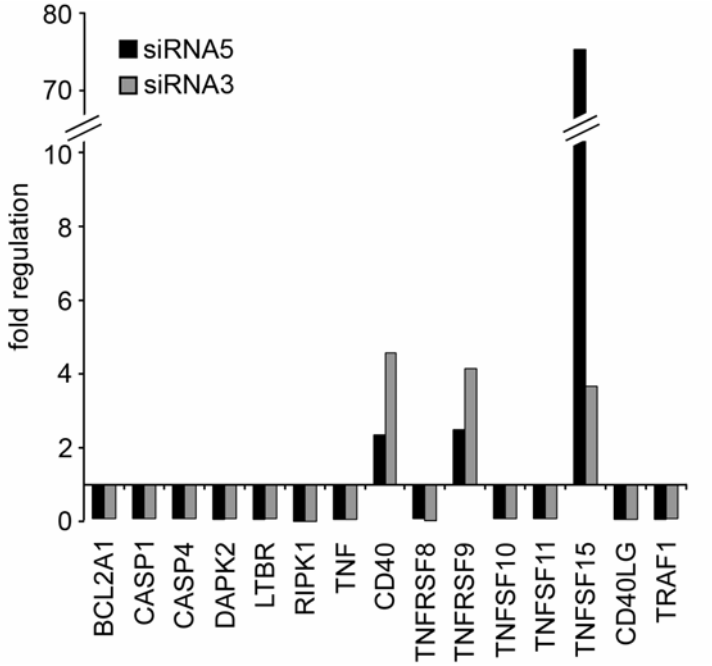

Figure 21 Apoptotic gene regulation in response to siRNA mediated HSD10 knock-down in HeLa cells. HeLa cells were treated with 20 pmol of two different siRNAs targeting HSD10, a negative control siRNA (40 pmol) and a vehicle control, respectively. Total RNA was isolated 48 h post transfection and transcribed into cDNA by M-MuLV-RT. This cDNA served as a template for the human apoptosis array primer library. Relative gene expression was determined by the ddCT method. Measured CT values were normalised against the mean of four different housekeeping genes (β-actin, β-2-microglobulin, glyceraldehyde-3-phosphate dehydrogenase and β-glucuronidase) in a first step. Since transfection reagents generally have a toxic effect on cells, the second normalisation was carried out against the vehicle control (0.5 µl Lipofectamine for each well in a 24-well-plate). Likewise, short dsRNA has been shown to influence gene expression, so the last normalisation was done against the CT values for the inert negative control siRNA. Shown in this graph are genes that are up- or downregulated more than 2-fold with both siRNAs targeting HSD10 in two independent experiments and their mean fold regulation.

Both specific siRNAs caused an efficient knock-down of HSD10 down to 22 and 31 % for siRNA3 and siRNA5, respectively, compared to control siRNA treated cells.

The CT values obtained with primers of the Human Apoptosis PCR Array for samples treated with siRNA specific for HSD10 were normalised against the mean of four different housekeeping genes, the vehicle and the negative siRNA control. Therefore, all changes that are unspecific and simply due to differences in total RNA concentration or to the transfection process should be eliminated. Also, only changes of more than 2-fold which were found in two independent experiments were taken into account.

Among the upregulated genes are two that are pro-apoptotic (TNFRSF9 and TNFSF15) and one (CD40) that is pro-apoptotic but can also be anti-apoptotic depending on the context (fig. 21). The downregulated genes comprise a mixture of pro- and anti-apoptotic genes. It has been shown that the knock-down of HSD10 causes an increase in apoptosis (Rauschenberger et al, 2010), thus the upregulation of pro-apoptotic and the downregulation of anti-apoptotic genes was expected. The opposite, the upregulation of anti- and the downregulation of pro-apoptotic genes might be a compensatory mechanism of the cells at the beginning of apoptosis.

In order to distinguish between the extrinsic and intrinsic pathway, the pattern of regulated genes upon transfection with FADD (Fas-Associated protein with Death Domain) or upon treatment with rotenone and sodium azide (NaN_3) was determined. FADD was used as a positive control because it bridges death receptors at the cell surface to caspase-8 through its death domain to form the DISC (death-inducing signalling complex) and thus extrinsically induces apoptosis.
Rotenone and NaN_3 both affect the mitochondrial respiratory chain. Rotenone induces oxidative stress by inhibiting complex I and NaN_3 inhibits complex IV by blocking the oxygen binding site in the active centre of cytochrome-c-oxidase irreversibly. Both inhibitors induce the intrinsic pathway of apoptosis and were found to cause a strong increase in BIRC3, CASP5 and TNFSF15 expression.

The pattern of genes that are regulated upon HSD10 knock-down (fig. 21) does not point to one well-defined apoptotic pathway. The upregulation of TNFSF15 might be specific for mitochondrial involvement in apoptosis, since a control treated with rotenone and NaN_3 as well as a knock-down of HSD10 strongly increased TNFSF15 expression. The transfection with FADD which triggers the extrinsic apoptosis pathway showed no upregulation of TNFSF15. However, usually the TNF superfamily is associated with the extrinsic apoptosis pathway.

Overexpression of HSD10 and especially the D86G and R130C mutation have been shown to induce apoptosis in *Xenopus* embryos (fig. 19). In order to analyse whether patient fibroblasts show a pattern of up- or downregulated genes that is characteristic for an increase in (intrinsic or extrinsic) apoptosis, the apoptosis PCR array was also used to determine up- or downregulated genes on a background where HSD10 is mutated (fig. 22).

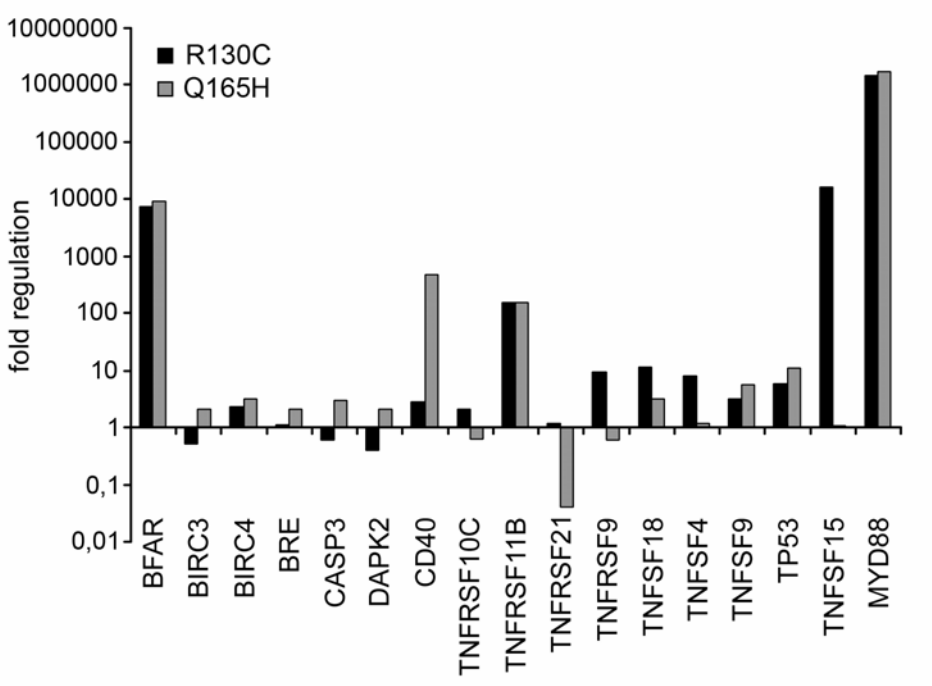

Figure 22 Apoptotic gene regulation in HSD10 deficiency patient fibroblasts. Total RNA was isolated from control fibroblasts or cells carrying the R130C or Q165H mutation, respectively. RNA was transcribed into cDNA by M-MuLV-RT and subsequently served as a template for the human apoptosis array primer library. Relative gene expression was determined by the ddCT method. Mean CT values of two experiments were normalised against the mean of four different housekeeping genes (β-actin, β-2-microglobulin, glyceraldehyde-3-phosphate dehydrogenase and β-glucuronidase) and afterwards to control fibroblasts. In this graph, genes that are up- or downregulated more than 2-fold for at least one of the tested mutations and their fold regulation in a logarithmic scale are shown.

The genes, which are up- or downregulated in patient fibroblasts in comparison to control cells, are a mixture of pro- and anti-apoptotic genes (fig. 22). Notably, half of the regulated genes and the ones that are highly changed in their expression in mutant fibroblasts are members of the TNF family. The pattern of regulated genes is not characteristic for the intrinsic or extrinsic apoptotic pathway but death receptors of the TNFR family mediate the extrinsic apoptotic pathway.

The following table (table 2) summarises the regulation of the expression of 88 apoptotic genes in response to HSD10 loss-of-function mediated by siRNA knock-down or mutation, tested with the human apoptosis PCR array.

	function in apoptosis		regulation upon HSD10 LOF					function in apoptosis		regulation upon HSD10 LOF			
GENE	pro-apoptotic	anti-apoptotic	siRNA3	siRNA5	R130C	Q165H	GENE	pro-apoptotic	anti-apoptotic	siRNA3	siRNA5	R130C	Q165H
APAF1	x		---	---	---	---	MCL1		x	---	---	---	---
ATM	x		---	↑	---	---	MYD88	x		↓	---	↑↑↑	↑↑↑
BAG1		x	---	---	---	---	CARD4	x		---	---	---	---
BAG3		x	---	---	---	---	RIPK1	x		↓↓↓	↓↓	---	---
BAG4		x	---	↑	---	---	RIPK2	x		---	---	---	---
BAK1	x		---	---	---	---	RPA3	x	x	---	---	---	---
BAX	x		↓	---	---	---	TANK	x		---	---	---	---
BCL10	x		---	---	---	---	TNF	x	x	↓	↓	---	---
BCL2		x	---	---	---	---	TNFRSF10A	x		---	---	---	---
BCL2A1		x	↓	↓	---	---	TNFRSF10B	x		---	---	---	---
BCL2L1		x	---	---	---	---	TNFRSF10C		x	---	---	↑	---
BCL2L11	x		---	---	---	---	TNFRSF10D		x	---	---	---	---
BCL2L2		x	---	---	---	---	CASP8	x		---	---	---	---
BFAR		x	---	---	↑↑	↑↑	CASP8AP2	x		---	---	---	---
BIK	x		↓	↑	---	---	CFLAR	x	x	---	---	---	---
BIRC1		x	---	---	---	---	CHEK1		x	---	---	---	---
BIRC2		x	---	---	---	---	TNFRSF11B	x	x	↓	---	↑↑	↑↑
BIRC3		x	---	---	---	↑	TNFRSF17		x	↓	---	---	---
BIRC4		x	---	---	↑	↑	TNFRSF1A	x		---	---	---	---
BIRC5		x	---	---	---	---	TNFRSF21	x		---	---	---	↓
BIRC6		x	---	↑	---	---	CD40	x		↑	↑	↑	↑↑
BNIP3		x	---	---	---	---	TNFRSF8	x		↓	↓	---	---
BRE		x	---	---	---	↑	TNFRSF9	x		↑	↑	↑	---
BOK	x		---	---	---	---	TNFSF10	x		↓	↓	---	---
CASP1	x		↓	↓	---	---	TNFSF11		x	↓	↓	---	---
CASP10	x		---	↓	---	---	TNFSF13	x		---	---	---	---
CASP4	x		↓	↓	---	---	TNFSF13B		x	---	---	---	---
CASP2		x	---	---	---	---	TNFSF15	x		↑	↑	↑↑	---
CASP3	x		---	---	---	↑	TNFSF18		x	---	↓	↑	↑
CASP5	x		---	---	---	---	TNFSF4		x	---	---	↑	---
CASP6	x		---	---	---	---	CD40LG		x	↓	↓	---	---
CASP7	x		---	---	---	---	FASLG	x		---	---	---	---
CHEK2	x		---	---	---	---	TNFSF7		x	---	---	---	---
CIDEA	x		---	---	---	---	TNFSF8	x		↓	---	---	---
CIDEB	x		---	---	---	---	TNFSF9	x	x	---	---	↑	↑
CRADD	x		---	---	---	---	TP53	x		---	---	↑	↑
DAPK1	x		---	---	---	---	TP73L	x		---	---	---	---

DAPK2	x		↓	↓	---	↑	TRAF1		x	↓	↓	---	---
DFFA		x	---	---	---	---	TRAF3	x		↓	---	---	---
DFFB	x		---	---	---	---	TRAF4		x	↓	---	---	---
FADD	x		---	---	---	---	TRAF5	x		↓	---	---	---
GADD45A	x		↑	---	---	---	TRAF6	x	x	---	---	---	---
HRK	x		---	---	---	---	TRIP	x		---	---	---	---
LTBR	x		↓	↓	---	---	DIABLO	x		---	---	---	---

Table 2 Regulation of the expression of 88 apoptotic genes in response to HSD10 loss-of-function. This table lists apoptotic genes that are up- or downregulated (↑ or ↓) or highly up- or downregulated (↑↑ or ↓↓) upon siRNA mediated knock-down of HSD10 or in fibroblasts carrying mutation R130C and Q165H, respectively.

There are several genes that are regulated upon treatment with one or both siRNAs or in response to the mutations in HSD10, but there are only three genes that are upregulated with both siRNAs and at least one mutation (highlighted in table 2). Those three genes, CD40, TNFRSF9 and TNFSF15, are regulated in both loss-of-function situations and all three have a pro-apoptotic function. Also, all three genes are members of the TNF (tumour necrosis factor) superfamily and this protein family is associated with the extrinsic pathway of apoptosis induction.

Therefore, they might be responsible for the increase in extrinsically activated apoptosis upon HSD10 knock-down or knock-out and upon overexpression of mutant HSD10.

4.4. HSD10 function and characterisation of mutations under cellular stress conditions

A protective effect of overexpressed HSD10 under conditions of oxidative stress was found in the setting of acute brain damage (Yan et al, 2000a) and in a mouse model of Parkinson disease (Tieu et al, 2004). Reduction or loss of HSD10 in *Xenopus*, mouse and humans has adverse effects on mitochondrial integrity and leads to enhanced apoptotic cell death and reduced viability (fig. 14-17; Rauschenberger et al, 2010).

Furthermore, clinical deterioration in HSD10 deficiency patients is triggered by infections or other stress situations. In response to metabolic stress, HSD10 protein translocates from the mitochondrial matrix to the inner mitochondrial membrane and this might be important for maintaining mitochondrial integrity as this is an essential site e.g. for assembly of the mitochondrial membrane permeability transition pore (Tieu et al, 2004, and fig. 13).

Thus, HSD10 may be a component serving to protect mitochondria at times of increased metabolic stress. It appears plausible that its protective effect might be disturbed by altered HSD10 protein structure due to specific mutations.

To determine whether mutated and control cells behave differently under various stress conditions and if mutated fibroblasts can still cope with stress like control cells can, cultured cells were put under various metabolic stress conditions. Metabolic stress was induced by sodium azid (NaN_3), hydrogen peroxide (H_2O_2) and heat (43°C). NaN_3 inhibits complex IV of the respiratory chain and the cells die due to an arrest of ATP production. H_2O_2 causes oxidative stress by accumulation of ROS (reactive oxygen species). Severe oxidative stress can cause cell death, since ROS alter fundamental structures of the cell like DNA, proteins and lipids. Elevated temperature turns on a more general stress response including the upregulation of heat shock proteins caused by an accumulation of denatured proteins. Heat shock proteins function as intra-cellular chaperones that e.g. assist proper protein folding and conformation.

Patient fibroblasts were exposed to these various stressors or left untreated and were subsequently scored for viability after one hour or after incubation overnight (fig. 23).

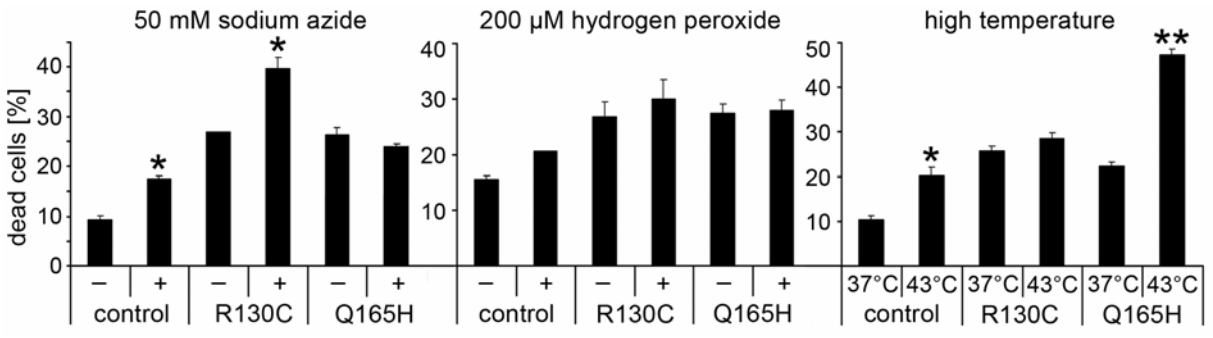

Figure 23 Sensitivity of HSD10 deficiency patient fibroblasts to different stress factors. Cultured fibroblasts were treated with 50 mM NaN_3 for 1 hour or 200 µM H_2O_2 for 1 hour or 43 °C overnight. Cell viability was then determined with trypan blue absorption and microscopic evaluation of the percentage of dead blue cells. Values represent the mean and standard error of 2, 4 or 5 biological replicates for H_2O_2, NaN_3 and heat, respectively. Significant differences between untreated cells and cells under stress were calculated using the student t-test. ** indicates significance at $p \leq 0.01$ and * denotes significance at $p = 0.0456–0.0691$ compared to the untreated control.

The applied concentration of chemicals and the appropriate temperature were titrated to a level where control cells show a small effect in cell viability. Mutated fibroblasts have a higher level of dying cells than control cells to begin with, but here the increase in non-viable cells elicited by the various stressors was monitored. Fibroblasts carrying the R130C mutation seem to be more sensitive to NaN_3 induced stress (fig. 23 left) whereas Q165H fibroblasts display an even lower reaction to this kind of stress than control cells. Likewise, Q165H fibroblasts might be less sensitive to H_2O_2 induced oxidative stress than R130C or control cells (fig. 23 middle). In contrast, fibroblasts with the Q165H mutation are more sensitive to heat induced cellular stress, whereas R130C fibroblasts display only a slight elevation comparable to control cells (fig. 23 right).

Although the alterations in mutated fibroblasts are not striking, one can conclude from this set of experiments that these cells behave differently from control cells under stress.

To investigate the effect of various stressors acting on mitochondrial components on patient fibroblasts in further detail and in a more quantifiable manner, the CellTiter-Glo® Luminescent Cell Viability Assay was used. A thermostable luciferase generates a stable "glow-type" luminescent signal proportional to the amount of ATP present, which signals the presence of metabolically active cells and thus this assay determines the number of viable cells in culture.

Cultured fibroblasts were put under various stress conditions and scored for viability with the CellTiter-Glo assay after six hours (fig. 24). A variety of inhibitors of the respiratory chain was applied to induce cellular stress (table 3). The four enzyme complexes that form the respiratory chain are partly encoded in the nucleus or in the mitochondrial genome. They are located at the inner mitochondrial membrane and transfer electrons from metabolites to oxygen through a sequence of redox reactions. This releases free energy which is used for the formation of ATP. Inhibition of each step of the respiratory chain can cause cellular stress or even cell death (Nelson & Cox, 2005).

A list of inhibitors used for this experiment together with their effect, the used concentration and the vehicle they are solved in is given below (table 3).

inhibitor	vehicle	concentration	effect
antimycin	ethanol	50 – 200 µM	binds to **complex III** (cytochrome c oxidoreductase) which results in the formation of large quantities of superoxide and inhibits the oxidation of ubiquinol and ultimately preventing the formation of ATP
2-decyl-4-quinazolinyl amine (DQA)	ethanol	500 nM – 2 µM	inhibits **complex I**
carbonylcyanide-3-chlorophenylhydrazone (CCCP)	ethanol	4 – 16 µM	**uncoupler** of the mitochondrial respiratory chain, that inhibits ATP production by the uncoupling of oxidative phosphorylation (Volkov et al, 2001)
malonic acid	water	4 – 16 mM	blocks **complex II** as a competitive inhibitor
sodium azide	water	25 – 100 mM	binds irreversibly to the oxygen binding site in the active centre of **complex IV** (cytochrome-c-oxidase)
oligomycin	ethanol	50 – 200 µM	inhibits **complex V** (ATP synthase) by blocking its proton channel
β-fluoropyruvic acid	water	250 µM – 1 mM	inactivates **pyruvate dehydrogenase** by acetylation of the active centre (Flournoy & Frey, 1989)
amyloid-β	water	500 nM – 2 µM	fragment 25-35 decreases the membrane potential in mitochondria as well as the activity of **complex I, II/III and IV** (Cardoso et al, 2001)
rotenone	ethanol	50 – 200 nM	inhibits the transfer of electrons from iron-sulfur centres in **complex I** to ubiquinone and thereby prevents the formation of ATP
hydrogen peroxide	water	50 – 200 µM	causes oxidative stress by accumulation of reactive oxygen species

Table 3 Various inhibitors used to induce cellular stress in HSD10 deficiency patient fibroblasts. Cultured fibroblasts were treated with a variety of inhibitors, which are listed here together with the used concentration and their effect in the cell.

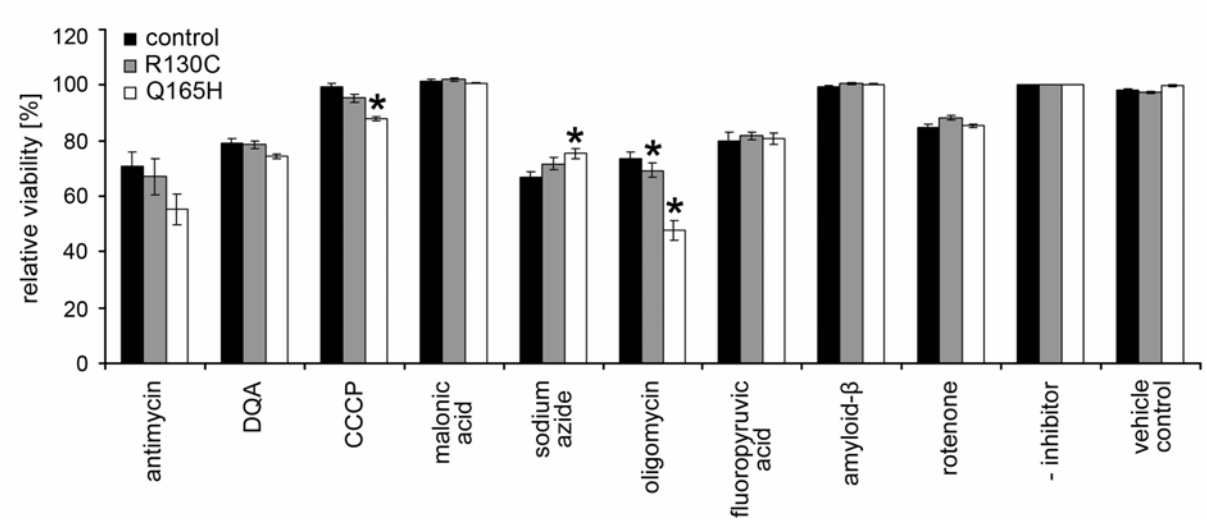

Figure 24 Viability of mutated fibroblasts under various stress conditions. Cultured fibroblasts were treated with a variety of inhibitors (see table 3). After six hours the CellTiter-Glo® Luminescent Cell Viability Assay was performed and relative fluorescence units were measured on a luminescence microplate reader according to the manufacturer's instructions. Shown in the diagram is the viability of fibroblasts relative to untreated cells. Values represent the mean of relative fluorescence units and standard error of 5 biological replicates. Significant differences between mutated and control cells were calculated using the student t-test. * indicates significance at $p \leq 0.01$.

This experiment was designed to determine whether mutated and control cells behave differently under various stress conditions. The analysis of cellular viability in response to a variety of inhibitors shows that under these experimental settings the mutated fibroblasts show only very little significant differences in their behaviour under stress (fig. 24). Fibroblasts with the Q165H mutation display significant changes in cellular viability in comparison with control cells upon treatment with the chemicals CCCP, NaN_3 and oligomycin. With the R130C mutation only oligomycin has a significant effect on cellular viability.

Since patients with the R130C mutation show a severe clinical phenotype which develops after times of increased metabolic stress, it was expected that this mutation is more sensitive to stress than control cells or cells with the Q165H mutation. However, in no case investigated here does the R130C mutation show higher sensitivity to stress than the Q165H mutation.

4.5. Identification of interaction partners of HSD10

In response to metabolic stress, HSD10 protein translocates from the mitochondrial matrix to the inner mitochondrial membrane and this might be important for maintaining mitochondrial integrity (Tieu et al, 2004; fig. 13). It appears plausible that interaction of HSD10 with an integral protein of the mitochondrial membrane or with a soluble protein in the mitochondrial matrix could mediate its protective effect and that this interaction is disturbed by altered HSD10 protein structure due to specific mutations. To better understand the implication of HSD10 in the maintenance of cellular integrity it would be of great interest to know which proteins it binds to under physiological or stress conditions and whether the mutated proteins show any differences in their ability to bind these potential interaction partners.

4.5.1. Homology based BLAST in yeast

The budding yeast (*Saccharomyces cerevisiae*) is a very well established model organism and a lot is known about its pathways and protein functions and interactions. Therefore, to gain a notion on potential binding partners of HSD10 a BLAST in yeast was performed. First, the yeast homolog of HSD10 was identified in a so-called WU-BLAST2, which stands for Washington University Basic Local Alignment Search Tool Version 2.0 (table 4). The emphasis of this tool is to find regions of sequence similarity quickly, with minimum loss of sensitivity. The query was carried out in the *Saccharomyces* Genome Database (more precisely, yeastORF.pep) with the human DNA (NM_004493 and NM_001037811) and protein sequence of HSD10 (NP_004484.1). The results of this BLAST are summarised in the table below (table 4).

Sequences producing significant alignments	Score (bits)	E-value	Identities
YKR009C FOX2 SGDID:S000001717, Chr XI from 456697-453995, reverse complement, Verified ORF, "Multifunctional enzyme of the peroxisomal fatty acid β-oxidation pathway; has 3-hydroxyacyl-CoA dehydrogenase and enoyl-CoA hydratase activities" Length = 901	266	2.5e-21	28 %
YDL114W YDL114W SGDID:S000002272, Chr IV from 255604-256530, Uncharacterised ORF, "Putative protein of unknown function with similarity to acyl-carrier-protein reductases; is not an essential gene" Length = 309	153	8.2e-10	25 %
YNL202W SPS19 SGDID:S000005146, Chr XIV from 259579-260457, Verified ORF, "Peroxisomal 2,4-dienoyl-CoA reductase, auxiliary enzyme of fatty acid β-oxidation; homodimeric enzyme required for growth and sporulation on petroselineate medium; expression induced during late sporulation and in the presence of oleate" Length = 293	151	1.2e-09	26 %
YKL055C OAR1 SGDID:S000001538, Chr XI from 335801-334965, reverse complement, Verified ORF, "Mitochondrial 3-oxoacyl-[acyl-carrier-protein] reductase, may comprise a type II mitochondrial fatty acid synthase along with Mct1p" Length = 279	141	1.4e-08	28 %
YMR226C YMR226C SGDID:S000004839, Chr XIII from 722395-721592, , reverse complement, Verified ORF, "NADP(+)-dependent dehydrogenase; acts on serine, L-allo-threonine, and other 3-hydroxy acids; green fluorescent protein fusion protein localises to the cytoplasm and nucleus; may interact with ribosomes, based on co-purification experiments" Length = 268	130	2.2e-07	30 %
YIR036C IRC24 SGDID:S000001475, Chr IX from 422862-422071, reverse complement, Uncharacterised ORF, "Putative benzil reductase; (GFP)-fusion protein localises to the cytoplasm and is induced by the DNA-damaging agent MMS; sequence similarity with short-chain dehydrogenase/reductases; null mutant has increased spontaneous Rad52p foci" Length = 264	116	8.3e-06	23 %
YLR426W YLR426W SGDID:S000004418, Chr XII from 987059-987138, 987210-988110, Uncharacterised ORF, "Putative protein of unknown function; the authentic, non-tagged protein is detected in highly purified mitochondria in high-throughput studies; proposed to be involved in resistance to mechlorethamine and streptozotocin" Length = 327	90	0.0099	21 %

Table 4 Yeast proteins homologous to human HSD10. This table shows the results of a WU-BLAST2 of human HSD10 protein (NP_004484.1) on the yeastORF.pep database at the *Saccharomyces* Genome Database. Seven yeast proteins display similarity to human HSD10 with an E-value < 0.01.

On nucleic acid level, the HSD10 gene has no similarity with the yeast genome. Based on protein sequence, some yeast genes have a low level of similarity (up to 35 %) with the HSD10 protein (table 4). On this low level of conservation, it is difficult to judge if there is also a functional conservation or not. The protein with the highest rank in similarities in yeast is FOX2. FOX2 (Multifunctional enzyme of the peroxisomal fatty acid β-oxidation pathway) has 3-hydroxyacyl-CoA dehydrogenase and enoyl-CoA hydratase activities.

Although it only has low similarity with human HSD10 (28 % identities), another interesting hit is OAR1, since it is the only protein that is localised in the same cellular compartment as HSD10 apart from one putative protein. OAR1 (Mitochondrial 3-oxoacyl-[acyl-carrier-protein] reductase) may comprise a type II mitochondrial fatty acid synthase along with Mct1p, a malonyl-CoA transferase.

Physical interaction between homologous proteins in yeast could point towards binding partners in humans or model organisms like *Xenopus* or mice, which could then be tested for actual binding to HSD10, e.g. in immunoprecipitation experiments. Therefore, a search for interaction partners of the protein with the highest level of similarities to human HSD10, FOX2, was performed on the *Saccharomyces* Genome Database, more precisely BioGRID (Biological General Repository for Interaction Datasets). The following table lists interaction partners of FOX2 (table 5). For the mitochondrial OAR1 no interaction partners were found.

Physical interaction			reference
bait/query	interaction type	hit	
Cdc34p	Affinity Capture-MS	Fox2p	Krogan et al, 2006
Fox2p	Affinity Capture-MS	Pby1p Cyk3p Rga2p	Krogan et al, 2006
Pex11p	Affinity Capture-Western	Fox2p	Marelli et al, 2004
Akl1p Cmk1p Ipl1p Pcl1p Pcl9p Pho80p Sky1p Snf1p Tos3p Tpk1p	Biochemical Activity	Fox2p	Ptacek et al, 2005
Smc3p	Co-fractionation	Fox2p	White et al, 2004
Rsp5p	Reconstituted Complex	Fox2p	Gupta et al, 2007

Table 5 Interaction partners of the yeast protein FOX2, a homolog to human HSD10. A search for physical interaction partners of the protein found to be most homologous to human HSD10 (table 4) was performed on the BioGRID database at the *Saccharomyces* Genome Database. This table lists published interactions between FOX2 and other proteins, their type of interaction and the according reference.

The interaction partners of FOX2 listed in table 5 are also putative interaction partners of HSD10 since FOX2 possibly is the yeast homolog to human HSD10. Among these interaction partners of FOX2 are many different protein classes.

The two most interesting interaction partners are Cmk1p and Rsp5p considering their cellular function. Cmk1p (Calmodulin-dependent protein kinase 1p) is involved in stress tolerance (Sakaguchi et al, 2010) and Rsp5p, an E3 ubiquitin ligase, plays important roles in stress resistance, heat shock and transcription initiation (Cardona et al, 2009).

Apart from that, FOX2 interacts with several kinases (Akl1p, Ipl1p, Sky1p, Snf1p, Tos3p, Tpk1p) that are involved in cellular processes like endocytosis (Henry et al, 2003), kinetochore-microtubule attachment (King et al, 2007), ion homeostasis (Porat et al, 2006) and glucose repression/derepression (Ye et al, 2008). It also plays a role in cell cycle regulation and cell division since it interacts with proteins like Cdc34p, Cyk3p, Rga2p, Pcl1p, Pcl9p and Pho80p which are a cell division cycle 34 homolog, a protein involved in cytokinesis (Korinek et al, 2000), a Cdc42p GTPase-activating protein (Zheng et al, 1993), G1-cyclin homologs and a cyclin-dependent kinase.

Pex11p regulates peroxisome biogenesis und morphogenesis (Kobayashi et al, 2007; Rottensteiner et al, 2003) and functions in medium-chain fatty acid oxidation (van Roermund et al, 2000) and Pby1p is a P-body associated protein. Smc3p is a member of the structural maintenance of chromosomes (SMC) family (Heidinger-Pauli et al, 2010) and a subunit of cohesion.

Taken together, all these interaction partners of FOX2 in yeast are also potential binding partners of HSD10 in humans. Considering the role of HSD10 for mitochondrial integrity and cell viability under normal or stress conditions, Cmk1p and Rsp5p are especially interesting candidates for a functional interaction with HSD10.

4.5.2. Functional interaction of human HSD10 and UXT in vivo

In a yeast-2-hybrid system, where HSD10 was used as bait and a HeLa cDNA library as prey, two potential interaction partners were identified: PCBP1 and UXT. PCBP1 (PolyC binding protein 1) binds to mRNAs that contain a DICE (differentiation control element) in the cytoplasm and thereby represses their translation. Upon phosphorylation it releases the mRNAs for translation and migrates to the nucleus where it functions as a transcription factor and plays a role in splicing. UXT (ubiquitously expressed transcript) is a small prefoldin-like protein implicated in several cellular functions. One of them is the promotion of the NFκB (nuclear factor kappa-light-chain-enhancer of activated B cells) enhanceosome in the nucleus and as such it plays a role in mitochondrial aggregation and apoptosis.

Since UXT is involved in regulation of apoptosis it was tested for functional interaction with HSD10. UXT is predominantly localised in the nucleus (Markus et al, 2002) but also present in the cytoplasm, e.g. as a component of centrosomes (Zhao et al, 2005). Although the greater part of HSD10 is detectable in mitochondria in immunofluorescence stainings (fig. 10) a small part might be distributed in the cytosol. Also, a Western Blot showing HSD10 overexpression in HEK cells pointed towards an additional cytosolic

fraction of HSD10 (data not shown). Based on this, it was assumed that UXT and HSD10 bind to each other in the cytosol. This might inhibit the transport of UXT to the nucleus, its binding to NFκB, and subsequently the induction of apoptosis. According to this hypothesis, an overexpression of UXT in *Xenopus* embryos should induce an increase in apoptosis which should be opposed by a simultaneous co-injection of HSD10. In this situation HSD10 could have a protective function in the cell.

The human constructs for UXT and HSD10 were used for the expression on the right body half of *Xenopus* embryos and after 2 days in culture (stage NF 33/34) the embryos were subjected to TUNEL staining ancelld scored for apoptosis on each side (fig. 25). The left side was used as an internal control and the amount of apoptotic spots on the right (injected) side was normalised against the left (uninjected) side.

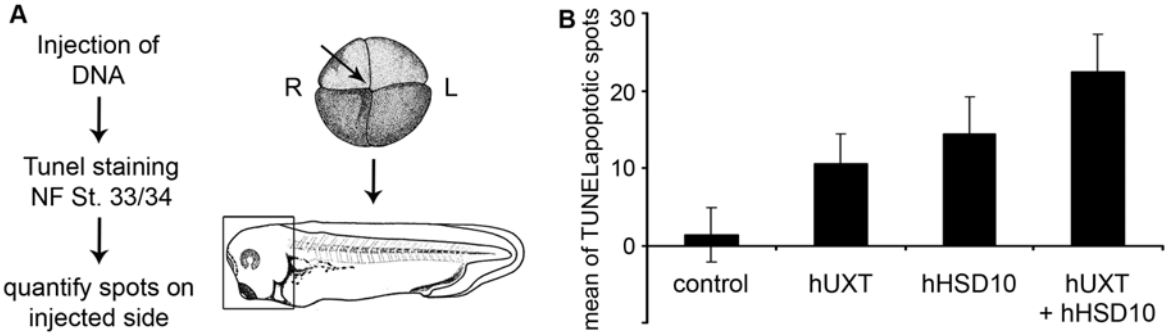

Figure 25 Induction of apoptosis by UXT in the presence of HSD10. (A) Experimental scheme. Embryos were injected into one blastomere of the 4-cell-stage with 150 pg of DNA (pT-Rex-DEST30_hHSD10 and pcDNA4/HisMaxB_hUXT). **(B)** Quantification of TUNEL staining on the right (injected) side of tailbud stage embryos (stage NF 33/34) normalised against the left (control) side. The standard error for 4 individual experiments (n = 36–62 embryos) is shown.

Human wildtype HSD10 has been shown before to induce a small increase in apoptosis rate (fig. 19). In line with previous publications on UXT function in humans, overexpression of UXT in *Xenopus* embryos leads to an increase in apoptosis (fig. 25). Co-injection of HSD10 together with UXT do not result in a rescue of the apoptotic phenotype elicited by UXT. In contrast, an additive effect of the apoptosis inducing functions of UXT and HSD10 can be observed. Thus, human UXT and HSD10 do not appear to interact functionally in *Xenopus* embryos.

4.5.3. Pull-down / IMAC approach to identify binding partners of HSD10

Pull-down experiments and IMAC (immobilised metal ion affinity chromatography) are tools to verify potential binding partners identified e.g. in yeast-2-hybrid systems or based on computational predictions. Here they were used to find proteins that bind to HSD10 *in vivo*.

The pull-down of potential binding partners of HSD10 was performed by overexpressing xHSD10_myc in *Xenopus* embryos and using an anti-myc antibody coupled to magnetic AG-beads. Overexpressed xHSD10_myc can bind to its interaction partners *in vivo* and after 1 day in culture (stage NF 19) the protein was extracted and an anti-myc antibody coupled to magnetic AG-beads was added. The beads are used to pull-down tagged HSD10 together with potential interaction partners which should still be bound under the experimental conditions. Only when the complexes are purified from the cell extract is the binding between HSD10 and potential binding partners released. In comparison with an unspecific pull-down where an IgG-antibody was used, the protein bands specific for HSD10 should be visible on a SDS-gel (fig. 26). Likewise, endogenous HSD10 was pulled-down from mitochondrial extract prepared from untreated HEK cells by an anti-HSD10 antibody (fig. 26). Isolating mitochondria before the pull-down enriches HSD10 in the input and should be more capable to find interaction partners in mitochondria.

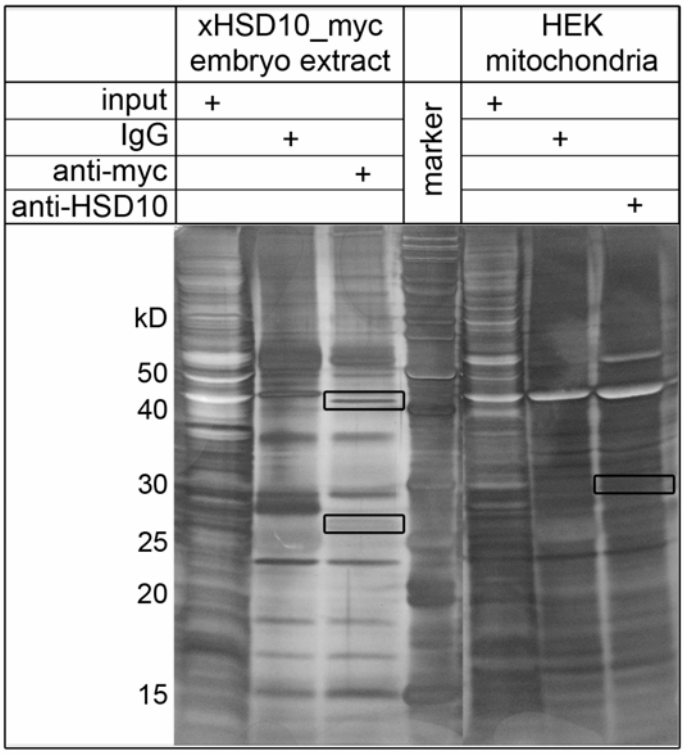

Figure 26 Pull-down of xHSD10_myc and endogenous HSD10 together with potential binding partners. 150 pg xHSD10_myc were injected into *Xenopus* embryos at the 4-cell-stage. Embryos were cultivated until stage NF 19 and their protein extract was used to pull-down overexpressed xHSD10_myc together with bound proteins with 1 µg anti-myc antibody coupled to magnetic AG beads. Mitochondrial extract from confluent HEK cells grown on three 10 cm plates was subjected to a pull-down with 2 µg anti-HSD10 antibody to isolate endogenous HSD10 together with its binding partners. All pulled-down proteins were run on a SDS-PAGE and detected by silver staining. Squares indicate bands which are specific for HSD10 pull-down opposed to a pull-down with IgG.

The comparison of the actual pull-down with the IgG control shows that there are several bands that are specifically pulled-down with anti-myc and anti-HSD10, respectively. With this method it was not possible to yield single neat bands on the SDS-gel.

In order to obtain more specific and identifiable bands on the silver stained gel, HSD10 protein was purified via IMAC prior to interaction partner binding. For this purpose *E.coli BL21(DE3)* were transformed with prokaryotic expression plasmids (pET15b_His/hHSD10 and p11/His for the mutations) for human wildtype and mutated HSD10. The proteins were isolated from bacteria and purified via IMAC. Prior to elution an extract of mitochondrial proteins prepared from HEK cells was added to the column (fig. 27). In this situation potential interaction partners in the mitochondrial extract can bind while they flow by the His-tagged HSD10 bound to the Ni^{2+} agarose in the column. Together they are eluted from the column and separated on a denaturing SDS-gel. Silver staining and the subsequent comparison of the proteins eluted with HSD10 or an unrelated His-tagged control protein yields bands that are specific for HSD10 and are not due to binding of proteins to the Ni^{2+} agarose or incomplete purification. A successive comparison between bands that eluted with HSD10 wildtype or one of the three mutations might reveal binding partners that show differences in their ability to bind to wildtype or mutated HSD10.

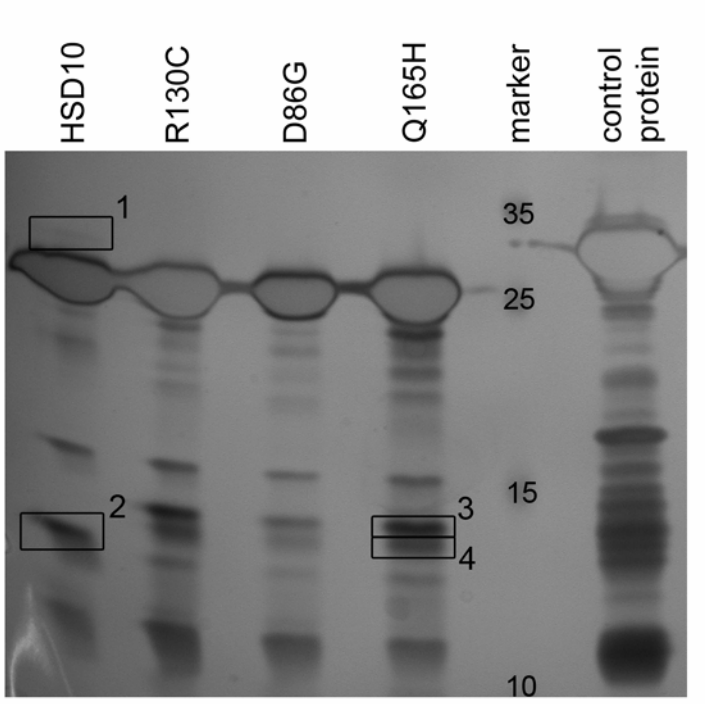

Figure 27 IMAC of wildtype and mutated HSD10 proteins together with potential binding partners. His-tagged HSD10 and a His-tagged control protein were expressed in *E.coli BL21(DE3)*. Purification of these proteins was carried out on an IMAC column. Prior to elution an extract of mitochondrial proteins prepared from confluent HEK cells grown on three 10 cm plates was added. Elution of His-tagged proteins from the Ni^{2+} agarose was achieved by addition of 250 mM imidazole. 80 µl of the eluate were subjected to SDS-PAGE on a large size gel and proteins were detected by a silver staining kit according to the manufacturer's instructions. Squares and numbers indicate bands which are specific for HSD10 wildtype protein (square 1 and 2) or the three mutations (square 3 and 4).

Comparison of the bands that come up with HSD10 or an unrelated control protein and comparison between wildtype and mutated HSD10 shows that indeed, there are two bands (band 1 and 2) visible with wildtype HSD10 that are not present with the mutations (fig. 27). The other way around, there are also two bands (band 3 and 4) that are found with all three mutations but not with wildtype HSD10.

To identify these proteins the four bands were analysed by MS (mass spectrometry). For this purpose they were cut out of the silver stained gel and enzymatically digested by trypsin into smaller peptides. Subsequently these peptides were introduced into the mass spectrometer and identified by tandem mass spectrometry, which involves multiple steps of mass spectrometry selection, with some form of fragmentation occurring in between the stages.

This analysis yields the amino acid sequence of several different peptides per band (table 6). Proteins that are bound to His-tagged HSD10 in the IMAC column can either be of bacterial origin and stem from the expression of HSD10 in *E.coli* or they can be human and originate from the mitochondrial extract applied to the columns. Therefore, these peptides were subjected to a BLAST search in a human or bacterial database at the NCBI (National Center for Biotechnology Information) and the results are listed in the table below (table 6).

peptides in band 1	peptides in band 2	peptides in band 3	peptides in band 4
K.DVQTALALAK.G	K.DVQTALALAKGK.F	R.VLDVNLMGTFNVIR.L	R.VVEPLITLAK.T
K.GGIVGMTLPIAR.D	K.IFVDEGPSMK.R	K.LFNELGPR.F	R.RVVEPLITLAK.T
K.GQTHTLEDFQR.V	R.TSHITVVVSDR.-	R.TRDNEIVAK.L	R.AGDNAPMAYIELVDR.S
R.VDVAVNCAGIAVASK.T	K.IFVDEGPSMKR.I	K.INALETVTIASK.A	R.TYLYQGIAER.N
K.VCNFLASQVPFPSR.L	K.VSQALDILTYTNKK.A		R.GANLVNGLLYIDLER.V
K.LGNNCVFAPADVTSEK.D	R.ALNAAGFR.I		R.NFDLSPLMR.Q
R.LVAGEMGQNEPDQGGQR.G	K.STPFAAQVAAER.A		R.IAISERPALNS.-
K.GLVAVITGGASGLGLATAER.L	K.AILAAAGIAEDVK.I		K.FNDAVLR.H
K.FGRVDVAVNCAGIAVASK.T	K.AILAAAGIAENVK.I		R.FNDAVIR.N
K.KLGNNCVFAPADVTSEK.D	R.FGGESVLAGSIIVR.Q		R.FNNAVIR.N
K.SQAHTLEDFQR.V	R.LQAFEGVVIAIR.N		R.AGLQFPVGR.I
K.LGEYGFQNALIVR.Y			R.AGIQFPVGR.I
K.DAFLGSFLYEYSR.R			R.FNNLGLR.G
R.KVPQVSTPTLVEVSR.S			K.FGGNLGLR.F
R.VATVSLPR.S			R.FGGDGLLR.E
K.LSSPATLNSR.V			K.AQLQEIAQTK.M
R.LGEHNIDVLEGNEQFINAAK.I			R.AQLQQIAQTK.A
R.VGYLVVSTDR.G			
K.VMLQAYDEGR.L			
R.VGYIVVSTDR.G			
K.LGEYGFQNALLVR.Y			
K.KVPQVSTPTLVEVSR.S			
R.VGYIVVTSDR.G			
R.VGYIVISSDR.G			
R.LVGQGASAVLLDLPNSGGEAQAK.K			

Table 6 MS results of proteins found in IMAC of wildtype and mutated HSD10 proteins together with potential binding partners. Bands distinguishable in the IMAC approach to find binding partners (fig. 27) that were detectable with wildtype HSD10 but not with the mutations or the other way around were analysed in MS. This table lists the peptides identified in MS that compose the indicated bands.

MS of four bands detected in the IMAC to be specific for wildtype or the three mutations (fig. 27 and table 6), respectively, and a successive BLAST search in a human or bacterial database at the NCBI revealed several potential binding partners for HSD10 (table 7). BLAST results that are only found with one peptide are assumed to be unspecific since the peptides that are used for the BLAST search are very short, and also unnamed protein products are not considered specific. Thus, the remaining specific results are listed in table 7.

BLAST results only found with wildtype HSD10 (bands 1 and 2)		BLAST results only found with mutated HSD10 (bands 3 and 4)	
human database	bacterial database	human database	bacterial database
3-ketodihydrosphingosine reductase	membrane-bound ATP synthase α-subunit AtpA	H2A histone family, member V	heat shock protein IbpA
α-fetoprotein	ATP synthase gamma subunit		50S ribosomal protein L11 and L17
albumin	Chain K and M, Ternary Complex 70s Ribosome (= 30S ribosomal protein S10 and S12)		Chain N, Ternary Complex 70s Ribosome (= 30S ribosomal protein S13)
	50S ribosomal protein L22		
	30S ribosomal protein S11 and S13		

Table 7 Potential binding partners of wildtype HSD10 and mutations R130C, D86G and Q165H. BLAST search results of peptides identified in MS of proteins that were co-purified with HSD10 wildtype or mutations (table 6) obtained from a human or bacterial database are listed in this table. BLAST search results that were only found with one short peptide or that belonged to unnamed protein products or were part of HSD10 itself were rendered unspecific. The remaining potentially specific interaction partners are listed here.

Proteins that are specific for wildtype HSD10 and came up in a BLAST search in a human database are 3-ketodihydrosphingosine reductase, α-fetoprotein and albumin. KDHSR (3-ketodihydrosphingosine reductase) plays a role in the biosynthesis of sphingolipids at the cytosolic side of the ER by reducing 3-keto-sphinganine to dihydrosphingosine (Takabe et al, 2008). Sphingolipids are essential membrane components of eukaryotic cells. Like HSD10, KDHSR belongs to the SDR (short-chain dehydrogenase/reductase) family. It shows the typical SDR active-site motif YXXXK, which is preceded by a conserved Ser 13 residues upstream as well as a Rossman fold in the nucleotide binding domain and the nucleotide binding motif GXXXGXG.

AFP (α-fetoprotein) is a mammalian glycoprotein and a member of the albuminoid gene superfamily. During normal development, AFP is synthesised in the fetal yolk sac endoderm and liver, and diffuses rapidly into the maternal circulation. After birth, the AFP level drops rapidly in the maternal serum, but remains high in the newborn for about four weeks associated with continued proliferation of hepatocytes in the liver until liver-cell proliferation ceases. Then the AFP level declines rapidly and only small quantities remain present in adults. AFP functions as a transporter protein carrying e.g. copper, nickel and fatty acids in fetal serum (Sell, 2008).

Albumin is a globular protein produced in liver cells. It is present in and outside of blood vessels and is responsible for the maintenance of osmotic pressure by retaining water molecules in the vessels. Hydrophobic compounds like fatty acids, some vitamins or

hormones need to be bound to albumins to be transported in the blood flow. Since albumins are H^+ acceptors and donors they also play a role in stabilising the pH of the blood (Chuang & Otagiri, 2007; Hankins, 2006; van der Vusse, 2009).

Proteins that are specific for wildtype HSD10 and came up in a BLAST search in a bacterial database are membrane-bound ATP synthase (α-subunit AtpA and gamma subunit) and several ribosomal proteins.

Membrane-bound ATP synthase is composed of the F_1 complex which is the catalytic core and comprises 5 subunits (alpha, beta, gamma, delta, epsilon) linked to the F_0 membrane-embedded proton channel that consists of at least three subunits (A-C), nine in mitochondria (A-G, F6, F8). Both the F_1 and F_0 complexes are rotary motors that rotate in opposite directions in order to drive ATP synthesis. The α-subunit AtpA can bind nucleotides in the F_1 catalytic cylinder formed by three alpha and three beta subunits whereas the gamma subunit forms the central shaft that connects the F_0 rotary motor to the F_1 catalytic core (Abrahams et al, 1994; Stock et al, 1999).

Ribosomal proteins that belong to the 30S subunit (S10, S11, S12 and S13) or the 50S subunit (L22), respectively, are found to be potential bacterial interaction partners of wildtype HSD10.

One protein that is only found with mutated HSD10 and came up in a BLAST search in a human database is H2A histone family, member V.

Histones are basic proteins that are responsible for the nucleosomal structure in eukaryotes. Nucleosomes consist of DNA wrapped around a histone octamer composed of two of each core histones (H2A, H2B, H3 and H4). The H2A family performs essential roles in maintaining structural integrity of the nucleosome, chromatin condensation, and binding of specific chromatin-associated proteins (Farris et al, 2005; Li et al, 2005; Raisner et al, 2005).

Proteins that are specific for mutated HSD10 and came up in a BLAST search in a bacterial database are heat shock protein IbpA and several ribosomal proteins.

Heat shock protein IbpA is a molecular chaperone that binds denatured proteins and facilitates their subsequent refolding by the ATP-dependent chaperones DnaK, DnaJ, GrpE and ClpB. It has been shown that IbpA can protect *E.coli* cells from oxidative damage caused by copper and from thermal stress (Matuszewska et al, 2008; Thomas & Baneyx, 1998)

Ribosomal protein S13 that belongs to the 30S subunit is found to be a potential bacterial interaction partner of mutated HSD10.

Among these possible binding partners (table 7) are three potentially specific results. Due to their localisation in mitochondria and their role in energy metabolism and stress

response, the ATP synthase subunits, ribosomal proteins and IbpA, might be specific binding partners of HSD10 in mitochondria.

In summary, there are several findings among these potential binding partners that are most likely unspecific. Proteins that are separated from HSD10 by their subcellular localisation, like AFP, albumin or H2A, are probably unspecific. Likewise, KDHSR might turn up in this BLAST search because it comprises the same motifs as HSD10 and the peptides that are used as a query are very short.

4.6. Function of HSD10 as a component of human mitochondrial RNaseP

Recently, HSD10 has been shown to be a component of the human mitochondrial RNaseP complex. This enzyme endonucleolytically cuts the 5' end of tRNAs. In contrast to other RNaseP complexes, human mtRNaseP (mitochondrial RNaseP) has been shown to be a RNA free, protein-only enzyme that consists of three proteins: MRPP1, MRPP2 (HSD10) and MRPP3.
Furthermore, it has been shown that knock-down of one of these proteins and a consequential loss of mtRNaseP activity in HeLa cells causes the accumulation of two mitochondrial tRNA precursors (Holzmann et al, 2008).

4.6.1. Accumulation of tRNA precursors after HSD10 loss-of-function

In order to establish a system to test the mutated HSD10 proteins for their mtRNaseP activity, the accumulation of several precursor (mt)tRNAs was determined in HeLa cells over a nine day time course after knock-down of HSD10 by two different siRNAs (fig. 28). The previously published accumulation (Holzmann et al, 2008) did only occur for one of two tested siRNAs for HSD10 and was only shown for two tRNA precursors, which were very different in their level of accumulation. Therefore, two previously used siRNAs targeting HSD10 (siRNA3 and siRNA5) were tested for their effect on accumulation of several tRNA precursors.

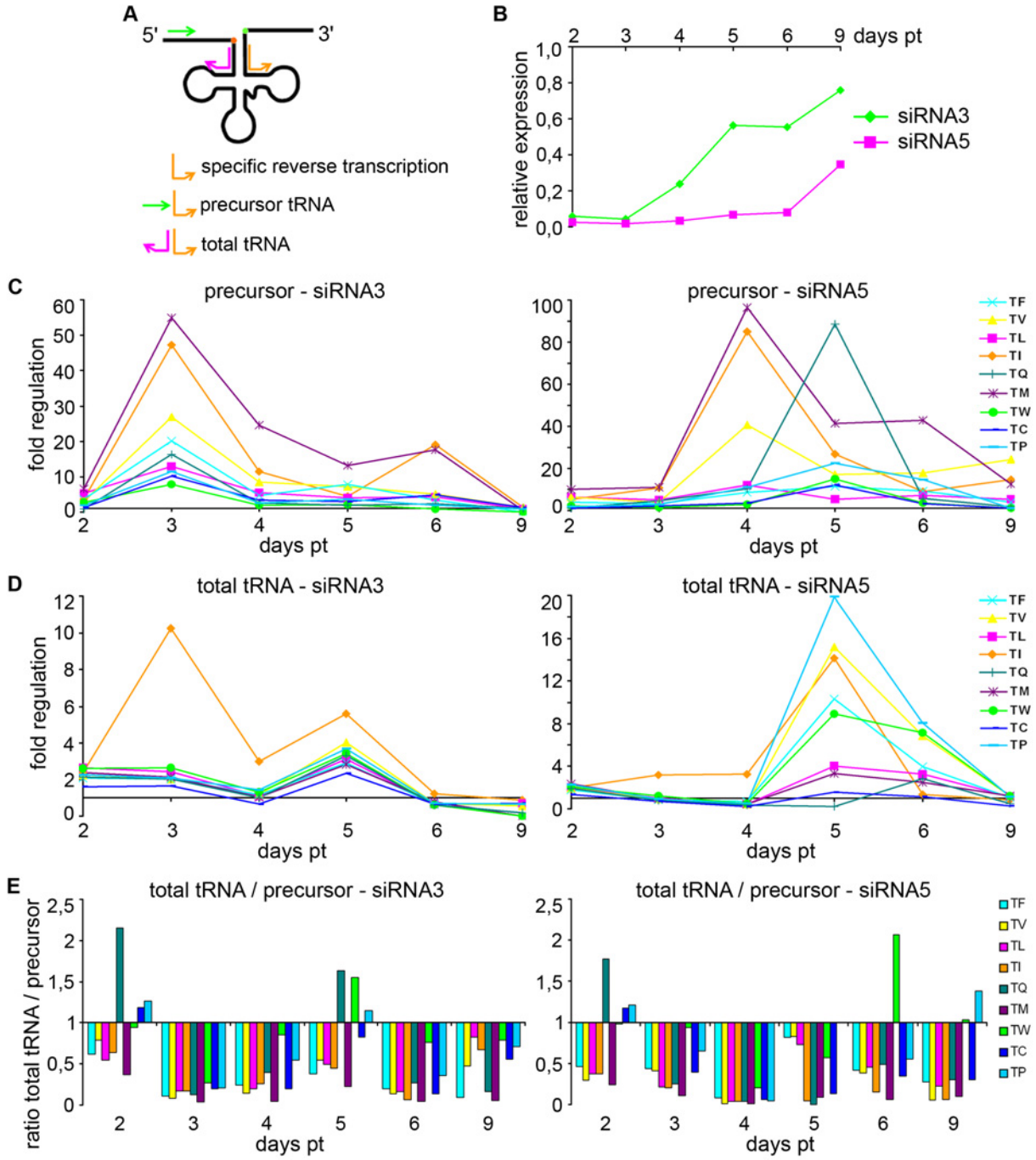

Figure 28 Accumulation of tRNA precursors after HSD10 knock-down. Transient transfection of HeLa cells was achieved using Lipofectamine and 60 pmol of two different siRNAs targeting HSD10 (siRNA3 and siRNA5). Total RNA was isolated from these cells after two to nine days post transfection and the RNA was transcribed into cDNA using Maxima Reverse Transcriptase and random primers or primers specific for (mt)tRNA sequences (orange arrow in **A**). This cDNA was subjected to qRT-PCR with internal tRNA primers for detection of the whole amount of mitochondrial tRNA transcript (precursor and mature, orange and pink arrows in **A**) and primers that cover the 5' leader sequence as well as part of the tRNA to quantify the amount of mitochondrial precursor tRNAs (orange and green arrows in **A**). **(A)** Displays the binding sites of tRNA specific primers and **(B)** shows the proof of knock-down efficiency by two different siRNAs against HSD10 over several days relative to cells treated with 60 pmol inert negative control siRNA. Random primed cDNA was subjected to qRT-PCR and CT values were normalised against GAPDH and control siRNA treated cells. Relative expression levels of HSD10 were calculated using a stan-

dard curve. **(C)** and **(D)** denote the accumulation of nine different mitochondrial tRNA precursors **(C)** and changes of the total amount of nine different mitochondrial tRNAs **(D)** in relativity to cells treated with an inert negative control siRNA (control siRNA = 1) over a time course of nine days. Specifically primed cDNA was subjected to qRT-PCR with tRNA specific primers and CT values were normalised against GAPDH. Relative expression levels of immature (mt)tRNA precursor and the total tRNA amount were calculated using the ddCT method. **(E)** Shows the ratio of total (mt)tRNA amount to immature precursor for nine different (mt)tRNAs over a time course of nine days after knock-down of HSD10. pt: post transfection, TF-TC: T stands for tRNA and the second letter denotes the specific amino acid according to the one letter code for amino acids.

Treatment of HeLa cells with 60 pmol of two different siRNAs results in an efficient knock-down of HSD10 over more than nine days (fig. 28B). Three days after knock-down of HSD10 with siRNA3 mitochondrial tRNA precursor levels increase to a temporary peak at 7- to 47-fold above those of control siRNA treated cells (fig. 28C, left). With siRNA5 the temporary maximum of mitochondrial tRNA precursor accumulation is found after four to five days post transfection and ranges from an 11- to 91-fold increase compared to cells treated with control siRNA (fig. 28C, right). In line with siRNA transfections being transient, HSD10 mRNA knock-down and concurrent precursor (mt)tRNA accumulation return to normal levels within the nine days examined (fig. 28B and C). The two different siRNAs used to knock-down HSD10 give rise to slightly different kinetics of precursor (mt)tRNA accumulation. In both cases precursors of $tRNA^M$, $tRNA^I$, $tRNA^F$ and $tRNA^V$ are among the tRNAs with the highest accumulation but the time point at which the highest accumulation can be detected varies.

The total amount of tRNAs also shows alterations upon treatment with siRNA targeting HSD10. It rises up to almost 20-fold above or 0,01-fold below the level of cells treated with control siRNA. In order to take into account the deviation of total tRNA amount and still be able to compare the accumulation of tRNA precursors, the ratio of total tRNA to tRNA precursor was calculated. In cases where the precursor increases more than the total amount of a certain tRNA the ratio falls below 1. Fig. 28E clearly shows that for almost all tRNAs and timepoints investigated here, this ratio is < 1.

In conclusion, a transient knock-down of HSD10 leads to the inhibition of RNaseP activity judged by the consequential accumulation of mitochondrial tRNA precursors.

4.6.2. Reconstitution of RNaseP activity using mutated HSD10 after HSD10 loss-of-function

The function of HSD10 in mitochondrial tRNA processing might be the underlying reason for the clinical phenotype in HSD10 deficiency patients. Mutations in mitochondrial tRNAs cause a disturbance of mitochondrial translation possibly resembling the mutation of one of the components of RNaseP. Mitochondrial tRNA mutations are known to elicit many different clinical syndromes including mitochondrial myopathy (Swalwell et al, 2006), CPEO (chronic progressive external ophtalmoplegia; Spagnolo et al, 2001), MELAS (mitochondrial encephalomyopathy, lactic acidosis, stroke-like episodes; Tzen et al, 2003) and ADPD (Alzheimer's disease and Parkinsons's disease; Wallace et al, 1992).

To test the mutations found in HSD10 deficiency patients for their residual activity in tRNA processing, a rescue experiment was performed (fig. 29). After siRNA mediated knock-down of endogenous HSD10 and co-transfection with constructs coding for HSD10 wildtype or mutations, the accumulation of several precursor (mt)tRNAs was determined in HeLa cells after three days.

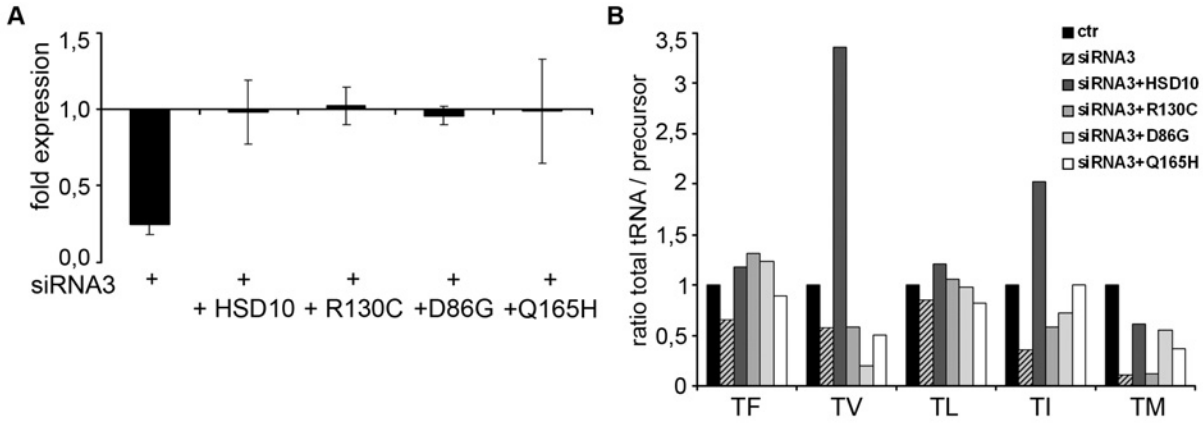

Figure 29 Accumulation of tRNA precursors after HSD10 knock-down and rescue. Transient co-transfection of HeLa cells was achieved using Lipofectamine and 60 pmol of siRNA3 as well as 1 µg of DNA (pT-Rex_DEST30 containing cDNA for HSD10 wildtype and mutations). Total RNA was isolated from these cells after three days post transfection and the RNA was transcribed into cDNA using Maxima Reverse Transcriptase and random primers or primers specific for (mt)tRNA sequences. This cDNA was subjected to qRT-PCR with internal tRNA primers for detection of the whole amount of mitochondrial tRNA transcript (precursor and mature) and primers that cover the 5' leader sequence as well as part of the tRNA to quantify the amount of mitochondrial precursor tRNAs. **(A)** Displays the relative expression levels of HSD10 in HeLa cells co-transfected with siRNA against HSD10 and cDNA coding for HSD10 wildtype or the mutations. Random primed cDNA was subjected to qRT-PCR and CT values were normalised against GAPDH. Relative expression levels of HSD10 were calculated using a standard curve. **(B)** Shows the ratio of total (mt)tRNA amount to immature precursor for five different (mt)tRNAs three days after knock-down of HSD10 with siRNA3 and rescue with HSD10 wildtype and mutations.

Co-transfection of siRNA targeting HSD10 and a concomitant overexpression of HSD10 wildtype and mutations resulted in very different expression levels of HSD10 (data not shown). The higher the expression level was compared to endogenous HSD10, the higher was the ability of wildtype or mutated HSD10 to re-establish the function of mtRNaseP and thus, to rescue the accumulation of mitochondrial tRNA precursors. Samples with equivalent HSD10 expression at the physiological level of HSD10 expression in cells treated with a negative control siRNA were chosen for analysis of tRNA levels to be able to draw a conclusion about the ability of mutated HSD10 to function in the (mt)RNaseP complex at physiological quantities (fig. 29A).

Three days after knock-down of HSD10 with siRNA3 mitochondrial tRNA precursors accumulate indicated by a decrease of the total amount/precursor ratio below the level of cells treated with control siRNA (control siRNA = 1). Co-transfection of HSD10 DNA does

rescue this accumulation in part depending on the tRNA in question and the respective DNA being wildtype or bearing a mutation (fig. 29B). HSD10 wildtype rescues the accumulation of tRNA precursors for all tested tRNAs. The R130C mutation rescues three out of five tested tRNAs (TF, TL and TI), the D86G mutation rescues all except for TV, and Q165H is able to bring tRNA precursor levels back to normal for three tRNAs (TF, TI, TM). Taken together to a mean of the five tested tRNAs despite the great variability between the different tRNAs, all mutations alike are able to rescue the accumulation of immature precursors from 200 % in the knock-down situation back to 143 % of the normal level (level of tRNA precursors in control siRNA treated cells = 100 %; ctr siRNA = 1, siRNA3 = 0.5, HSD10 wildtype = 1.7, all mutations = 0.7). The mutations are not as active in their RNaseP activity as the wildtype protein, which even over-compensates and reduces tRNA precursor levels to 59 % of the normal level.

This experiment does not show a clear pattern of rescue with HSD10 wildtype or the mild Q165H mutation but not with the two severe mutations as it was the case for the rescue of the apoptosis phenotype (Rauschenberger et al, 2010). Nevertheless, it gives clear evidence that the expression of the two severe mutations R130C and D86G does not have a dominant-negative effect on (mt)RNaseP activity in contrast to the apoptotic phenotype shown before (fig. 19).

4.6.3. RNaseP activity in patient fibroblasts under physiological and oxidative stress conditions

To investigate if the disturbed function of (mt)RNaseP is the cause for the observed disease phenotype in HSD10 deficiency patients, mitochondrial tRNA levels were determined in patient fibroblasts. The severe R130C but not the mild Q165H mutation should display a considerable accumulation of (mt)tRNA precursors comparable to a HSD10 knock-down.

Transfection of cells is only a transient effect which does not necessarily reflect the condition of patient cells that carry a mutation right from the start. Furthermore, co-transfection of siRNA and DNA that can be targeted by the siRNA does probably result in the expression of a mixture of endogenous wildtype HSD10 and transfected wildtype or mutated HSD10. To eliminate these factors mitochondrial tRNA levels were determined in HSD10 deficiency patient fibroblasts directly (fig. 30).

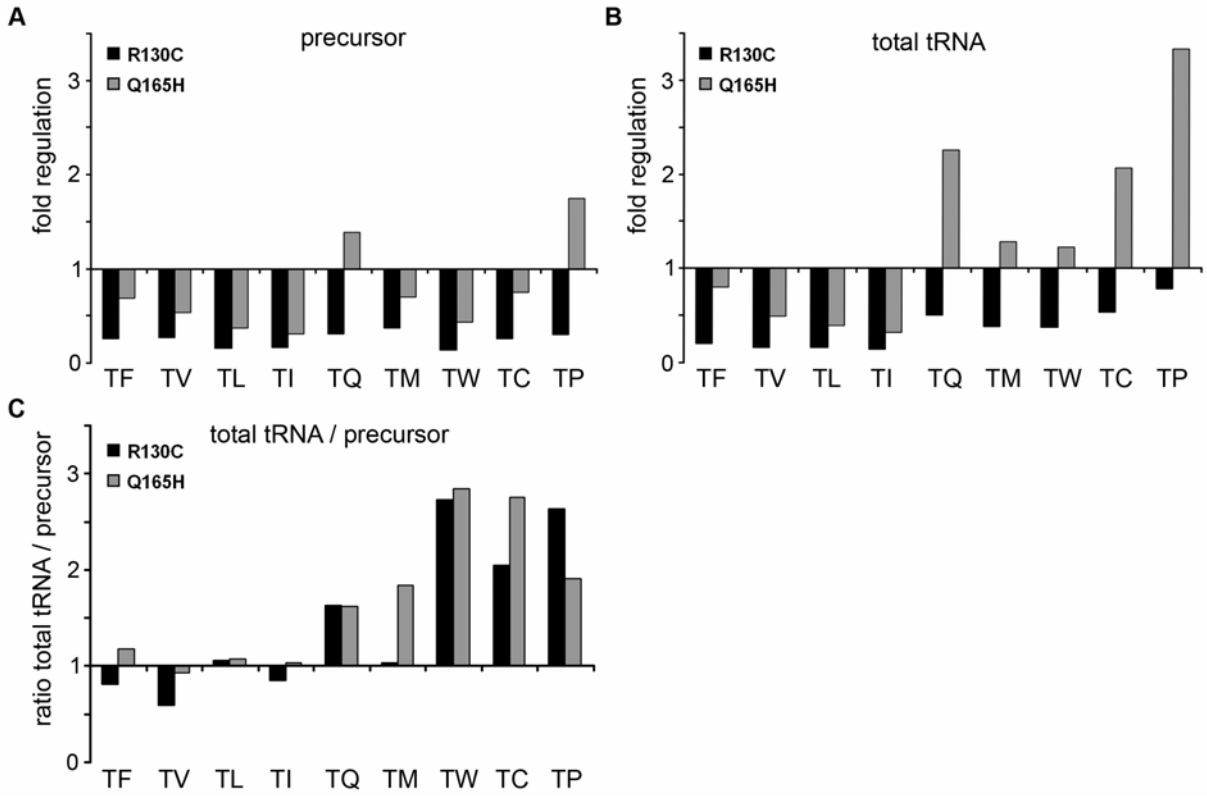

Figure 30 tRNA levels in HSD10 deficiency patient fibroblasts. Total RNA was isolated from control cells or cells carrying the R130C or Q165H mutation and the RNA was transcribed into cDNA using Maxima Reverse Transcriptase and random primers or primers specific for (mt)tRNA sequences. This specifically primed cDNA was subjected to qRT-PCR with internal tRNA primers for detection of the whole amount of mitochondrial tRNA transcript (precursor and mature) and primers that cover the 5' leader sequence as well as part of the tRNA to quantify the amount of mitochondrial precursor tRNAs. CT values were normalised against GAPDH. Relative expression levels were calculated using the ddCT method whereat levels in control cells were set to 1. **(A)** Denotes the amount of nine different (mt)tRNA precursors in relativity to control cells (control = 1). **(B)** Displays changes of the total amount of (mt)tRNAs in relativity to control cells. **(C)** Shows the ratio of total (mt)tRNA amount to immature precursor.

In patient fibroblasts mitochondrial tRNA precursors are not accumulated as expected. The total amount of mitochondrial tRNA (fig. 30B) as well as the level of precursors (fig. 30A) is strongly decreased compared to control cells. In both cases the reduction is higher for cells with the R130C mutation than in fibroblasts with the Q165H mutation. The ratio of total amount of tRNA to precursors is only slightly altered for some tRNAs compared to control cells which points to a concurrent reduction of both tRNA forms (fig. 30C). For other tRNAs the ratio is > 1, indicating the stronger decrease of immature precursor relative to the total amount of tRNAs. The reduction of all tRNA forms might be the long-term response of the cells to the mutations and the permanently impaired (mt)RNaseP activity in patients in contrast to the transient effects upon siRNA mediated knock-down of HSD10 shown before (fig. 28).

As described above, HSD10 seems to play a role in the protection of cells against metabolic stress and this protective effect might be disturbed by altered HSD10 protein structure due to specific mutations. Under physiological conditions, the amount of total

(mt)tRNA as well as (mt)tRNA precursors is reduced in fibroblasts with the R130C and the Q165H mutation (fig. 30). In order to investigate whether mutated and control fibroblasts respond differently to cellular stress conditions, their ability to process (mt)tRNAs was examined (fig. 31). Oxidative stress was induced by two different concentrations of rotenone and the cells were scored for their level of total and precursor (mt)tRNA after one or two days.

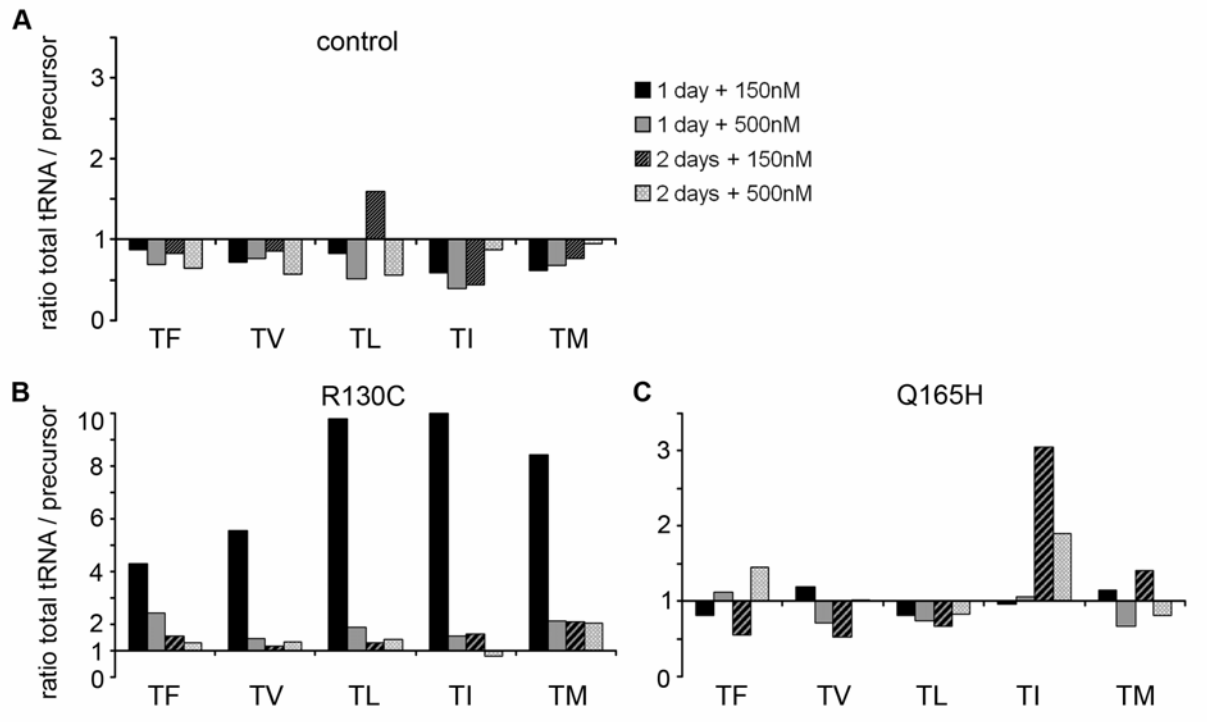

Figure 31 Amount of tRNA precursors in HSD10 deficiency patient fibroblasts under oxidative stress. Fibroblasts were treated with 150 nM or 500 nM rotenone for one or two days. Total RNA was isolated from control cells or cells carrying the R130C or Q165H mutation and the RNA was transcribed into cDNA using Maxima Reverse Transcriptase and random primers or primers specific for (mt)tRNA sequences. This specifically primed cDNA was subjected to qRT-PCR with internal tRNA primers for detection of the whole amount of mitochondrial tRNA transcript (precursor and mature) and primers that cover the 5' leader sequence as well as part of the tRNA to quantify the amount of mitochondrial precursor tRNAs. CT values were normalised against GAPDH. Relative expression levels were calculated using the ddCT method whereat levels in untreated cells were set to 1. **(A)** Shows the ratio of total (mt)tRNA amount to immature precursor for five different tRNAs in control fibroblasts. Changes in control cells under various oxidative stress conditions are shown in comparison to untreated control cells (control = 1). **(B)** Displays the ratio of total (mt)tRNA amount to immature precursor in R130C fibroblasts. Alterations in cells with the R130C mutation under various oxidative stress conditions are shown in comparison to untreated R130C cells (control = 1). **(C)** Shows the ratio of total (mt)tRNA amount to immature precursor for five different tRNAs in Q165H fibroblasts. Changes under various oxidative stress conditions are shown in comparison to untreated Q165H cells (control = 1).

Interestingly, the amount of mitochondrial tRNA precursors increases in control fibroblasts under all oxidative stress conditions tested, as indicated by the ratio of total tRNA to precursor < 1 (fig. 31A). In contrast, cells carrying the R130C mutation display a decrease of mitochondrial tRNA precursors upon oxidative stress induced by rotenone

treatment indicated by the ratio of total tRNA to immature precursors > 1 (fig. 31B). Cells carrying the benign Q165H mutation exhibit a mixture of slightly increased and decreased (mt)tRNA precursors (fig. 31C). In these cells, there is an obvious trend of precursor accumulation upon oxidative stress like in control fibroblasts. But also a slight decrease of mitochondrial tRNA precursors that is found in fibroblasts with the R130C mutation can be observed with the Q165H mutation. The overall amount of total tRNA varies slightly but does not change significantly in all cases.

Thus, mutated fibroblasts behave differently under oxidative stress. Control fibroblasts react to oxidative stress by an accumulation of unprocessed mitochondrial tRNA precursors. Mutated fibroblasts are not able to respond in the same way but rather display a decrease depending on the mutation.

4.6.4. Effect of impaired RNaseP activity on mitochondrial translation

HSD10 plays a role in the correct post transcriptional processing of mitochondrial tRNAs and concurrently functions in the maturation of mitochondrial mRNAs and rRNAs according to the "tRNA punctuation model of RNA processing in human mitochondria" (Ojala et al, 1981). Therefore, in a HSD10 loss-of-function scenario polycistronic mitochondrial transcripts are not processed correctly and consequentially not only the immature precursors of (mt)tRNAs but also the level of unprocessed mitochondrially encoded mRNAs accumulate. The concurrent lack of mature (mt)tRNAs and mature mRNAs caused by impaired (mt)RNaseP function due to HSD10 knock-down or mutation should lead to a reduction or stop of protein translation for all proteins that are encoded mitochondrially. Proteins that are transcribed from nuclear DNA and that are imported into mitochondria after they have been translated in the cytosol should not be affected.

To analyse on a translational level, whether a decrease in mitochondrial protein translation occurs after HSD10 loss-of-function and whether mutated and control fibroblasts respond differently to oxidative stress conditions, protein amounts of two different subunits of complex IV were determined. Complex IV (cytochrome c oxidase, COX) is a large integral membrane protein complex of the respiratory electron transport chain in mitochondria. It transfers electrons from cytochrome c to oxygen, converting them to water. In addition, it transports protons across the membrane, helping to establish the membrane potential that drives the motor force of ATP synthase. The complex consists of 13 subunits in mammals, ten of which originate in the nucleus (e.g. subunit COXIV) and three in mitochondria (e.g. subunit COXI). The amount of the nuclear encoded subunit IV of complex IV (COXIV) should not be affected by HSD10 loss-of-function by knock-down or mutation. In contrast, the amount of the mitochondrially encoded subunit I of complex IV (COXI) should display a decrease upon HSD10 knock-down. In this situation the correct processing of mitochondrial transcripts and consequentially the translation of proteins encoded in mitochondria is abolished. Existing endogenous protein is not concerned but every protein becomes degraded after a certain time and is newly synthesised. A disturbance in the synthesis should cause a decrease in mitochondrially encoded proteins (in this case subunit COXI) which would probably arise with a delay to the accumulation of tRNAs after 3-4 days. Thus, the impact of impaired

mitochondrial translation will be detectable at least 4 days after HSD10 knock-down depending on the stability of the tested protein subunits.

HSD10 was knocked-down in HeLa cells and the amount of COXIV and COXI was determined on a Western Blot (fig. 32A). This system also provides the possibility to test the mutations found in HSD10 deficiency patients for differences in their behaviour under physiological and oxidative stress conditions (fig. 32B). Therefore, untreated fibroblasts or fibroblasts treated with rotenone were analysed for their amount of nuclear and mitochondrially encoded protein subunits, respectively.

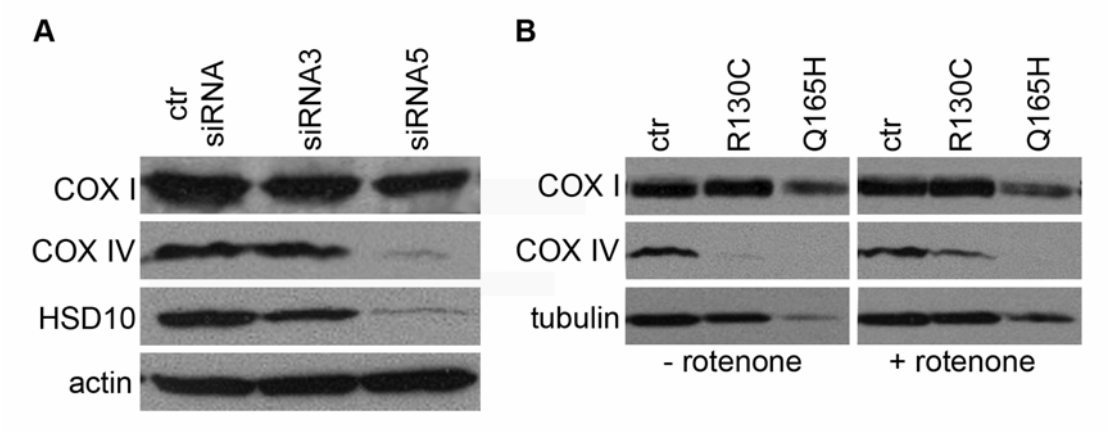

Figure 32 Comparison of nuclear and mitochondrial translation after HSD10 loss-of-function. (A) Transient transfection of HeLa cells was achieved using Lipofectamine and 60 pmol of an inert negative control siRNA or siRNA3 and 5 targeting the ORF of HSD10. Protein extract was prepared four days post transfection and analysed by SDS-PAGE and Western Blot using anti-COXI and anti-COXIV antibodies. HSD10 and actin levels were analysed as knock-down and loading controls. **(B)** Fibroblasts from HSD10 deficiency patients were left untreated or were treated with 500 nM rotenone for three days before protein extract was prepared and analysed by SDS-PAGE and Western Blot using anti-COXI and anti-COXIV antibodies. Tubulin levels were detected as a loading control. ctr: control.

The comparison of COXI and COXIV protein levels in cells where HSD10 is efficiently knocked-down indicates that the amount of mitochondrially encoded subunit COXI is slightly reduced upon HSD10 knock-down (fig. 32A top). However, the nuclear encoded subunit COXIV is significantly stronger reduced. In patient fibroblasts the mitochondrially encoded subunit COXI is not reduced but rather increased (fig. 32B left, top) under physiological conditions (- rotenone), whereas the nuclear encoded subunit COXIV is again strongly reduced compared to control cells (fig. 32B left, middle). There are no significant changes in protein amounts (COXI, COXIV or tubulin) upon rotenone treatment.

This suggests that mitochondrial translation is slightly impaired upon HSD10 knock-down but not affected in patient fibroblasts under physiological or oxidative stress conditions.

4.6.5. RNaseP dependency of apoptosis induced by HSD10 loss-of-function

It has been shown previously in *Xenopus* embryos, in human cells and in cells from conditional knock-out mice that HSD10 loss-of-function elicits an increase in apoptosis (Rauschenberger et al, 2010). This phenotype has been attested to be specific for HSD10 knock-down since it can be rescued by the addition of human HSD10 wildtype and partially by the mild Q165H mutation.

Unfortunately, the deployed apoptotic pathway is still unknown but next it was analysed if the induction of apoptosis is dependent on the function of HSD10 as a component of the (mt)RNaseP complex. To address this question, a siRNA mediated knock-down of nuclear encoded HSD10 was performed in cells that have been depleted of mitochondrial DNA (fig. 33). Low doses of ethidium bromide inhibit replication of mitochondrial DNA and thus generate so-called rho zero (rho0, ρ^0) cells which lack mitochondrial DNA and as a consequence critical subunits of the respiratory chain. Those cells still have small mitochondria but they cannot support normal oxidative phosphorylation and depend on supplementation of pyruvate (2.5 mM) and uridine (100 µg/ml) in the culture medium. Rho0 cells are generally used to examine the role that mitochondria play in distinct physiological pathways e.g. apoptosis (Chandel & Schumacker, 1999; Lee et al, 2004).

If the induction of apoptosis upon knock-down of HSD10 is due to impaired (mt)RNaseP activity and thus dependent on mitochondrial translation, rho0 cells that do not comprise mitochondrial DNA and consequentially mitochondrial translation should not be affected by the apoptotic phenotype caused by HSD10 knock-down.

BTK-143 osteogenic sarcoma cells were used for HSD10 knock-down either as untreated wildtype cells or as rho0 cells depleted of their mitochondrial DNA (fig. 33). As a control BTK-143 rho0 cells were re-substituted with mitochondrial DNA (haplotype H or T). Transient knock-down of HSD10 in these cells was performed and the ratio of apoptotic cells was determined by DAPI staining and microscopic evaluation of the morphological structure of nuclei. DAPI (4', 6-diamidino-2-phenylindole) preferentially binds to AT rich parts of DNA and fluoresces in bright blue when excited with ultraviolet light. It is used as a specific marker for nuclei and enables the analysis of nuclear morphology. Apoptotic nuclei are discernible by an irregular nuclear membrane and beginning chromatin condensation early in apoptosis. At later stages nuclear fragmentation and the formation of nuclear apoptotic bodies takes place. Nuclear apoptotic bodies are irregular blebbings of the nuclear membrane containing membrane-bound chromatin.

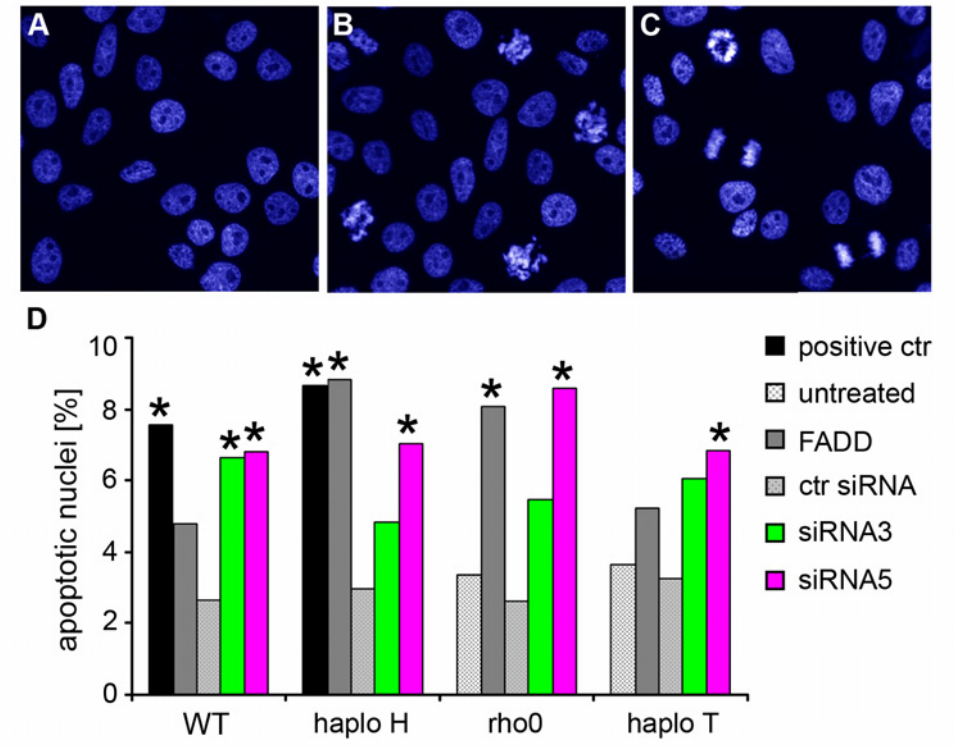

Figure 33 Apoptosis induced by HSD10 knock-down in BTK-143 cells. BTK-143 osteogenic sarcoma cells were used as wildtype cells (WT), rho0 cells (depleted of mitochondrial DNA) or as two control cell lines haplotype H and haplotype T (depleted of mitochondrial DNA and re-substituted with mitochondrial DNA). BTK-143 cells were transfected with 1 µg of FADD plasmid or 60 pmol of inert negative control siRNA, siRNA3 or siRNA5, using Lipofectamine. 48 hours post transfection cells were fixed and samples used as a positive control were treated with DNaseI for 10 min prior to the labelling procedure. Chamber slides were then transferred to DAPI for 10 min, mounted in Mowiol and observed by fluorescent microscopy. Exemplary pictures of normal nuclei **(A)** and apoptotic nuclei **(B)** in contrast to mitotic nuclei **(C)** stained with DAPI are shown. **(D)** Indicates the percentage of apoptotic nuclei for each sample scored by their morphological appearance in DAPI staining. Significant differences compared to cells treated with negative control siRNA were calculated by the student t-test. * indicates significance at $p \leq 0.01$. ctr: control, WT: wildtype, haplo H and T: haplotypes H and T.

The normal ratio of apoptotic BTK-143 cells in culture lies between 2.6 and 3.6 % judged by the percentage of apoptotic nuclei in the untreated control and in cells treated with an inert negative control siRNA (fig 32D). This applies to all BTK-143 cells: wildtype, rho0 or haplotype T and H, respectively. DNaseI incubation and transfection with apoptosis inducing FADD (Fas-Associated protein with Death Domain) were used as a positive control. These treatments increase the ratio of apoptotic cells to 4.8-8.8 %. Likewise, transfection with HSD10 targeting siRNA3 and siRNA5 raises the ratio of apoptotic cells to 4.8-6.6 % for siRNA3 and 6.8-8.6 % for siRNA5 in control as well as in rho0 BTK-143 cells.

Interestingly, HSD10 knock-down in rho0 BTK-143 cells causes an increase in apoptosis although these cells do not comprise mitochondrial translation and thus, (mt)RNaseP function. Therefore, the induction of apoptosis upon HSD10 loss-of-function is not dependent on RNaseP function in mitochondria.

To verify these results obtained with DAPI staining, the activity of a key mediator in apoptosis, caspase-3, was determined (fig. 34). Caspase-3 is activated in apoptotic cells both by extrinsic and intrinsic signals. It is an executioner caspase that is responsible for chromatin condensation and DNA fragmentation.

Again, BTK-143 osteogenic sarcoma cells were used for HSD10 knock-down with siRNA3 either as untreated wildtype cells or as rho0 cells depleted of their mitochondrial DNA. As a control BTK-143 osteogenic sarcoma rho0 cells were re-substituted with mitochondrial DNA (haplotype H or T). The ratio of apoptotic cells was determined by microscopic evaluation of active caspase-3 positive cells in immunofluorescent stainings (fig. 34).

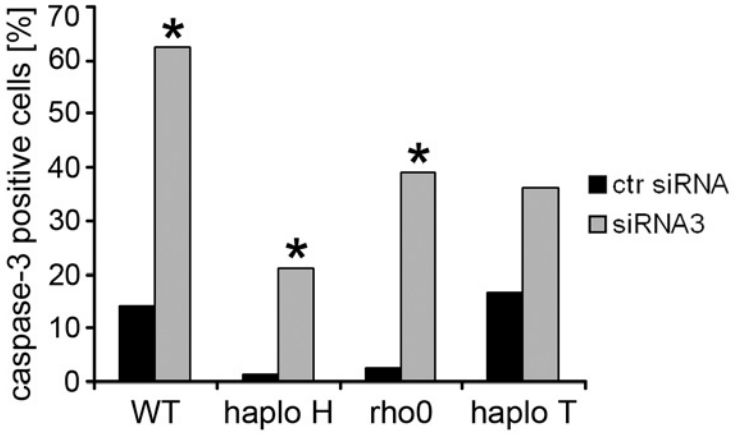

Figure 34 Caspase-3 activity induced by HSD10 knock-down in BTK-143 cells. BTK-143 osteogenic sarcoma cells were used as wildtype cells (WT), rho0 cells (depleted of mitochondrial DNA) or as two control cell lines haplotype H and haplotype T (depleted of mitochondrial DNA and re-substituted with mitochondrial DNA). BTK-143 cells were transfected with 60 pmol of inert negative control siRNA or siRNA3, using Lipofectamine. 48 hours post transfection cells were fixed and active caspase-3 was detected using polyclonal rabbit anti-cleaved caspase-3 antibody (1:100). After incubation with the secondary antibody (anti-rabbit Alexa 594, 1:1000) cells were washed, counterstained with DAPI nuclear stain and mounted in Fluorescence Mounting Media. Cells were counted in five randomly chosen visual fields and the percentage of caspase-3 positive cells is indicated here for each sample. Significant differences compared to cells treated with negative control siRNA were calculated by the student t-test. * indicates significance at $p \leq 0.01$. ctr: control, WT: wildtype, haplo H and T: haplotypes H and T.

The knock-down efficiency of the transient transfection of BTK-143 cells with siRNA3 was confirmed by a simultaneous immunostaining for HSD10 protein (data not shown). Since the fluorescent signal for active caspase-3 and HSD10 was captured under comparable conditions for each sample a semi-quantitative conclusion can be drawn about the abundance of HSD10 in the knock-down samples compared to controls. The fluorescent signal was categorised as "normal" or "weaker than normal". On average, 7.6 % of control siRNA treated cells have a weaker signal for HSD10 than normal (2.7 % in haplotype H cells to 13.9 % in haplotype T cells, data not shown). In contrast, 34.4 % of

siRNA3 treated cells display a lower signal for HSD10 than normal (27.3 % in haplotype H cells to 39.3 % in wildtype cells).

The ratio of BTK-143 cells, that are positive for active caspase-3 after transfection with an inert negative control siRNA, lies between 1.4 and 16.7 % judged by the percentage of fluorescent cells in all BTK-143 cells (wildtype, rho0, haplotype H and T). Transfection with siRNA3 targeting HSD10 raises the ratio of apoptotic cells to 21-62.5 % judged by the percentage of cells that are positive for active caspase-3 (fig. 34). This verifies the result shown before, that HSD10 knock-down in rho0 BTK-143 cells causes an increase in apoptosis (fig. 34) although these cells do not comprise mitochondrial translation and thus, (mt)RNaseP function.

In conclusion, these experiments show that the induction of apoptosis after HSD10 loss-of-function is not dependent on the mitochondrial transcription and translation machinery including RNaseP. An as yet unknown function of HSD10 that is independent of its dehydrogenase and tRNA 5’ processing function is required for cellular integrity and viability.

5 DISCUSSION

5.1. A dehydrogenase-independent function of HSD10 is essential for mitochondrial integrity

Several lines of evidence support the suggestion that HSD10 has an additional function apart from its important dehydrogenase role in mitochondrial metabolism. HSD10 loss-of-function led to enhanced apoptotic cell death (Rauschenberger et al, 2010) and had adverse effects on mitochondrial structural integrity (fig. 14-17).

First, complete loss of the HSD10 protein in *Drosophila* is embryonic lethal (Torroja et al, 1998). Also in mouse causes the complete HSD10 knock-out lethality at very early stages of embryogenesis (day 5 p.f.; Rumig, 2006). It is unlikely that the embryonic lethality is due to the lack of enzyme activity, because it was shown for defects in comparable metabolic enzymes that toxic metabolites are efficiently eliminated by the placenta. A conditional knock-out in mice led to severely disrupted mitochondrial morphology in neurons of the CNS in the locus coeruleus and in some neurons of the PNS in the superior cervical ganglia (fig. 15 and 16), indicating that HSD10 is essential for mitochondrial integrity.

Knock-down of HSD10 in *Xenopus* was not embryonic lethal since HSD10 is also provided maternally and the knock-down was only carried out in specific regions of the body by targeted microinjection. Knock-down of HSD10 in *Xenopus* animal caps resulted in a severe disruption of mitochondrial structure, and also mitochondrial function was impaired (fig. 17 and 18). Both effects could be rescued by co-injection of a human wildtype HSD10 construct. Additionally, the knock-down of HSD10 in *Xenopus* led to enhanced apoptosis in injected tissue and this effect could also be rescued by human HSD10 wildtype protein (Rauschenberger et al, 2010). The mutated HSD10 proteins found in human patients, however, showed remarkable differences in their ability to rescue the apoptotic phenotype. The Q165H mutation, which has less than 3 % residual enzymatic activity but was identified in three neurologically normal boys, partially rescued HSD10 Mo^{ATG}-induced apoptosis. In contrast, injection of the mutations R130C and in particular D86G failed to rescue, and instead further enhanced apoptosis (Rauschenberger et al, 2010). D86G has considerable residual enzyme activity (28 %) despite being associated with a very severe clinical phenotype.

Thus, HSD10 is required for mitochondrial integrity in *Xenopus* and mice. Apoptosis after HSD10 loss-of-function is not dependent on the dehydrogenase activity of HSD10, arguing for a non-dehydrogenase function of this protein.

Secondly, HSD10 deficiency in humans causes an atypical organic aciduria (Zschocke et al, 2000; Ensenauer et al, 2002; Olpin et al, 2002). Neurological abnormalities in organic acidurias are usually attributed to accumulation of toxic substrates proximal to a specific enzymatic block, causing secondary interference with energy metabolism (Deodato et al, 2006). Primary apoptotic nerve cell death as it was observed in HSD10 deficiency is not usually a feature of organic acidurias. Measurements of enzymatic activity in patient fibroblasts revealed that the R130C and D86G mutations associated with classical and neonatal neurodegenerative forms of HSD10 deficiency had up to 64 % residual activity

compared to the wildtype protein. In contrast, the Q165H mutation that was identified in three children with normal neurological development was associated with less than 3 % residual enzymatic activity (Rauschenberger et al, 2010). Thus, the severity of the clinical phenotype is not at all correlated with the enzymatic activity of the mutated HSD10 proteins. Also, symptoms observed in patients are not due to the accumulation of toxic metabolites in the isoleucine pathway. 3-ketothiolase deficiency, the enzyme catalysing the last step in the breakdown of isoleucine, causes the same metabolites in urinary organic acid assays but a completely different clinical picture not including progressive neurodegeneration but rather the classical symptoms of an organic aciduria (Ozand et al, 1994). Also, an isoleucine restrictive diet that avoids the accumulation of potentially toxic metabolites failed to improve the condition of patients (unpublished data).

In contrast to most other metabolic disorders, no null mutations that completely eliminate the protein have been identified in HSD10 deficiency patients. One particular mutation, R130C, is found in more than half of the cases and has usually occurred *de novo* in the respective patients (Ofman et al, 2003; Perez-Cerda et al, 2005). There is no evidence that the corresponding nucleotide change c.388C>T represents a hypermutable position, raising the possibility that most other mutations in the HSD17B10 gene are not observed because they are incompatible with life. This again is highly unusual for organic acidurias that usually manifest after birth only, since prenatally toxic metabolites are removed via the placenta.

Protein localisation of mutated HSD10 was not altered in patient fibroblasts (fig. 10) indicating that simple mis-localisation of the mutations cannot be causative for the clinical phenotype.

Therefore, the loss of enzyme activity, the accumulation of toxic metabolites, and the protein localisation, are not the reason for the clinical phenotype of HSD10 deficiency patients.

In contrast to an immuno fluorescent staining of the mitochondrial protein porin which did not show any differences in the mitochondrial network between control and mutated fibroblasts (fig. 10), the staining with a Mitotracker and the electron microscopic analysis (fig. 14) revealed alterations of the reticular network as well as the subcellular structure of mitochondria. Fibroblasts from HSD10 deficiency patients carrying the two severe mutations displayed aberrant mitochondria in contrast to control cells and cells with the Q165H mutation. The observed fragmentation of the mitochondrial network is known to be a feature of apoptotic cell death (Karbowski & Youle, 2003). This indicates that a non-dehydrogenase effect of HSD10 is required for mitochondrial integrity and a loss-of HSD10 function triggers mitochondrial disintegration and apoptosis (Rauschenberger et al, 2010 and fig. 14).

Cellular energy failure caused by mitochondrial dysfunction is thought to play an important role in the development of AD (Alzheimer's disease), and several studies indicated that this effect is caused by a direct interaction of amyloid β with HSD10 (Yan et al, 1997; Lustbader et al, 2004). HSD10 protein or transcript was found to be increased in affected neurons in human AD as well as in AD mouse models and it has been suggested that overexpression of HSD10 amplifies amyloid β -mediated

mitochondrial toxicity (Chen & Yan, 2007). However, a recent study showed that a mitochondrial bioenergetic deficit precedes HSD10 overexpression and Alzheimer's pathology in an AD mouse model (Yao et al, 2009). The results of our study, the first to examine the effect of HSD10 loss-of-function, indicate that adverse effects observed as a consequence of the binding of amyloid β to HSD10 are more likely due to the loss of a non-enzymatic HSD10 function, and that increased amounts of (non-functional) HSD10 protein may be produced as a secondary or compensatory mechanism. It thus remains possible that the mitochondrial interaction of amyloid β with HSD10, triggering early dysfunction of energy homeostasis, is one of the first steps in the pathogenesis of AD.

5.2. HSD10 function in apoptosis, RNaseP activity and cellular stress

5.2.1. HSD10 function in apoptosis

Not only the loss-of-function of HSD10 but also its overexpression led to a mild induction of apoptosis (fig. 19). The two mutations R130C and D86G strongly induced apoptosis and may have a dominant-negative effect on the initiation of apoptosis which is not due to the UPR of the ER or mitochondria that is often triggered by overexpression of (mutated) proteins (fig. 20). Interestingly, the R130C mutation induced apoptosis in a dominant-negative manner (fig. 19) although it has been shown that the mutated protein is less stable (Rauschenberger et al, 2010).

The characterisation of the apoptotic pathway that is initiated by HSD10 loss-of-function revealed three genes, CD40, TNFRSF9 and TNFSF15, that were upregulated with both siRNAs targeting HSD10 (table 2). Interestingly, two of these genes, TNFRSF9 and TNFSF15 were also upregulated in fibroblasts with the R130C mutation, which is associated with a severe clinical disease course, but not with the benign Q165H mutation. All three genes are members of the TNF (tumour necrosis factor) superfamily and have a pro-apoptotic function (Georgopoulos et al, 2006; Schwarz et al, 1996; Simon et al, 2001; Yu et al, 2001). Proteins of this family are associated with the extrinsic pathway of apoptosis induction, although ligand binding to CD40 has been reported to also trigger the intrinsic pathway and upregulation of Bax expression (Georgopoulos et al, 2006). TNFSF15 is a cytokine that can activate NFκB signalling (Wen et al, 2003) and was found to inhibit angiogenesis by blocking endothelial cell proliferation (Yu et al, 2001). Both functions are very interesting since UXT, a potential binding partner of HSD10, is also involved in NFκB signalling (see 5.3.) and angiogenesis was found to be impaired in *Xenopus* embryos upon HSD10 knock-down (Guerra, 2010; Rauschenberger, 2007). In addition mice with a conditional knock-out of HSD10 in vascular endothelium (Tie2-cre mice) indicated that these animals have an aberrant blood system (Rumig, 2006). Organisation and structure of endothelial tissue appears normal but blood flow and the ability of blood vessels to dilate after a contraction are seriously inhibited (unpublished data). In contrast, *Xenopus* embryos depleted of HSD10 exhibited a severe reduction of endothelial blood vessels in the injected region which would be in line with the upregulation of TNFSF15 in human cells and the impaired blood vessel function in mice (Guerra, 2010; own unpublished data).

HSD10 loss-of-function might activate the extrinsic apoptosis pathway as indicated by the upregulation of three pro-apoptotic genes associated with the extrinsic pathway, CD40, TNFRSF9 and TNFSF15. Therefore, the mitochondrial disintegration observed upon HSD10 loss-of-function (fig. 14, 15, 16 and 17) would be a secondary effect. The loss of an essential non-dehydrogenase function of HSD10 can induce apoptosis which is not necessarily initiated but followed by mitochondrial disintegration. One possible explanation could be that the loss of the small amount of HSD10 which has been shown to be localised in the cytosol triggers the initiation of the extrinsic apoptotic pathway (see 5.3.).

Nevertheless, the regulation of apoptotic genes upon HSD10 loss-of-function should be interpreted with caution because this regulation of gene expression was a result of a transient transfection evaluated after 48 h post transfection. Hence, it is not surprising that there was a mixture of pro- and anti-apoptotic genes within the regulated genes because the cells might try and compensate the apoptotic signals at first. This transient effect does probably not fully reflect the situation in patients. Also in patient fibroblasts a mixture of pro- and anti-apoptotic genes was regulated compared to control cells. This was to be expected because these cells are viable and not undergoing apoptosis in culture. Also, these results are based solely on transcriptional analysis of genes that are regulated upon HSD10 knock-down. Transcriptional regulation is by far not the only and not the main regulatory level of apoptosis. The strongest and the most immediate regulation occurs on protein level. For example, caspases are present in inactive pro-forms and are activated by proteolytic cleavage, as well as posttranslational modifications such as phosphorylation which regulate protein activity. Another level of regulation is the subcellular re-distribution of proteins like BAX and cytochrome c that leak from mitochondria and then set off apoptosis in the cytosol.

Therefore, the induction of extrinsic apoptosis upon HSD10 loss-of-function should also be confirmed on protein level. Antibody-protein-arrays which simultaneously detect the relative level of several (active) apoptosis related proteins in cell lysates are commercially available. Alternatively active cleaved caspase-8 and caspase-9 can be detected specifically on a Western Blot. Activation of these two caspases distinguishes clearly between intrinsic and extrinsic apoptosis pathways.

5.2.2. HSD10 function under cellular stress

Reduction, loss or mutation of HSD10 in *Xenopus*, mouse and humans had adverse effects on mitochondrial integrity and led to enhanced apoptotic cell death and reduced viability (Rauschenberger et al, 2010). Consistently, a protective effect in mitochondria at times of increased oxidative stress has been implied for overexpressed HSD10 in the setting of acute brain damage (Yan et al, 2000a) and in a mouse model of Parkinson's (Tieu et al, 2004). One dehydrogenase-independent function of HSD10 may be to protect mitochondria at times of increased metabolic stress. The described induction of apoptosis upon overexpression of mutated HSD10 (mutation R130C and D86G; fig. 19) could be due to a disturbance of this protective function.

This interpretation is compatible with the observation that infections or other stress situations in patients with HSD10 deficiency may trigger clinical deterioration. In response to metabolic stress, HSD10 protein translocates from the mitochondrial matrix to the inner mitochondrial membrane (fig. 13) and this might be important for maintaining mitochondrial integrity as this is an essential site for assembly of the mitochondrial membrane permeability transition pore (Tieu et al, 2004). It appears plausible that interaction of HSD10 with a soluble protein in the mitochondrial matrix or with an integral protein of the mitochondrial membrane could mediate its protective effect and that this interaction is disturbed by altered HSD10 protein structure due to specific mutations. One such protein could be CypD (cyclophilin D; Ren, 2008), which is localised in the mitochondrial matrix and is recruited to the inner membrane under oxidative stress in order to form the MPTP (mitochondrial permeability transition pore; Connern & Halestrap, 1994). Binding of HSD10 and CypD in the mitochondrial matrix might block its participation in pore formation and thus, HSD10 might have a protective, anti-apoptotic dehydrogenase-independent function in the mitochondrial matrix (Yan & Stern, 2005). This function might be disturbed upon mutation of HSD10. The functional interaction of HSD10 and CypD remains to be confirmed. An additional candidate for an interaction with HSD10 at the mitochondrial membrane that might mediate the protective function of HSD10 is ATP synthase (fig. 27, table 6 and 7). This interaction has been found in an IMAC approach for wildtype HSD10 but not for the mutated proteins.

Several potential interaction partners of HSD10 inside mitochondria were identified by the purification of HSD10 together with bound proteins on an IMAC column. The comparison of the proteins eluted together with HSD10 wildtype or the mutations and a control protein on a silver stained gel revealed binding partners of HSD10 that show differences in their ability to bind to wildtype or mutated HSD10. The finding that mutated HSD10 protein cannot interact with certain proteins in the mitochondrial matrix or at the mitochondrial membrane could explain why mutant HSD10 cannot execute the protective function in mitochondria. In this experimental approach three proteins were of particular interest because they are localised in mitochondria and they play a role in energy metabolism and stress response: ATP synthase subunits, ribosomal proteins and IbpA (table 7).

IbpA plays a role in the cellular heat shock response (Matuszewska et al, 2008; Thomas & Baneyx, 1998), and might interact with HSD10 under stress conditions in the

mitochondrial matrix. Once HSD10 is re-distributed upon oxidative stress, the wildtype but not the mutated protein might bind to ATP synthase at the mitochondrial membrane. It is interesting to note that ATP synthase also co-purified in an approach to partially purify RNaseP (Holzmann et al, 2008). This could be due to a physical interaction of HSD10 and ATP synthase subunits. Binding of HSD10 to integral proteins of the mitochondrial membrane like ATP synthase might protect them from oxidative stress or could stimulate ATP production that helps the cell to cope with increased stress. In order to investigate if those proteins functionally interact in the human cellular stress response, the physical interaction of these proteins has to be confirmed in *in vitro* assays like Co-IP or GST pull-down.

In our IMAC approach to identify novel interaction partners of HSD10 none of the previously reported binding proteins in mitochondria like CypD, estrogen receptor α and MRPP1 and MRPP3 emerged. Therefore, an additional technique like SPINE (Strep-protein interaction experiment; Herzberg et al, 2007) or combination of techniques like the "partial purification overlap proteome" employed to purify RNaseP (Holzmann et al, 2008) could help to verify the interaction of these candidate proteins with HSD10 or identify additional binding partners of HSD10.

Since patients with the R130C mutation show a severe clinical phenotype which develops after times of increased metabolic stress, it was expected that cells with this mutation are more sensitive to stress than control cells or cells with the Q165H mutation. When patient fibroblasts were assayed for general cell viability under stress, no stress conditions tested in this study caused fibroblasts with the R130C mutation to be more sensitive than the Q165H cells (fig. 23 und 24)

It is possible that fibroblasts are not the most appropriate cell type to investigate the effect of stress on cell viability. Cells that depend on a higher energy metabolism like heart or muscle cells are probably more susceptive to increased stress and could display differences for the two mutations upon stress that fibroblasts do not. Also, cell viability might not be the only possible readout for these stress experiments. The cellular stress response might be very different in mutated cells without displaying a reduced viability.

Rotenone treatment causes enhanced transcription in cell culture (Greene et al, 2010; MacKenzie et al, 2008; Ishikawa et al, 2009). Accordingly, control cells apparently reacted to oxidative stress by an activation of mitochondrial transcription and a subsequent accumulation of unprocessed transcripts (fig. 31). Since HSD10 has been found to play a role in the 5' processing of mitochondrial tRNAs (Holzmann et al, 2008) these transcripts were used as a readout for mitochondrial transcription upon oxidative stress.

When patient fibroblasts carrying different mutations in the HSD17B10 gene were assayed for tRNA precursor accumulation they displayed different behaviour upon oxidative stress than control cells. Control fibroblasts responded to oxidative stress by an increase in the amount of immature mitochondrial tRNA precursors (fig. 31A). Mutated fibroblasts were not able to respond in the same way but the R130C mutation rather

displayed a decrease in tRNA precursors (fig. 31B). Fibroblasts with the Q165H mutation appeared to behave more like wildtype cells than like the R130C mutation (fig. 31C).

Therefore, fibroblasts with the R130C and Q165H mutation seem to be unable or less able, respectively, to stimulate tRNA transcription upon oxidative stress.

Activation of transcription appears to be a protective reaction of mitochondria compensating cellular stress. HSD10 expression has been shown to be upregulated in stress situations like hypoxia-ischemia, nutritional stress and the presence of amyloid plaques (Yan et al, 2000a; Yan et al, 2000b; Yan & Stern, 2005). Similarly, oxidative stress induced by rotenone could stimulate HSD10 transcription, since it has been shown to have a protective effect in mitochondria at times of increased oxidative stress. Binding of HSD10 to (potential) binding partners in mitochondria that play a role in cellular stress response (like ATP synthase, IbpA, Rsp5p and Cmk1p) might be important for this protective effect of HSD10 in mitochondria. Mutation of HSD10 could abolish the binding to its usual interaction partners and thereby its protective function. This could cause general mitochondrial damage including disruption of mitochondrial structure (fig. 14). Consequentially, impaired mitochondria of fibroblasts with the R130C and Q165H mutation are unable to stimulate mitochondrial transcription in the same way as control cells.

5.2.3. Function of HSD10 as a component of human mitochondrial RNaseP

HSD10 is a component of the human mitochondrial RNaseP complex and functions in the 5' processing of mitochondrial tRNAs (Holzmann et al, 2008). Consequentially, a knock-down of HSD10 causes the accumulation of immature mitochondrial tRNA precursors. The previously published accumulation (Holzmann et al, 2008) did only occur for one of two tested siRNAs for HSD10 and was only shown for two tRNA precursors, which were very different in their level of accumulation. Also the level of total tRNA was not considered.

Therefore, this effect was confirmed in this study with two siRNAs targeting HSD10 and for several tRNA precursors. All tested tRNA precursors accumulated upon HSD10 knock-down but with different kinetics (fig. 28). The previously published accumulation occurred nine days after HSD10 knock-down and ranged from a 5- to 65-fold increase. In contrast, the siRNAs used here gave rise to an accumulation of immature tRNA precursors after three or four/five days and ranged from a 7- to 91-fold increase. The total amount of tRNAs was also altered upon HSD10 knock-down but in a smaller range than tRNA precursors, indicated by the ratio of total tRNA to tRNA precursor below 1.

On a translational level, the reduced amount of mitochondrially encoded complex IV subunit COXI indicates an inhibition of mitochondrial translation caused by impaired mtRNaseP function (fig. 32). This indicates that the processing of mitochondrial transcripts is impaired upon HSD10 knock-down which, in turn, impairs mitochondrial translation.

Interestingly, the nuclear encoded subunit COXIV was significantly stronger reduced upon HSD10 knock-down than the mitochondrially encoded subunit COXI. Just like

COXIV, one component of RNaseP, MRPP1, has been shown to be reduced upon HSD10 knock-down. Both reductions of nuclear encoded protein complex subunits could be explained by the instability of proteins that are not integrated into a protein complex. Although it is possible that COXIV may need mitochondrially encoded proteins such as COXI in order to be stable, a secondary effect caused by primary reduction of COXI upon HSD10 knock-down is not very likely since the nuclear encoded subunit is reduced in a much higher degree than the mitochondrially encoded subunit. In contrast, it is not surprising that MRPP1 could be unstable if HSD10 is not present, causing deficient assembly of the RNaseP complex.

An alternative explanation for the concurrent reduction of nuclear encoded COXIV and MRPP1 upon HSD10 knock-down could be an effect of HSD10 on general nuclear transcription. In fact there is preliminary evidence that a link between HSD10 and the transcriptional machinery may exist. Two proteins, UXT and PCBP1 that were found to interact with HSD10 in a yeast-2-hybrid analysis, are known regulators of transcription (see 5.3.). Provided that there is a cytosolic fraction of HSD10, this interaction could influence nuclear gene expression (see 5.3.).

To address this question, the level of MRPP1 and COXIV mRNA upon HSD10 knock-down should be determined. A concurrent reduction of MRPP1 and COXIV mRNA together with HSD10 would suggest an effect of HSD10 on the transcriptional level. Also, protein and transcript levels for proteins that do not bind to HSD10 should be determined to exclude protein subunit instability as a cause for reduced protein amounts.

The function of HSD10 in mitochondrial tRNA processing could be the underlying reason for the clinical phenotype in HSD10 deficiency patients. Mutations in mitochondrial tRNAs cause disturbances of mitochondrial translation that elicit many different clinical syndromes including MERRF (myoclonic epilepsy and ragged red muscle fibres; Finnila et al, 2001), mitochondrial myopathy (Swalwell et al, 2006), CPEO (chronic progressive external ophtalmoplegia; Spagnolo et al, 2001), progressive respiratory failure (Bruno et al, 2003), MELAS (mitochondrial myopathy, encephalopathy, lactic acidosis, stroke-like episodes; Tzen et al, 2003) and ADPD (Alzheimer's and Parkinson's disease; Wallace et al, 1992). Like HSD10 deficiency some of these mitochondriopathies feature a progressive neurodegenerative clinical phenotype. MELAS patients exhibit blood vessel abnormalities such as dysfunction of endothelium-dependent vasodilation (Koga et al, 2006) which could be similar to the effect of a HSD10 knock-out observed in conditional Tie2 knock-out mice and *Xenopus* embryos (Guerra, 2010; Rauschenberger, 2007).

Mutation of one of the components of RNaseP also disrupts mitochondrial translation but this seems not to be the underlying reason for the clinical phenotype in HSD10 deficiency patients since all three mutations found in patients had considerable residual mtRNaseP activity in a rescue experiment. All mutations alike were able to rescue the accumulation of immature precursors in the knock-down situation (fig. 29). The mutations were not as active in their RNaseP activity as the wildtype protein, but no dominant-negative effect on (mt)RNaseP activity was observed. Reduced (mt)RNaseP activity of the HSD10 mutations could result from impaired interaction of mutated HSD10 with the other two components of RNaseP.

The interpretation of this finding is somehow difficult because co-transfection of siRNA and DNA that can be targeted by the siRNA does probably not result in an effective knock-down of endogenous wildtype HSD10 combined with full expression of transfected HSD10. Rather it will cause mixed translation of endogenous wildtype HSD10 and transfected wildtype/mutated HSD10. Still, there was an effect with the mutated and the wildtype protein compared to the knock-down situation and the wildtype and the mutated proteins displayed some differences in their ability to rescue, so there had to be at least some expression from the transfected plasmids.

In order to eliminate the difficulties of this kind of co-transfection, mitochondrial tRNA levels were determined in patient fibroblasts directly but tRNA precursors were not found to be accumulated as expected (fig. 30). In contrast, the total amount of mitochondrial tRNA as well as the level of precursors was strongly decreased in mutant cells. This effect was stronger in fibroblasts with the R130C mutation than in cells carrying the Q165H mutation.

On a translational level, there was also no evidence for an inhibition of mitochondrial translation, since the amount of mitochondrially encoded complex IV subunit COXI was not reduced. Interestingly, the nuclear encoded subunit COXIV was strongly reduced comparable to the HSD10 knock-down situation. Thus, mitochondrial transcript processing and translation is not affected in patient fibroblasts like it is upon HSD10 knock-down.

The reduction of all tRNA forms might be the long-term response to the mutations and the permanently impaired (mt)RNaseP activity in patients (fig. 30) in contrast to the transient effects upon siRNA mediated knock-down of HSD10 shown before (fig. 28). Permanent impairment of RNaseP activity might cause the cells to reduce overall transcription since the polycistronic transcripts cannot be processed. Also, the likewise reduction of mitochondrial total tRNA and nuclear encoded COXIV protein levels could indicate an effect of HSD10 on mitochondrial and nuclear transcription which can be measured e.g. by the new nanostring technique or by microarrays (see 5.3.). The degradation of protein subunits that are not incorporated into their respective complexes appears unlikely to play a role in this situation since COXI was not reduced in patient fibroblasts. Holzmann et al, 2008, introduced an elaborate assay to measure (mt)RNaseP activity *in vitro*. The analysis of (mt)RNaseP activity of purified mutant HSD10 proteins would help a great deal to characterise these mutations, their impact on cellular functions and the contribution of possibly impaired (mt)RNaseP activity to the clinical phenotype of HSD10 deficiency patients.

The induction of apoptosis upon HSD10 loss-of-function has been shown previously not to be dependent on the enzymatic dehydrogenase function of HSD10 (Rauschenberger et al, 2010). In this study it has also been shown to be independent of the function of HSD10 as a component of the (mt)RNaseP complex. Rho0 cells lack mitochondrial DNA and thus do not depend on mitochondrial transcript processing and translation. These cells induced apoptosis upon HSD10 loss-of-function just as well as wildtype cells (fig. 33 and 34).

This suggests that apoptosis upon HSD10 loss-of-function is triggered by a function of HSD10 that is independent of its function in mitochondria and that an as yet unknown function of HSD10 that is independent of its dehydrogenase and tRNA 5' processing function is required for cellular integrity and viability.

5.3. Dehydrogenase- and RNaseP-independent function of HSD10 outside of mitochondria?

As elaborated above, the function of HSD10, that is essential for cell viability and mitochondrial integrity, is independent of its dehydrogenase and RNaseP activity. Although the greater part of HSD10 is detectable in mitochondria, a small part seems to be distributed in the cytosol. Immunostaining and an overexpression experiment indicated that about 5 % of HSD10 appears to be localised in the cytosol (fig 10). Also, when cells initiate apoptosis and mitochondria start to permeabilise HSD10 could leak into the cytosol.

Several potential interaction partners of HSD10 and with that several potential functions in the cytosol have been proposed previously (fig. 25, table 5 and 7).

In an attempt to identify novel interaction partners of HSD10 a search in yeast was performed (table 4). Physical interaction between homologous proteins in yeast could point towards binding partners in humans. The yeast protein with the highest level of homology to HSD10 (up to 35 %) was FOX2 (multifunctional enzyme of the peroxisomal fatty acid β-oxidation pathway). This protein has 3-hydroxyacyl-CoA dehydrogenase activity but is not localised in mitochondria suggesting that HSD10 could also have a function outside of mitochondria. Also, none of the binding partners of FOX2 are mitochondrial proteins. Two interesting potential binding partners are Rsp5p and Cmk1p. Both proteins play a role in cellular stress response and might interact with HSD10 under stress conditions. Rsp5p is an E3 ubiquitin ligase involved in many different cellular events including transcription initiation and both, stress resistance upon heat shock (like IbpA, another potential binding partner of HSD10) and adaptation to a change of nutrients (Cardona et al, 2009). Cmk1p is a calmodulin-dependent protein kinase implicated in signal transduction in stress tolerance (Sakaguchi et al, 2010). Both yeast proteins have homologous proteins in humans: NEDD4L (neural precursor cell expressed, developmentally down-regulated 4-like; NP_001138439.1) and CAMK1D (calcium/ calmodulin-dependent protein kinase ID; NP_705718.1). In order to investigate if those proteins functionally interact in human cellular stress response, first of all this potential interaction has to be confirmed in *in vitro* assays like Co-IP or GST pull-down.

Two potential interaction partners were identified in a yeast-2-hybrid system with HSD10 as bait: PCBP1 and UXT. Again, both proteins interacting with HSD10 are not localised in mitochondria. Nevertheless, the interaction found in the yeast-2-hybrid system might play a role *in vivo* although the proteins are normally separated by compartments, but there also is the possibility of a HSD10 function outside of mitochondria.

The interaction of HSD10 with UXT (ubiquitously expressed transcript) seems possible since both proteins play a role in apoptosis and have been shown to act synergistically on the induction of apoptosis. When mutated HSD10 instead of wildtype HSD10 was used in a yeast-2-hybrid as bait the interaction of UXT and HSD10 appeared to be weaker for the two mutations associated with a severe clinical disease, although colonies in the yeast-2-hybrid system can in fact not be analysed quantitatively. The currently available data on the function of UXT in cell survival or cell death are contradictory (McGilvray et al, 2007; Moss et al, 2007; Zhao et al, 2005; Sun et al, 2007).

UXT is located predominantly in the nucleus and functions in androgen receptor-dependent transcription as a cofactor that binds to the androgen receptor (Markus et al, 2002). It has an inhibitory effect on a subset of AR-dependent genes (Taneja et al, 2004) including regulators of DNA damage checkpoint and cell cycle progression (Nwachukwu et al, 2009). Additionally a role for UXT in the cytoplasm has been proposed. UXT is located in centrosomes and associated with γ-tubulin (Zhao et al, 2005) and also a component of a multidomain organizer associated with mitochondria. This organizer integrates mitochondria and the microtubular cytoskeleton with chromosome remodelling, transcription and cytokinesis (Moss et al, 2007; Liu et al, 2002).

UXT also seems to be regulated in tumour tissue but again overexpression as well as decreased expression of UXT is found in tumours (Schroer et al, 1999; Zhao et al, 2005; Taneja et al, 2004).

Some publications postulate an inhibitory function of increasing amounts of UXT on cell proliferation and/or survival (McGilvray et al, 2007; Moss et al, 2007) others report an increase in apoptosis upon UXT knock-down (Zhao et al, 2005; Sun et al, 2007). UXT specifically interacts with NFκB in the nucleus and activates the expression of NFκB dependent genes (Sun et al, 2007). The knock-down of UXT inhibits NFκB dependent gene expression, which sensitizes cells to apoptosis by tumour necrosis factor α (Sun et al, 2007).

Similarly, all apoptotic genes that were upregulated upon HSD10 loss-of-function, CD40, TNFRSF9 and TNFSF15, are pro-apoptotic members of the TNF superfamily, which is usually associated with the extrinsic pathway. If HSD10 functions together with UXT in the activation of gene expression by NFκB, the loss of this essential non-dehydrogenase function of HSD10 could induce apoptosis via the extrinsic pathway associated with TNF family members. As mentioned above, the involvement of TNFs and NFκB in HSD10 function or the loss-of-function phenotype is very interesting. For example, TNFSF15, which is upregulated upon HSD10 loss-of-function, and UXT, which is a potential interaction partner of HSD10, both can activate NFκB signalling (Wen et al, 2003; Sun et al, 2007). NFκB signalling can regulate pro- and anti-apoptotic genes and can switch between both upon certain regulatory signals. NFκB also plays a role in the resistance of tumours against chemotherapeutic drugs and ionising radiation (Wang et al, 1996). In this connection it is interesting to note that HSD10 upregulation in tumour tissue has been found to be protective against chemotherapy and is thus correlated with poor response to chemotherapy (Salas et al, 2009).

Nevertheless, a functional interaction of UXT and HSD10 in the cytosol, which prevents the induction of apoptosis by UXT in the nucleus, was not detected in the *Xenopus*

system (fig. 25). Instead, UXT and HSD10 had an additive effect on the induction of apoptosis but the mechanism remains to be investigated. The most straight forward approach to clarify if those two proteins interact does not involve functional studies because little is known about the function of both proteins. In order to elucidate the participation of HSD10 in UXT/ NFκB signalling, first of all the physical interaction between UXT and HSD10 should be confirmed in *in vitro* assays like Co-IP, GST pull-down or FRET (fluorescence resonance energy transfer). Secondly, the regulation of NFκB dependent gene expression upon HSD10 loss- or gain-of-function could be assayed e.g. by qRT-PCR.

Another potential interaction partner of HSD10 in the cytosol is PCBP1. PCBP1 (PolyC binding protein 1), like UXT, could be a link between HSD10 and transcriptional regulation. It binds to mRNAs that contain a DICE (differentiation control element) in the cytoplasm and thereby represses their translation, e.g. the endogenous L1 cell adhesion molecule mRNA. Upon phosphorylation it releases the mRNAs for translation and migrates to the nucleus where it is a transcription factor for several target genes like eIF4E (eukaryotic translation initiation factor 4E; Lynch et al, 2005) and GDF15 (growth differentiation factor 15; Huo et al, 2009). *In vitro* assays like Co-IP might confirm physical interaction of PCBP1 and HSD10 wildtype and especially the mutations. If PCBP1 and HSD10 interact functionally *in vivo* a HSD10 gain-of-function should bind PCBP1 and inhibit its repressive effect on target mRNAs. So, the detection of proteins whose translation is normally repressed by PCBP1 should be determined on a Western Blot after HSD10 knock-down. In turn, the knock-down of HSD10 might release PCBP1 which further represses the translation of target genes. Similarly an effect of HSD10 loss- or gain-of-function would be detectable on target gene transcription.

The potential binding of HSD10 to UXT and PCBP1 in the cytoplasm, might mediate an effect of HSD10 on transcription. A convenient experiment to analyse hundreds of transcripts in one sample is a microarray gene expression analysis or the nanostring technique. This new technique allows direct multiplexed measurement of gene expression with a high sensitivity (< 1 copy per cell). Thus, the effect of HSD10 loss-of-function on gene expression could be measured in patient fibroblasts and after efficient knock-down of HSD10 in cell culture. It would also be interesting to assay the effect of HSD10 knock-down on mitochondrial transcription. There are commercially available gene expression assays that are especially designed to quantify mitochondrial transcription.

If there actually is cytosolic HSD10, the suggested interaction with UXT and even PCBP1 might be an important function *in vivo*. Also this function of HSD10 in the cytosol could mediate extrinsically induced apoptosis. Therefore, it has to be confirmed if HSD10 really is restricted to mitochondria under normal conditions and if it leaks into the cytosol upon mitochondrial permeabilisation during apoptosis and then assumes a cytosolic function.

Very potent evidence that HSD10 has a function in the cytosol would be a rescue experiment with HSD10 depleted of its mitochondrial localisation signal. If this cytosolic form of HSD10 is able to rescue the apoptotic phenotype observed upon HSD10 knock-down it would very strongly suggest a function of HSD10 outside of mitochondria. But to

be able to investigate this, the mitochondrial import sequence of HSD10 has to be identified. Eleven N-terminal amino acids that form a positively charged amphiphilic α helix have been proposed to be sufficient but not required for mitochondrial import (He et al, 2001). HSD10 might have one or more additional mitochondrial localisation signals, although an internal or C-terminal targeting signal was not found in the protein sequence. Preliminary own data suggest that the N-terminal sequence is not only sufficient but also required to direct HSD10 to mitochondria.

Taken together, several experiments show that the induction of apoptosis after HSD10 loss-of-function is not (exclusively) dependent on mitochondrial transcription and translation including RNaseP activity. An as yet unknown function of HSD10 that is independent of its dehydrogenase and tRNA 5′ processing function appears to be required for cellular integrity and viability.

6 MATERIALS

6.1. Chemicals

All chemicals, if not stated otherwise, were obtained from J.T.Baker, Merck, Carl Roth GmbH, and Sigma-Aldrich.

ABsolute™ qPCR SYBR Green ROX Mix	Thermo Scientific
Acetone	Merck
Acrylamide (30 %)	Carl Roth GmbH
Ammonium persulfate	Grüssing
Amphotericin	Sigma Aldrich
Ampicillin	biomol
Antibody diluent with background reducing	DAKO
Bacto tryptone	Carl Roth GmbH
Bacto yeast extract	Carl Roth GmbH
Boric acid	Merck
Bromophenol Blue	Serva
Calciumnitrat-Tetrahydrat ($Ca(NO_3)x4H_2O$)	Merck
Calciumchlorid-Dihydrat ($CaCl_2x2H_2O$)	Merck
Chloroform	Zentrallager INF
4',6-diamidino-2-phenylindole (DAPI)	Roth
Dimethylsulfoxid (DMSO)	Acros Organics
Dithiothreitol (DTT)	Invitrogen
dNTP-mix, 2 and 10 mM	Fermentas
Dodecylsulfat (SDS)	Serva
Dulbecco's modified Eagle's medium (DMEM, ready mix)	GibcoBRL
Ethanol absolut (EtOH)	Sigma Aldrich
Ethidium bromide	Merck
Ethylendiamintetraacetat (EDTA)	Merck
Ethylenglycol-bis[β-aminoethyl ether]-N, N, N' N'-Tetraacetat (EGTA)	Sigma Aldrich
Fluorescence mounting media	DAKO
Formaldehyde (37 %)	Merck
Formamide	J.T. Baker
Gelatine from cold water fish skin	Sigma
GeneRuler 1 kb and 100 bp DNA Ladder	Fermentas
Glutaraldehyde	Serva
Glycerol	GibcoBRL
Glycine	Sigma Aldrich
2-[4-(2-hydroxyethyl)-1-piperazinyl]-ethansulfonic acid (HEPES)	biomol
Hoechst nuclear stain	Immunochemistry Technologies
Hyamine	Merck
Hydrochloric acid (HCl)	Merck
Hydrogen peroxid (33 %) (H_2O_2)	Merck

IPTG	Fermentas
Imidazole	Sigma
Isopropanol	Zentrallager INF
L-cysteine	biomol
LE Agarose	Biozym
Lead citrate	Serva Electrophoresis
Lipofectamine2000	Invitrogen
Magnesium sulfate	Merck
Magnesium sulphate heptahydrate ($MgSO_4x7H_2O$)	Merck
Malate	Sigma Aldrich
Methanol absolut (MeOH)	J.T. Baker and Zentrallager INF
Mitotracker Green FM	Invitrogen
MOPS (3-(N-Morpholino)propane sulfonic acid)	Biomol
Mowiol	Calbiochem
Ni-NTA Agarose	GE Healthcare
NP40	Calbiochem
Opti-MEM® I medium	Invitrogen
Osmium tetroxide	Serva Electrophoresis
PageRuler Prestained Protein Ladder	Fermentas
Paraformaldehyde (PFA)	Merck
PBS for cell culture	PAA Laboratories
Penicillin	PAA Laboratories
Phenol-chloroform-isoamylalcohol	Fluka
Polyoxyethylensorbitanmonolaurat (Tween-20)	Carl Roth GmbH
Ponceau S concentrate	Sigma Aldrich
Potassium chloride (KCl)	AppliChem
Potassium dihydrogen phosphate (KH_2PO_4)	Gerbu
1-C^{14} pyruvate	GE Healthcare
Pyruvate	Sigma Aldrich
RNAse-free water	Ambion
Sheep serum	Sigma
Skimmed milk powder	Saliter
SOC medium	Invitrogen
Sodium acetate (NaAc)	Merck
Sodium citrate	AppliChem
Sodium chloride (NaCl)	Sigma Aldrich
Sodium hydrogen carbonate ($NaHCO_3$)	Merck
Sodium hydrogen phosphate dihydrate ($Na_2HPO_4x2H_2O$)	J.T. Baker
Sodium hydroxide (NaOH)	Merck
Sodium-ortho-vanadate	Sigma Aldrich
Streptomycin (Strep)	PAA Laboratories GmbH
Streptomycin sulfate	Merck
Sucrose	Merck

N, N, N' N'-Tetramethylethylenediamine (TEMED)	biomol
Tris-(Hydroxymethyl)-aminomethane (Tris)	Carl Roth GmbH
Triton X-100	Serva
TRIZOL reagent	Invitrogen
Trypan blue	Invitrogen
UltimaGold	PerkinElmer
Uranyl acetate	Serva Electrophoresis
Urea (CH_4N_2O)	Invitrogen
Uridine	Merck

6.2. Buffers, solutions and cell culture media

antigen retrieval buffer	1 mM EDTA, 0.05 % Tween-20 in PBS, pH 8.0
bacteria lysis buffer for IMAC	8 M CH_4N_2O, 50 mM Tris-HCl pH 8.0, 1 mM DTT in PBS
bleaching solution	1 % H_2O_2, 5 % formamide, 0.5 x SSC
cell culture lysis buffer	1 % Triton X-100, 2 % NP40, 0.1 mM sodium-ortho-vanadate, 0.05 mg aprotinin, 25 µM APMSF, 3 U benzonase, 1 x complete protease inhibitor
cell culture medium (HEK293 and HeLa)	DMEM ready mix, 1 % Pen/Strep
cell culture medium (fibroblasts)	DMEM ready mix, 1 % Pen/Strep, 1 % Amphotericin B
cystein solution	2 % L-cystein, pH 8.0
DNA loading buffer (6 x)	40 % glycerol, 0.25 % Bromphenol Blue
embryo lysis buffer	10 mM Tris-HCl pH 7.5, 100 mM NaCl, 2 mM EDTA, 1 mM EGTA, 0.5 % NP40, 10 % glycerol, protease inhibitors
homogenisation buffer (pyruvate turnover)	250 mM sucrose, 50 mM KCl, 5 mM $MgCl_2$, 20 mM Tris-HCl, pH 7.4
IMAC binding buffer	500 mM NaCl, 5 % glycerol, 50 mM HEPES pH 7.5, 50 mM imidazole
IMAC elution buffer	500 mM NaCl, 5 % glycerol, 50 mM HEPES pH 7.5, 250 mM imidazole
LB medium	1 % (w/v) Bactotrypton, 1 % (w/v) NaCl, 0.5 % (w/v) yeast extract
LB-Amp	50 µg/ml ampicillin in LB
LB-Amp plate	1.5 % agar in LB-Amp
MBSH buffer	88 mM NaCl, 1 mM KCl, 2.4 mM $NaHCO_3$, 0.82 mM $MgSO_4$, 0.33 mM $Na(NO)_3$, 0.41 mM $CaCl_2$, 10 mM HEPES pH 7.4, 10 µg/ml streptomycin-sulfate, 10 µg/ml penicillin

Modified Eagle's medium (MEM) (10 x)	1 M MOPS, 20 mM EGTA, 10 mM $MgSO_4$, pH 7.4
MEMFA	0.1 M MOPS pH 7.4, 2 mM EGTA, 1 mM $MgSO_4$, 3.7 % formaldehyde
milk buffer	5 % powdered milk, 0.1 % Tween-20 in PBS
mitochondria isolation buffer	0.25 M sucrose, 5 mM Tris-HCl, pH 7.4, 1 mM EDTA, 1 x complete protease inhibitor
Mowiol	20 mg Mowiol, 80 ml PBS, 50 ml glycerol
PBS (10 x)	1.37 M NaCl, 27 mM KCl, 20 mM KH_2PO_4, 100 mM Na_2HPO_4, pH 7.4
PBS-T	1 x PBS, 0.1 % (v/v) Tween-20
pH 9 buffer	100 mM Tris pH 9.5, 100 mM NaCl, 50 mM $MgCl_2$
SDS-PAGE running buffer	24.8 mM Tris, 192 mM glycine, 0.1 % SDS
SDS-PAGE sample buffer (3 x)	150 mM Tris-HCl pH 6.8, 6 % SDS (w/v), 0.3 % Bromphenol Blue (w/v), 30 % glycerol (v/v), 300 mM DTT
standard saline citrate (20 x SSC)	3 M NaCl, 0.3 M sodium citrate, pH 7.0
TBE (10 x)	890 mM Tris-borate, 0.2 mM EDTA, pH 8.0
TE buffer	10 mM Tris-HCl, 1 mM EDTA, pH 8.0
Tris/NaCl	100 mM Tris-HCl pH 7.4, 100 mM NaCl
trypan blue stain	0.4 % trypan blue in PBS
Western Blot transfer buffer (10 x)	24.8 mM Tris, 192 mM glycine, 20 % methanol

6.3. Equipment

ABI 7500 Fast Real-Time PCR cycler	Applied Biosystems
Blotting chambers	Bio-rad
CC-12 digital camera	Olympus
Cellstar Tissue culture dishes, 6 and 24 well and 10 cm	Greiner Bio-one
Cell culture flasks, 75 cm² and 25 cm²	Greiner bio-one
Cold plate	Julabo
Cronex 5 film	Agfa
Cryostat CM 30505	Leica
Dounce homogeniser	Wheaton USA
Dumont Nr. 5, forceps	NeoLab
EasyCast electrophoresis system	Owl Scientific
Eclipse 90i upright automated microscope	Nikon
electron microscope Philips CM10	Philips
Epi Chemi II Darkroom gel documentation system	UVP Laboratory Product
Eppi-pestle, stainless steel, for 1.5 ml reaction vessels	Schuett biotec
Folded Filters	Schleicher & Schuell
Glass vials 2.0 and 4.0 ml	neoLab
hemocytometer	Biochrom
IM300 Microinjector	Narishige
JC-5 centrifuge	Beckman Coulter
KL 1500 electronic cold light source	Zeiss
Micromanipulator	Micro Instruments
NanoDrop ND-1000 Spectrophotometer	Thermo Scientific
NC2010 Gel cassettes 1.0 mm	Invitrogen
Novex xCell SureLock Mini-cell system	Invitrogen
Optimax Typ TR x-ray film processor Protec	Medizintrechnik
PCR Plate cover foil Star Seal	Star Lab
PCR strips	Sarstedt
PD-5 Puller for producing microneedles	Narishige
Peltier Thermocycler PTC-200	MJ Research
Petri dishes	Greiner bio-one
pH-Meter Delta 320	Mettler
Pipettes	Gilson
Pipette tips	Sarstedt and Greiner bio-one
Power Pac 300	BioRad
PROTRAN Nitrocellulose Transfer Membrane	Whatman

Reaction tubes 0.5, 1.0 and 2.0 ml	Sarstedt
Reaction tubes 15 and 50 ml	Greiner bio-one
scintillation counter	Beckman Coulter
scintillation vial	Perkin Elmer
Sonicator	HeatSystems Ultrasonics
Sorvall RC 5B refrigerated superspeed centrifuge	Du Pont Instruments
spinning disc confocal ERS-FRET on Nikon TE2000 inverted microscope	Perkin Elmer
Stemi SV6	Zeiss
Stripette	Costar
Superfrost Plus	Thermo Scientific
SZX12 stereo microscope	Olympus
tabletop centrifuge 5415D	Eppendorf
Thermo Fast 96-well PCR Plates	Applied Biosystems
Thermocycler TGradient	Biometra
Whatman 3MM paper	Sartorius

6.4. Kits

JETquick Plasmid Miniprep Spin Kit	Genomed
JETstar Plasmid Purification Midi Kit	Genomed
Lumi-LightPLUS Western Blotting Substrat	Roche
Qiagen Plasmid Midi Kit	Qiagen
SilverQuest™ Silver Staining Kit	Invitrogen
MasterPure™ Complete DNA and RNA Purification Kit	Epicentre Biotechnologie

6.5. Enzymes, proteins and markers

All enzymes were obtained from Fermentas, Roche, and New England Biolabs if not stated otherwise.

AG beads (magnetic)	ademtech
4-Amidinophenylmethanesulfonyl fluoride hydrochloride (APMSF)	AppliChem
anti-cleaved caspase-3 (polyclonal rabbit)	Cell Signaling Technology
anti-digoxygenin antibody coupled to alkaline phosphatase (sheep)	Roche
anti-Grp75 antibody	Stressgen Bioreagents
anti-HSD10 antibody (mouse monoclonal)	Abcam
anti-myc antibody 9E10 (mouse)	Merck
anti-porin antibody (polyclonal rabbit)	Abcam
aprotinin	Sigma Aldrich
benzonase	Merck
BM Purple AP Substrat	Roche
DNAse I	Fermentas
GeneRuler kb DNA ladder Plus	Fermentas
goat anti-mouse Alexa 488	Molecular probes
goat anti-rabbit Alexa 594	Molecular probes
goat anti-mouse antibody coupled to alkaline phosphatase (GAM-AP)	dianova
goat anti-mouse antibody coupled to peroxidase (GAM-PO)	dianova
goat anti-mouse antibody coupled to horseradish peroxidase (GAM-HRP)	Biorad
human chorionic gonadotropin	Sigma
Maxima Reverse Transcriptase	Fermentas
mouse IgG antibody	dianova
normal goat serum	Dako
PageRuler Prestained protein ladder	Fermentas
Poly-L-Lysine	Sigma
protease inhibitor complete Mini (10 x)	Roche
RevertAidH-Minus M-MuLV Reverse Transcriptase	Fermentas
RiboLock RNAse inhibitor	Fermentas
RNaseOUT RNase inhibitor	Invitrogen
Terminal deoxynucleotidyl transferase (5 U/µl)	Fermentas
Trypsin	PAA Laboratories
TurboDNase	Ambion

6.6. Oligonucleotides

The following Morpholino antisense oligonucleotides were purchased from Gene Tools LLC.

Morpholino	sequence 5′ → 3′
Mo^{Co}	cctcttacctcagttacaatttata
$MoHSD10^{ATG}$	ccttcaggttcctcacatgcgccat

Table 8 Morpholino antisense oligonucleotides used for HSD10 knock-down in *Xenopus* embryos.

The following siRNAs were obtained from Qiagen.

siRNA	Target sequence 5′ → 3′
ctr siRNA	---
siRNA3	aagacttccagcgagttcttg
siRNA5	cagcgagttcttgatgtgaat

Table 9 siRNA oligonucleotides used for HSD10 knock-down in human cells.

The following oligonucleotides were ordered from Operon, Metabion, Sigma-Aldrich and Realtimeprimers.com.

primer	organism	forward primer sequence 5′ → 3′	reverse primer sequence 5′ → 3′
apoptosis primer library	human		
CHOP	*Xenopus*	aaagtgtcccatttgttagctgaaa	cctggtctgctccacttcctt
GAPDH	human	ccatgttcgtcatgggtgt	ccaggggtgctaagcagtt
HSD10	human	gtatccgggtgatgaccatt	tggccaagaagttgcaca
ODC	*Xenopus*	gtcaatgatggagtgtatggatc	tccattccgctctcctgagcac
oligo-dT			
random $d(N)_6$			
TOMM20	human	gcttctgactaagctcccaaca	gttgacatttgtttctcattccac

tRNA for amino acid	primer used for specific reverse transcription	primer	sequence 5′ → 3′	product size
tRNAs encoded on the H-strand				
TF	x	MT-TF-R1	ggtgatgtgagcccgtctaa	
		MT-TF-F	tgtagcttacctcctcaaagca	57
		HSP1-F	ccaaagacacccccaca	80
TV	x	MT-TV-R	caagttaagttgaaatctcctaagtg	
		MT-TV-F2	agaggagacaagtcgtaacatgg	113
		MT-TV-F1	gcttaacacaaagcacccaac	50
TL	x	MT-TL-R	aagaggaattgaacctctgactg	
		MT-TL-F2	tatacccacacccacccaag	98
		MT-TL-F1	cccggtaatcgcataaaact	53
TI	x	MT-TI-R	agggggtttaagctcctatt	
		MT-TI-F2	ttcctaccactcaccctagca	141
		MT-TI-F1	aaatatgtctgataaaagagttactttg	59
TM	x	MT-TM-R	cgggaagggtataaccaaca	
		TM-F	aaggtcagctaaataagctatcg	60
		TQ-F	agaatcgaacccatccctga	125
TW	x	MT-TW-R	tgcaacttactgagggctttg	
		TW-F	gaaatttaggttaaatacagaccaaga	53
		ND2-F	ccacgctactcctacctatctcc	99
tRNA for amino acid	primer used for specific reverse transcription	primer	sequence 5′ → 3′	product size
tRNAs encoded on the L-strand				
TQ	x	MT-TQ-F	agaatcgaacccatccctga	
		TQ-R	aggatggggtgtgataggtg	60
		TM-R	cgggaagggtataaccaaca	125
TC	x	MT-TC-int-F	ccccggcaggtttgaag	
		TC-R	agctccgaggtgattttcat	63
		15-R	aatagtcaacggtcggcgaac	163
TP	x	MT-TP-F	agaaaaagtctttaactccacca	
		TP-R	agaatcttagctttgggtgct	46
		TyrPro11-R	tggtacccaaatctgcttcc	95

Table 10 Primer oligonucleotides used for amplification of different mRNA and tRNA transcripts.

6.7. Plasmids

clone	source
Fadd	J.W.G. Janssen
pcDNA4/HisMaxB_hUXT	J. Zschocke (Susanne Theiß)
pCS2+_myc/xHSD10	xHSD10 was amplified from pCS2+/xHSD10 and ligated into an empty pCS2+_myc
pET15b/hHSD10	J. Zschocke (Beate Grziwa)
p11_His/ R130C	J. Zschocke (Astrid Nümann)
p11_His/ D86G	J. Zschocke (Astrid Nümann)
p11_His/ Q165H	J. Zschocke (Astrid Nümann)
pT-Rex-DEST30/hHSD10	J. Zschocke (Katja Schöler)
pT-Rex-DEST30/R130C	J. Zschocke (Katja Schöler)
pT-Rex-DEST30/D86G	J. Zschocke (Katja Schöler)
pT-Rex-DEST30/Q165H	J. Zschocke (Katja Schöler)

Table 11 Plasmids used for expression in *Xenopus* embryos, human cells or bacteria.

6.8. Bacteria

E.coli BL21(DE3) Rosetta

E.coli XL1 chemocompetent

6.9. Cell lines

cell line	source
BTK-143	Hans Mayr, Kinderspital Salzburg
fibroblasts N18 (control)	Jürgen Okun, Kinderklinik Heidelberg
fibroblasts N32 (control)	Jürgen Okun, Kinderklinik Heidelberg
fibroblasts NHDF (control)	Jürgen Okun, Kinderklinik Heidelberg
fibroblasts R130C	Jürgen Okun, Kinderklinik Heidelberg
fibroblasts D86G	Jürgen Okun, Kinderklinik Heidelberg
fibroblasts Q165H	Jürgen Okun, Kinderklinik Heidelberg
HeLa Kyoto	Heiko Runz, Humangenetik Heidelberg
HEK293	LGC Promochem

Table 12 List of cell lines used in this study.

6.10. Animals

Xenopus laevis used for experiments in embryos were obtained from Xenopus Express. Material from mice was kindly prepared by Afsaneh Majdazari (Max Planck Institute for Brain Research, Frankfurt) or B. Arnold (Molecular Immunology, DKFZ). All experiments with model organisms were performed in agreement with the applying Protection of Animals Act.

6.11. Software

AnalySIS	Soft Imaging System GmbH
Adobe Photoshop™ 7.0 and Adobe Photoshop CS	Adobe
endnote	endnote
LabWorks analysis software	UVP laboratory prodcut
Microsoft Office	Microsoft
NIS-Elements 2.30 Nikon	Nikon
PhotoStudio 5	ArcSoft
SAS 9.1	SAS Institute

6.12. Online databases

National Center for Biotechnology Information	www.ncbi.nlm.nih.gov/
primer design	http://biotools.umassmed.edu /bioapps/primer3_www.cgi
proteomics tools	www.expasy.org/tools
tRNA database	http://mamit-trna.u-strasbg.fr/Sequences.asp
Xenopus Web Resource	www.xenbase.org
Saccharomyces Genome database	http://www.yeastgenome.org
Human gene compendium	http://www.genecards.org
apoptosis database	http://deathbase.org/index.php

7 METHODS

7.1. Embryological methods

7.1.1. Embryo culture and microinjection

In vitro fertilisation and manipulation of embryos was performed as previously described (Rauschenberger, 2007). In brief, eggs were obtained from female *Xenopus laevis* injected with 500 U human chorionic gonadotropin, and were fertilised *in vitro*. Embryos were dejellied using 2 % L-cysteine (pH 7.8-8.0), cultured in 0.1 x MBSH and microinjected in 1 x MBSH. For microinjections antisense Morpholino oligonucleotides or DNA plasmids diluted in an injection volume of 5 nl were injected into 2- or 4-cell stage embryos. The dorsal blastomeres of 4-cell embryos were identified according to Klein (Klein, 1987). Animal caps were dissected at stage 8 or 9 and cultured in 0.5 x MBSH until they reached the desired stage. Embryo stages were determined according to Nieuwkoop and Faber (Nieuwkoop & Faber, 1967).

7.1.2. TUNEL assay (Terminale deoxynucleotidyl transferase-mediated dUTP digoxygenin nick end labelling)

The TUNEL assay specifically stains apoptotic cells. An enzyme called TdT (terminal deoxynucleotidyl transferase) adds labelled dNTPs coupled to a DIG-dUTP (digoxygenin) to the single strand DNA breaks that happen during apoptosis. This DIG label is then detected by an anti-DIG antibody (Hensey & Gautier, 1997).

Embryos that reached the desired stage according to Nieuwkoop and Faber were fixed in MEMFA for 2 h at RT, washed twice with methanol for 30 min and stored in methanol at -20 °C. The following TUNEL assay protocol takes 4 days:

- 2 x PBS-T for 15 min at RT
- 2 x PBS for 15 min at RT
- 1 x TdT-buffer for 30 min at RT
- 1 x TdT-Puffer containing 0,5 µM digoxygenin-dUTP and 150 U/ml TdT o/n at RT

- 2 x PBS-T containing 1 mM EDTA for 1 h at 65 °C
- 4 x PBS for 1 h at RT
- Blocking: PBS-T with 20 % goat serum for 1 h at RT
- Blocking solution containing anti-DIG antibody coupled to alkaline phosphatase 1 : 10,000 o/n at 4 °C

- 6 x PBS for 1 h at RT
- PBS o/n at RT

- pH 9 buffer for 30 min at RT
- pH 9 buffer / BM Purple 1 : 1 until the staining is visible (usually 3-4 h)
- Stop: 2 x PBS for 5 min at RT
- Postfixation: 3.7 % formaldehyd in PBS o/n at 4 °C (no agitation)
- 2 x PBS for 5 min at RT

Subsequently, *Xenopus laevis* embryos that were stained with the TUNEL assay were bleached for a better visualisation of apoptotic spots. Bleaching solution was applied and the embryos were incubated for several hours on a light source at 4 °C until the pigmentation of the embryos was gone. The embryos were washed once with methanol and stored in methanol at -20 °C.

7.1.3. Tissue preparation from mice

Animals were killed and immediately dissected to collect brains or ganglia. Tissues were fixed in 4 % formaldehyde and 1 % glutaraldehyde in PBS. Fixed brains were cut in Vibratome sections (50 µm) and the appropriate regions of the brain (locus coeruleus) were identified by pigmentation and dissected from these Vibratome sections prior to electron microscopy.

Fixed ganglia were embedded for cryosectioning (15 µm). For that reason ganglia were washed in PBS, incubated in Tris/NaCl for 1 h and rinsed again in PBS. Ganglia were then embedded in 15 % cold water fish gelatine and 15 % sucrose o/n followed by 25 % cold water fish gelatine and 15 % sucrose o/n. Specimens were frozen in 15 % cold water fish gelatine at -80 °C. 15 µm sections were cut in a Cryostat CM 30505 at -19 °C, collected on Superfrost Plus precoated glass slides and dried at 37 °C o/n. The dried cryosections were fixed with acetone and mounted in Mowiol.

7.2. Molecular biology

7.2.1. Isolation of DNA (midiprep)

Transformation of competent bacteria was achieved by mixing 100 ng of purified plasmid DNA with 50 µl chemocompetent cells and incubating them on ice for 20 min. Bacteria were heat shocked for 30 s at 42 °C and then put on ice for 1 min. After the addition of 1 ml LB or 250 µl SOC medium bacteria were incubated for 1 h shaking at 37 °C and then 20-150 µl were plated on LB plates containing antibiotics and cultured o/n at 37 °C.

One of the resulting colonies was picked and cultured in 50 ml LB-medium containing antibiotics o/n shaking at 37 °C. Plasmid DNA was isolated from bacteria with the appropriate kit (see 6.4.) according to the manufacturer's instructions.

7.2.2. Isolation of RNA

Total RNA from approximately 15 *Xenopus* animal caps was isolated using 1 ml TRIZOL reagent. The tissue was homogenised with an Eppi-pestle and incubated at RT for 10 min. Subsequently, 200 µl of chloroform were added and samples were mixed thoroughly by vortexing. Centrifugation for 15 min at 13,000 rpm at 4 °C separates the upper aqueous phase which was transferred to a new tube and RNA was precipitated by the addition of 250 µl isopropanol and 250 µl 0.8 M sodium citrate/1.2 M NaCl and incubation at RT for 10-30 min. Subsequently, RNA was pelleted by centrifugation for 15 min at 13,000 rpm at 4 °C and the pellet was washed twice with 75 % ethanol and resuspended in an appropriate volume of nuclease-free water.

Isolation of total RNA from cells was achieved with the appropriate kit (see 6.4.) according to the manufacturer's instructions.

To avoid possible genomic DNA contaminations a DNAse I digest was performed within the scope of the RNA isolation procedure. 1 µg of total RNA was incubated with 1 µl DNAse I or TurboDNase and incubated for up to 1 h at 37 °C. DNAse was inactivated by the precipitation of proteins during the RNA isolation procedure.

7.2.3. Phenol-chloroform purification of nucleic acids

Purification of nucleic acids from lipids and proteins was performed by phenol-chloroform extraction. The aqueous solution of nucleic acids was mixed with the same volume of phenol-chloroform-isoamylalcohol and centrifuged for 15 min at 13,000 rpm at RT. The upper phase containing the nucleic acids was transferred to a new tube, mixed with the same volume of chloroform and centrifuged again for 15 min. The upper phase was transferred to a new tube and the nucleic acid was precipitated with ethanol or isopropanol.

7.2.4. Precipitation of nucleic acids

Alcohol precipitation of nucleic acids was performed to purify RNA or DNA. To precipitate nucleic acids from aqueous solutions 1/10 volume 3 M sodium acetate (pH 5.2) and 2.5 volume 100 % ethanol or 1 volume isopropanol were added, and the mixture was incubated on ice for 15 min or o/n at -20 °C and centrifuged at 13,000 rpm. The nucleic acid pellet was washed once with 75 % ethanol and resuspended in a suitable volume of water or TE buffer.

7.2.5. Concentration and quality of nucleic acids

The concentration and quality of nucleic acid solutions were measured photometrically using a NanoDrop ND-1000.

Quality of total RNA was additionally assessed by gel electrophoresis. RNA samples were mixed with 6 x loading buffer and loaded onto 1 % agarose gels in 1 x TBE-buffer containing 5 µg/ml ethidium bromide. RNA fragments were then electrophoretically separated in 1 x TBE buffer at 100-135 V for 30-60 min. To visualise the separated nucleic acids, the agarose gel was illuminated by UV light and imaged on a gel documentation system.

7.2.6. cDNA synthesis (reverse transcription)

To detect the relative expression level of a target gene RT-PCR (reverse transcription Polymerase Chain Reaction) followed by qPCR (quantitative Polymerase Chain Reaction) was used.

Total RNA was reverse transcribed by RevertAidH-Minus-MuLV-RT or Maxima Reverse Transcriptase using random hexamer or oligo-dT primers or specific primers listed in table 10. Maxima Reverse Transcriptase and specific primers were used for RT-PCR of tRNA genes, since this enzyme can tolerate higher temperatures than RevertAidH-Minus-MuLV-RT and this and the binding of specific primers helps to dissolve the secondary structure of tRNA genes that otherwise disturbs reverse transcription. RT-PCR of mRNA transcripts was performed according to the following protocol:

- heat 1 µg RNA and 250 ng $d(N)_6$ in a volume of 11 µl to 70 °C for 10 min
- cool down to 4 °C
- add 4 µl 5 x M-MuLV RT buffer, 1 µl 10 mM dNTP, 0.5 µl RNase inhibitors and 2.5 µl water
- incubate at 25 °C for 5 min
- cool down to 4 °C
- add 1 µl RevertAidH-Minus-MuLV-RT to a final volume of 20 µl

- use PCR program:
  25 °C 10 min
  42 °C 2h
  70 °C 10 min
  4 °C ∞

For further use the reaction was filled to a total volume of 100 µl with nuclease-free water.

cDNA synthesis for tRNA genes was performed according to the following protocol:

- heat 1 ng - 5 µg RNA, 10 mM dNTP and 100 µM primer in a volume of 7 µl to 70 °C for 3 min
- cool down to 4 °C for oligo-dT and $d(N)_6$ and keep on 55 °C for specific primers
- add 2 µl 5 x first strand buffer, 0.5 µl RNaseOUT RNase inhibitor and 0.5 µl Maxima Reverse Transcriptase to a final volume of 10 µl
- use PCR program for

oligo-dT primers	$d(N)_6$ primers	specific primers
50 °C 30 min	25 °C 10 min	55 °C 5 min
55 °C 10 min	50 °C 30 min	50 °C 30 min
60 °C 10 min	55 °C 10 min	55 °C 10 min
65 °C 10 min	60 °C 10 min	60 °C 10 min
85 °C 5 min	65 °C 10 min	65 °C 10 min
	85 °C 5 min	85 °C 5 min

Table 13 PCR programs for cDNA synthesis using different primers.

For further use the reaction was filled to a total volume of 20 µl with nuclease-free water.

7.2.7. Quantitative PCR

To quantify gene expression qPCR (quantitative realtime PCR) was performed on an ABI 7500 Fast Real-Time PCR cycler. The qPCR reaction was set up in the following 20 µl or 10 µl PCR reaction and the following PCR programs were used.

qPCR for mRNA transcripts		qPCR for tRNA transcripts
2 µl	cDNA	0,6 µl
10 µl	ABsolute™ qPCR SYBR Green ROX Mix	5 µl
0.4 µl (10 µM each)	Primer	4 µl (0.2 µM each)
7.6 µl	H_2O	1 µl
20 µl	**total**	10 µl

Table 14 qPCR reaction for the quantification of mRNA or tRNA transcripts.

qPCR for mRNA transcripts			qPCR for tRNA transcripts		
temperature	time	cycle	temperature	time	cycle
25 °C	15 min	1 x	25 °C	20 min	1 x
95 °C	15 min	1 x	95 °C	1 min	1 x
95 °C	15 s	40 x	96 °C	2 s	40 x
60 °C	1 min		63 °C	40 s	40 x
Dissociation stage			72 °C	30 s	40 x
			25 °C	10 s	1 x
			Dissociation stage		

Table 15 PCR program used for the quantitative amplification of mRNA or tRNA transcripts.

CT values measured in the qPCR were normalised against housekeeping genes like GAPDH in human and ODC in *Xenopus* samples and relative expression levels were calculated using a standard curve or the ddCT method.

7.3. Proteinbiochemistry

7.3.1. SDS-PAGE

Discontinuous SDS-PAGE (polyacrylamid-gel electrophoresis) was performed according to Laemmli, 1970. Protein extracts boiled with 1 x SDS sample buffer and stained protein molecular weight standards were separated at constant voltage of 100-200 V in a 12-15 % separating gel topped with 6 % stacking gel. A 12 % separating gel topped with 6 % stacking gel was prepared as follows for a standard size SDS gel; amounts used for large size gels were adapted according to the size of the gels:

	10 ml separating gel	3 ml stacking gel
H_2O [ml]	4.18	1.69
1 M Tris pH 8.8 [ml]	1.67	---
0.5 M Tris pH 6.8 [µl]	---	760
30 % acrylamide	4 ml	500 µl
20 % SDS [µl]	50	15
10 % APS [µl]	100	30
TEMED [µl]	4	3

Table 16 Separating and stacking gel for discontinuous SDS-PAGE.

7.3.2. Silver staining

Proteins separated in a large size SDS-PAGE were silver stained using the SilverQuest™ Silver Staining Kit by Invitrogen according to the manufacturer's instructions. This technique specifically detects proteins in the polyacrylamide gel with a very high sensitivity. The SilverQuest™ Silver Staining Kit from Invitrogen is compatible with subsequent mass spectrometry.

7.3.3. Western Blot

Proteins that were separated in SDS-PAGE were transferred electrophoretically to a nitrocellulose membrane by wet transfer at constant amperage (400 mA, 80 min) in Western blot transfer buffer. A correct transfer as well as protein amounts in each sample were checked by Ponceau S staining and the membrane was blocked in 5 % milkpowder in PBS-T for 1 h at RT. Antibody incubation times were o/n at 4 °C for primary, and 1 h at RT for secondary antibodies with six washing steps in PBS-T at RT before and after each incubation step.

Specific protein bands were visualised by chemoluminescence using the Lumi-LightPLUS Western Blotting substrate (Roche). The luminescence was detected on X-ray film, which was developed using an X-ray film processor (Protec Medizintechnik).

7.3.4. Co-immuno precipitation of protein complexes

This pull-down method was used to isolate HSD10 together with potential binding partners from injected *Xenopus* embryos overexpressing xHSD10_myc or endogenous HSD10 from mitochondrial lysate from untreated HEK cells.

For the preparation of embryo extract injected embryos were washed once with lysis buffer and then lysed in lysis buffer containing proteinase inhibitors by pipetting up and down. The lysate was incubated on a head-over-head rotator at 4 °C for 5-10 min and then centrifuged for 5 min at 10,000 rpm at 4 °C. After separating the proteins from the pigment pellet and the overlaying yolk they were centrifuged again for 5 min at 10,000 rpm at 4 °C.

For the preparation of mitochondrial proteins see 7.4.3.

An aliquot "input" was removed from both, embryo extract and mitochondrial proteins, and prepared for SDS-PAGE. The remaining input was divided in two parts and mixed with 2 µg IgG and anti-myc or anti-HSD10 antibody, respectively. Proteins and antibodies were incubated on a head-over-head rotator for 1 h at 4 °C. Subsequently, the mixture was centrifuged for 15 min at 10,000 rpm at 4 °C and the supernatant was processed by the addition of 30 µl magnetic AG beads. The protein/antibody-complexes were incubated for 2-3 h or o/n on a head-over-head rotator at 4 °C with the magnetic AG beads. Afterwards the beads were washed 4-5 times with lysis buffer and finally resuspended in 1 x SDS-PAGE sample buffer, incubated at 95° C for 5 min and the supernatant was used for SDS-PAGE.

7.3.5. IMAC (immobilised metal ion affinity chromatography)

Protein purification of HSD10 wildtype and mutations was achieved by the expression of the proteins in *E.coli BL21(DE3) Rosetta*. For that reason 50 µl competent bacteria were transformed with 100 ng prokaryotic expression plasmids (pET15b_His/hHSD10 and p11_His for the mutations) by incubating cells and DNA on ice for 10 min, heat shocking at 42 °C for 90 s and cultivating shaking in 1 ml LB at 37 °C for 1 h before plating them on LB/Amp plates and cultivation at 37 °C o/n.

For protein expression an o/n pre-culture of 2-3 ml was inoculated with a single colony. This small o/n pre-culture was then used to start a 250 ml culture that was incubated shaking until $OD_{600} \geq 0.5$. Then protein expression was induced by the addition of 0.4 mM IPTG and again incubated shaking at 37 °C for 3 h. Subsequently, cells were centrifuged for 15 min at 6,000 rpm and the pellet stored at -80 °C.

For cell lysis the pellet was resuspended and incubated shaking for 30 min at 4 °C in bacteria lysis buffer. Centrifugation at 12,000 rpm and 4 °C for 15 min yielded the protein containing supernatant. This supernatant was charged on a column filled with 1 ml Ni-NTA agarose and then washed with 10-20 ml IMAC binding buffer and 20-30 ml PBS. Mitochondrial lysate (see 7.4.3.) was subjected to the column and subsequently washed again with 10 ml PBS. Elution was achieved by adding 3 ml IMAC elution buffer to the column.

7.3.6. Pyruvate turnover

Xenopus animal caps were homogenised in 500 µl homogenisation buffer using a Potter-Elvehejm-system and 7 downstrokes. The suspension was incubated with 50 µl 10 mM malate and 50 µl 1-C^{14} pyruvate (5 µCi/ml) for 1 h at 37 °C in a scintillation vial that contains a tube with 200 µl hyamine. This tube was transferred in a new scintillation vial containing 7 ml UltimaGold and measured in a scintillation counter.

7.3.7. Protein extract from cell culture cells

Adherent cells were washed with PBS and then incubated pivoting on ice for 15 min in cell lysis buffer. The cells were scraped from the culture dish, transferred to tubes and cell debris was pelleted by centrifugation for 20 min at 4 °C at 13,200 rpm. The supernatant was mixed with SDS-PAGE sample buffer and boiled for 5 min at 95 °C.

7.3.8. Acetone precipitation

Acetone precipitation of proteins was performed to concentrate proteins in aqueous solutions. Four volumes cold acetone were added, vortexed vigorously and incubated for 60 min at -20 °C. Centrifugation at 13,000 x g for 10 min pellets the proteins and the pellet was washed once with acetone. The remaining acetone was allowed to evaporate and the protein pellet was resuspended in an appropriate volume of buffer.

7.4. Cell culture methods

7.4.1. Cultivation of cell lines

All adherent cell lines used in this study were grown in DMEM Ready Mix supplemented with 100 µg/ml penicillin and streptomycin at 37 °C in a humidified 5 % CO_2 incubator. These cell lines are HEK293, HeLa Kyoto, BTK-143 osteogenic sarcoma cells and fibroblasts. Patient and control fibroblasts are additionally protected from fungal growth by 100 µg/ml amphotericin B.

BTK-143 osteogenic sarcoma cells were used as wildtype or rho0 cells. Rho0 cells are depleted of their mitochondrial DNA and hence do not assemble a functional respiratory chain in mitochondria. These cells were supplemented with 2.5 mM pyruvate and 100 µg/ml uridine.

At 80-90 % confluence cells were subcultured using trypsin and a split ratio of 1 : 20 for HEK293 cells and trypsin/EDTA for all other cell lines and a split ratio of 1 : 10 for HeLa and BTK-143 cells and 1 : 3 for fibroblasts.

For microscopic analyses cells were seeded onto coverslips coated with poly-L-lysine.

7.4.2. Transfection of cultured cells

HeLa and BTK-143 cells were transfected using Lipofectamine2000 and Opti-MEM according to the manufacturer's instructions. For efficient HSD10 knock-down 60 pmol siRNA (3 µl 20 µM siRNA) were used with 2 µl Lipofectamine to yield a final concentration of 30 nM in 2 ml culture medium. For rescue experiments 60 pmol siRNA were transfected together with 1 µg DNA using 2 µl Lipofectamine.

7.4.3. Isolation and fractionation of mitochondria from HEK293 cells

For the preparation of mitochondrial proteins HEK293 cells were harvested and the cell pellet was resuspended in 5 volumes of mitochondria isolation buffer. Cells lysis was achieved by 10 downstrokes and cellular debris was removed by centrifugation at 750 x g for 10 min. Mitochondria were pelleted by centrifugation at 16,400 x g for 10 min. The resulting supernatant represents the cytosol fraction and the resuspended pellet the isolated mitochondria. After washing the mitochondrial pellet once, an aliquot "mitochondria" was removed and prepared for SDS-PAGE or the mitochondrial proteins were subjected to pull-down or IMAC experiments. Alternatively, isolated mitochondria were sonicated for 20 s and the matrix and membrane fraction were separated by centrifugation at 44,000 x g for 1 h.

7.4.4. Trypan blue staining

Trypan blue is a negatively charged chromophore that only enters cells when the membrane is damaged. Therefore, all cells that exclude the dye are viable (Freshney, 1987). 0.1 ml of 0.4 % trypan blue stain was added to 0.5 ml cell suspension and mixed thoroughly. After 5 min incubation at RT the cells were counted in a hemocytometer.

7.4.5. Immunofluorescent staining of cultured cells

Adherent cells were washed twice with PBS and then fixed for 20 min at RT in 4 % formaldehyde in methanol. After washing the cells 3 x for 3 min with PBS, they were incubated for 20 min in antigen retrieval buffer at 95 °C followed by another 3 x for 3 min in PBS. The cells were permeabilised for 15 min with 0.1 % Triton X-100 in PBS, washed 3 x for 3 min with PBS and once 3 min with PBS-T (0.5 % Tween-20). Unspecific antibody binding sites were blocked with 10 % normal goat serum in PBS-T for 30 min and the first antibody was incubated for 1 h at RT in "antibody diluent with background reducing". After 3 x 3 min washing with PBS-T the cells were incubated for 1 h at RT with the second antibody diluted in PBS-T. The cells were washed again 3 x with PBS-T, stained with 20 µg/ml DAPI in PBS-T for 10 min, washed again 2 x for 3 min with water and mounted on slides with "fluorescence mounting media".

7.4.6. Nuclear staining of cultured cells

Cultured fibroblasts were washed with PBS and then fixed for 20 min at RT in 4 % formaldehyde in methanol or 3.7 % formaldehyde in PBS. After washing the cells 3 x for 3 min with PBS, they were permeabilised for 15 min with 0.1 % Triton X-100 in PBS, washed again 3 x for 3 min with PBS and once 3 min with PBS-T. The cells were stained with 20 µg/ml DAPI or Hoechst in PBS-T for 10 min, washed again 2 x for 3 min with water and mounted on slides with "fluorescence mounting media" or Mowiol.

7.4.7. Mitochondrial staining of cultured cells

Fibroblasts were fixed for 15 min at 37 °C in 3.7 % formaldehyde in culture medium. Cells were rinsed with PBS and incubated for 15 min with 300 nM Mitotracker Green FM in PBS. The cells were rinsed again with PBS followed by mounting in Mowiol.

7.5. Microscopy

Fluorescent images were obtained on an Eclipse 90i upright microscope or a spinning disc confocal ERS-FRET on Nikon TE2000 inverted microscope at the Nikon Imaging Centre at the University of Heidelberg.

7.5.1. Electron microscopy

Primary fixation was done with 2.5 % glutaraldehyde in PBS. For easier handling tissue culture cells were scraped off and embedded in 2 % agarose. All samples were postfixed with 1 % osmium tetroxide in 100 mM phosphate buffer pH 7.2 for 1 h on ice, washed extensively with water, block-stained with 1 % aqueous uranyl acetate for 1 h at 4 °C, dehydrated in a graded series of ethanol at RT, infiltrated with mixtures of ethanol/Epon and finally embedded in Epon. Ultrathin sections were stained with uranyl acetate and lead citrate (Venable & Coggeshall, 1965) and viewed in a Philips CM10 electron microscope at 60 kV using a 30 µm objective aperture. Mitochondria were quantitatively classified into groups according to their morphology by examiner who was blinded to the nature (wt/mutant/knock-out) of the samples. Group 1 is distinguished by a regular arrangement and shape of the cristea stacks. Group 3 characteristics are a reduced cristae compartment resulting in less electron dense material in the mitochondria and an irregular arrangement and shape of the cristae stacks. Group 2 is represented by an intermediate morphological phenotype (fig. 14, 15, 16 and 17).

All samples were sectioned at random angles resulting in cross and longitudinal sections of mitochondria. For the morphological analyses the plain of sections was not relevant.

7.6. Statistics

For the statistical evaluation of mitochondrial morphology the density of each mitochondrium was used as an ordinal variable (dense, medium or depleted). The variable was evaluated as a categorical variable within a logistic model framework. The hypothesis of equal density distribution rates for different treatments was tested controlling for a suitable covariante (animal cap, brain sections or patient) in the respective experiment. All analyses have been performed with SAS 9.1 on PC (SAS Institute, Inc, cary, NC). Differences were counted as significant if the p-values were lower than 5 % adjusted for multiple testing within one experiment.

Significance in all other experiments was calculated by the student t-test. Differences were counted as significant if the p-values were ≤ 0.01.

8 REFERENCES

Abrahams JP, Leslie AG, Lutter R, Walker JE (1994) Structure at 2.8 A resolution of F1-ATPase from bovine heart mitochondria. *Nature* **370**(6491)**:** 621-628

Anderson S, Bankier AT, Barrell BG, de Bruijn MH, Coulson AR, Drouin J, Eperon IC, Nierlich DP, Roe BA, Sanger F, Schreier PH, Smith AJ, Staden R, Young IG (1981) Sequence and organization of the human mitochondrial genome. *Nature* **290**(5806)**:** 457-465

Banner DW, D'Arcy A, Janes W, Gentz R, Schoenfeld HJ, Broger C, Loetscher H, Lesslauer W (1993) Crystal structure of the soluble human 55 kd TNF receptor-human TNF beta complex: implications for TNF receptor activation. *Cell* **73**(3)**:** 431-445

Bates S, Vousden KH (1999) Mechanisms of p53-mediated apoptosis. *Cell Mol Life Sci* **55**(1)**:** 28-37

Bauer DV, Huang S, Moody SA (1994) The cleavage stage origin of Spemann's Organizer: analysis of the movements of blastomere clones before and during gastrulation in Xenopus. *Development* **120**(5)**:** 1179-1189

Bosetti F, Brizzi F, Barogi S, Mancuso M, Siciliano G, Tendi EA, Murri L, Rapoport SI, Solaini G (2002) Cytochrome c oxidase and mitochondrial F1F0-ATPase (ATP synthase) activities in platelets and brain from patients with Alzheimer's disease. *Neurobiol Aging* **23**(3)**:** 371-376

Brown WM, George M, Jr., Wilson AC (1979) Rapid evolution of animal mitochondrial DNA. *Proc Natl Acad Sci U S A* **76**(4)**:** 1967-1971

Bruno C, Sacco O, Santorelli FM, Assereto S, Tonoli E, Bado M, Rossi GA, Minetti C (2003) Mitochondrial myopathy and respiratory failure associated with a new mutation in the mitochondrial transfer ribonucleic acid glutamic acid gene. *J Child Neurol* **18**(4)**:** 300-303

Cardona F, Aranda A, del Olmo M (2009) Ubiquitin ligase Rsp5p is involved in the gene expression changes during nutrient limitation in Saccharomyces cerevisiae. *Yeast* **26**(1)**:** 1-15

Cardoso SM, Santos S, Swerdlow RH, Oliveira CR (2001) Functional mitochondria are required for amyloid beta-mediated neurotoxicity. *FASEB J* **15**(8)**:** 1439-1441

Chandel NS, Schumacker PT (1999) Cells depleted of mitochondrial DNA (rho0) yield insight into physiological mechanisms. *FEBS Lett* **454**(3)**:** 173-176

Chen JX, Yan SD (2007) Amyloid-beta-induced mitochondrial dysfunction. *J Alzheimers Dis* **12**(2)**:** 177-184

Chuang VT, Otagiri M (2007) Recombinant human serum albumin. *Drugs Today (Barc)* **43**(8)**:** 547-561

Clayton DA (1982) Replication of animal mitochondrial DNA. *Cell* **28**(4)**:** 693-705

Connern CP, Halestrap AP (1994) Recruitment of mitochondrial cyclophilin to the mitochondrial inner membrane under conditions of oxidative stress that enhance the opening of a calcium-sensitive non-specific channel. *Biochem J* **302 (Pt 2):** 321-324

Dauer W, Przedborski S (2003) Parkinson's disease: mechanisms and models. *Neuron* **39**(6)**:** 889-909

Deodato F, Boenzi S, Santorelli FM, Dionisi-Vici C (2006) Methylmalonic and propionic aciduria. *Am J Med Genet C Semin Med Genet* **142C**(2)**:** 104-112

Dudgeon (2009) Transcriptional Regulation of Apoptosis *Essentials of Apoptosis***:** 239-260

Eaton S, Pourfarzam M, Bartlett K (1996) The effect of respiratory chain impairment of beta-oxidation in rat heart mitochondria. *Biochem J* **319 (Pt 2):** 633-640

Ensenauer R, Niederhoff H, Ruiter JP, Wanders RJ, Schwab KO, Brandis M, Lehnert W (2002) Clinical variability in 3-hydroxy-2-methylbutyryl-CoA dehydrogenase deficiency. *Ann Neurol* **51**(5)**:** 656-659

Farris SD, Rubio ED, Moon JJ, Gombert WM, Nelson BH, Krumm A (2005) Transcription-induced chromatin remodeling at the c-myc gene involves the local exchange of histone H2A.Z. *J Biol Chem* **280**(26)**:** 25298-25303

Finnila S, Autere J, Lehtovirta M, Hartikainen P, Mannermaa A, Soininen H, Majamaa K (2001) Increased risk of sensorineural hearing loss and migraine in patients with a rare mitochondrial DNA variant 4336A>G in tRNAGln. *J Med Genet* **38**(6)**:** 400-405

Finsterer J (2004) Diagnostic approach for adult mitochondriopathy with limited resources. *Neurol India* **52**(4)**:** 511-512; author reply 512-513

Flournoy DS, Frey PA (1989) Inactivation of the pyruvate dehydrogenase complex of Escherichia coli by fluoropyruvate. *Biochemistry* **28**(25)**:** 9594-9602

Frackowiak J, Mazur-Kolecka B, Kaczmarski W, Dickson D (2001) Deposition of Alzheimer's vascular amyloid-beta is associated with decreased expression of brain L-3-hydroxyacyl-coenzyme A dehydrogenase (ERAB). *Brain Res* **907**(1-2)**:** 44-53

Freshney I (1987) Measurement of cytotoxicity and viability; in Culture of animal cells—a manual of basic techniques *I Freshney (New York: A Liss)* pp 245–256

Froyen G, Corbett M, Vandewalle J, Jarvela I, Lawrence O, Meldrum C, Bauters M, Govaerts K, Vandeleur L, Van Esch H, Chelly J, Sanlaville D, van Bokhoven H, Ropers HH, Laumonnier F, Ranieri E, Schwartz CE, Abidi F, Tarpey PS, Futreal PA, Whibley A, Raymond FL, Stratton MR, Fryns JP, Scott R, Peippo M, Sipponen M, Partington M, Mowat D, Field M, Hackett A, Marynen P, Turner G, Gecz J (2008) Submicroscopic duplications of the hydroxysteroid dehydrogenase HSD17B10 and the E3 ubiquitin ligase HUWE1 are associated with mental retardation. *Am J Hum Genet* **82**(2)**:** 432-443

Furuta S, Kobayashi A, Miyazawa S, Hashimoto T (1997) Cloning and expression of cDNA for a newly identified isozyme of bovine liver 3-hydroxyacyl-CoA dehydrogenase and its import into mitochondria. *Biochim Biophys Acta* **1350**(3)**:** 317-324

Garcia-Villoria J, Gort L, Madrigal I, Fons C, Fernandez C, Navarro-Sastre A, Mila M, Briones P, Garcia-Cazorla A, Campistol J, Ribes A (2010) X-inactivation of HSD17B10 revealed by cDNA analysis in two female patients with 17beta-hydroxysteroid dehydrogenase 10 deficiency. *Eur J Hum Genet* **18**(12)**:** 1353-1355

Garcia-Villoria J, Navarro-Sastre A, Fons C, Perez-Cerda C, Baldellou A, Fuentes-Castello MA, Gonzalez I, Hernandez-Gonzalez A, Fernandez C, Campistol J, Delpiccolo C, Cortes N, Messeguer A, Briones P, Ribes A (2009) Study of patients and carriers with 2-methyl-3-hydroxybutyryl-CoA dehydrogenase (MHBD) deficiency: difficulties in the diagnosis. *Clin Biochem* **42**(1-2)**:** 27-33

Georgopoulos NT, Steele LP, Thomson MJ, Selby PJ, Southgate J, Trejdosiewicz LK (2006) A novel mechanism of CD40-induced apoptosis of carcinoma cells involving TRAF3 and JNK/AP-1 activation. *Cell Death Differ* **13**(10)**:** 1789-1801

Gilley J, Coffer PJ, Ham J (2003) FOXO transcription factors directly activate bim gene expression and promote apoptosis in sympathetic neurons. *J Cell Biol* **162**(4)**:** 613-622

Giovanni A, Keramaris E, Morris EJ, Hou ST, O'Hare M, Dyson N, Robertson GS, Slack RS, Park DS (2000) E2F1 mediates death of B-amyloid-treated cortical neurons in a manner independent of p53 and dependent on Bax and caspase 3. *J Biol Chem* **275**(16)**:** 11553-11560

Green D, Kroemer G (1998) The central executioners of apoptosis: caspases or mitochondria? *Trends Cell Biol* **8**(7)**:** 267-271

Green DR (1998) Apoptotic pathways: the roads to ruin. *Cell* **94**(6)**:** 695-698

Green DR, Kroemer G (2004) The pathophysiology of mitochondrial cell death. *Science* **305**(5684)**:** 626-629

Green DR, Reed JC (1998) Mitochondria and apoptosis. *Science* **281**(5381)**:** 1309-1312

Greene JG, Dingledine R, Greenamyre JT (2010) Neuron-selective changes in RNA transcripts related to energy metabolism in toxic models of parkinsonism in rodents. *Neurobiol Dis* **38**(3)**:** 476-481

Gross A, McDonnell JM, Korsmeyer SJ (1999) BCL-2 family members and the mitochondria in apoptosis. *Genes Dev* **13**(15)**:** 1899-1911

Guerra V (2010) Formation of blood vessels in HSD10 deficient *Xenopus* embryos.

Guerrier-Takada C, Gardiner K, Marsh T, Pace N, Altman S (1983) The RNA moiety of ribonuclease P is the catalytic subunit of the enzyme. *Cell* **35**(3 Pt 2)**:** 849-857

Gupta R, Kus B, Fladd C, Wasmuth J, Tonikian R, Sidhu S, Krogan NJ, Parkinson J, Rotin D (2007) Ubiquitination screen using protein microarrays for comprehensive identification of Rsp5 substrates in yeast. *Mol Syst Biol* **3:** 116

Halestrap AP, Brenner C (2003) The adenine nucleotide translocase: a central component of the mitochondrial permeability transition pore and key player in cell death. *Curr Med Chem* **10**(16)**:** 1507-1525

Hankins J (2006) The role of albumin in fluid and electrolyte balance. *J Infus Nurs* **29**(5)**:** 260-265

Hartmann E, Hartmann RK (2003) The enigma of ribonuclease P evolution. *Trends Genet* **19**(10)**:** 561-569

He XY, Merz G, Chu CH, Lin D, Yang YZ, Mehta P, Schulz H, Yang SY (2001) Molecular cloning, modeling, and localization of rat type 10 17beta-hydroxysteroid dehydrogenase. *Mol Cell Endocrinol* **171**(1-2)**:** 89-98

He XY, Merz G, Mehta P, Schulz H, Yang SY (1999) Human brain short chain L-3-hydroxyacyl coenzyme A dehydrogenase is a single-domain multifunctional enzyme. Characterization of a novel 17beta-hydroxysteroid dehydrogenase. *J Biol Chem* **274**(21)**:** 15014-15019

He XY, Merz G, Yang YZ, Pullakart R, Mehta P, Schulz H, Yang SY (2000a) Function of human brain short chain L-3-hydroxyacyl coenzyme A dehydrogenase in androgen metabolism. *Biochim Biophys Acta* **1484**(2-3)**:** 267-277

He XY, Schulz H, Yang SY (1998) A human brain L-3-hydroxyacyl-coenzyme A dehydrogenase is identical to an amyloid beta-peptide-binding protein involved in Alzheimer's disease. *J Biol Chem* **273**(17)**:** 10741-10746

He XY, Wegiel J, Yang SY (2005a) Intracellular oxidation of allopregnanolone by human brain type 10 17beta-hydroxysteroid dehydrogenase. *Brain Res* **1040**(1-2)**:** 29-35

He XY, Wegiel J, Yang YZ, Pullarkat R, Schulz H, Yang SY (2005b) Type 10 17beta-hydroxysteroid dehydrogenase catalyzing the oxidation of steroid modulators of gamma-aminobutyric acid type A receptors. *Mol Cell Endocrinol* **229**(1-2)**:** 111-117

He XY, Wen GY, Merz G, Lin D, Yang YZ, Mehta P, Schulz H, Yang SY (2002) Abundant type 10 17 beta-hydroxysteroid dehydrogenase in the hippocampus of mouse Alzheimer's disease model. *Brain Res Mol Brain Res* **99**(1)**:** 46-53

He XY, Yang YZ, Peehl DM, Lauderdale A, Schulz H, Yang SY (2003) Oxidative 3alpha-hydroxysteroid dehydrogenase activity of human type 10 17beta-hydroxysteroid dehydrogenase. *J Steroid Biochem Mol Biol* **87**(2-3)**:** 191-198

He XY, Yang YZ, Schulz H, Yang SY (2000b) Intrinsic alcohol dehydrogenase and hydroxysteroid dehydrogenase activities of human mitochondrial short-chain L-3-hydroxyacyl-CoA dehydrogenase. *Biochem J* **345 Pt 1:** 139-143

Heidinger-Pauli JM, Onn I, Koshland D (2010) Genetic evidence that the acetylation of the Smc3p subunit of cohesin modulates its ATP-bound state to promote cohesion establishment in Saccharomyces cerevisiae. *Genetics* **185**(4)**:** 1249-1256

Helm M, Brule H, Friede D, Giege R, Putz D, Florentz C (2000) Search for characteristic structural features of mammalian mitochondrial tRNAs. *RNA* **6**(10)**:** 1356-1379

Henry KR, D'Hondt K, Chang JS, Nix DA, Cope MJ, Chan CS, Drubin DG, Lemmon SK (2003) The actin-regulating kinase Prk1p negatively regulates Scd5p, a suppressor of clathrin deficiency, in actin organization and endocytosis. *Curr Biol* **13**(17)**:** 1564-1569

Hensey C, Gautier J (1997) A developmental timer that regulates apoptosis at the onset of gastrulation. *Mech Dev* **69**(1-2)**:** 183-195

Herzberg C, Weidinger LA, Dorrbecker B, Hubner S, Stulke J, Commichau FM (2007) SPINE: a method for the rapid detection and analysis of protein-protein interactions in vivo. *Proteomics* **7**(22)**:** 4032-4035

Holland M, Huffine E (2001) Molecular Analysis of the Human Mitochondrial DNA Control Region for Forensic Identity Testing. *Current Protocols in Human Genetics* **UNIT 14.7**

Holzmann J, Frank P, Loffler E, Bennett KL, Gerner C, Rossmanith W (2008) RNase P without RNA: identification and functional reconstitution of the human mitochondrial tRNA processing enzyme. *Cell* **135**(3)**:** 462-474

Huo LR, Ju W, Yan M, Zou JH, Yan W, He B, Zhao XL, Jenkins EC, Brown WT, Zhong N (2009) Identification of differentially expressed transcripts and translatants targeted by knock-down of endogenous PCBP1. *Biochim Biophys Acta* **1804**(10)**:** 1954-1964

Hurto RL (2011) Unexpected Functions of tRNA and tRNA Processing Enzymes. *RNA Infrastructure and Networks, Landes Bioscience*

Ishikawa F, Akimoto T, Yamamoto H, Araki Y, Yoshie T, Mori K, Hayashi H, Nose K, Shibanuma M (2009) Gene expression profiling identifies a role for CHOP during inhibition of the mitochondrial respiratory chain. *J Biochem* **146**(1)**:** 123-132

Ivell R, Balvers M, Anand RJ, Paust HJ, McKinnell C, Sharpe R (2003) Differentiation-dependent expression of 17beta-hydroxysteroid dehydrogenase, type 10, in the rodent testis: effect of aging in Leydig cells. *Endocrinology* **144**(7)**:** 3130-3137

Jazbutyte V, Kehl F, Neyses L, Pelzer T (2009) Estrogen receptor alpha interacts with 17beta-hydroxysteroid dehydrogenase type 10 in mitochondria. *Biochem Biophys Res Commun* **384**(4)**:** 450-454

Karbowski M, Youle RJ (2003) Dynamics of mitochondrial morphology in healthy cells and during apoptosis. *Cell Death Differ* **10**(8)**:** 870-880

Kashiwaya Y, Takeshima T, Mori N, Nakashima K, Clarke K, Veech RL (2000) D-beta-hydroxybutyrate protects neurons in models of Alzheimer's and Parkinson's disease. *Proc Natl Acad Sci U S A* **97**(10)**:** 5440-5444

King EM, Rachidi N, Morrice N, Hardwick KG, Stark MJ (2007) Ipl1p-dependent phosphorylation of Mad3p is required for the spindle checkpoint response to lack of tension at kinetochores. *Genes Dev* **21**(10)**:** 1163-1168

Kish SJ, Bergeron C, Rajput A, Dozic S, Mastrogiacomo F, Chang LJ, Wilson JM, DiStefano LM, Nobrega JN (1992) Brain cytochrome oxidase in Alzheimer's disease. *J Neurochem* **59**(2)**:** 776-779

Kissinger CR, Rejto PA, Pelletier LA, Thomson JA, Showalter RE, Abreo MA, Agree CS, Margosiak S, Meng JJ, Aust RM, Vanderpool D, Li B, Tempczyk-Russell A, Villafranca JE (2004) Crystal structure of human ABAD/HSD10 with a bound inhibitor: implications for design of Alzheimer's disease therapeutics. *J Mol Biol* **342**(3)**:** 943-952

Klein SL (1987) The first cleavage furrow demarcates the dorsal-ventral axis in Xenopus embryos. *Dev Biol* **120**(1)**:** 299-304

Kobayashi A, Jiang LL, Hashimoto T (1996) Two mitochondrial 3-hydroxyacyl-CoA dehydrogenases in bovine liver. *J Biochem* **119**(4)**:** 775-782

Kobayashi S, Tanaka A, Fujiki Y (2007) Fis1, DLP1, and Pex11p coordinately regulate peroxisome morphogenesis. *Exp Cell Res* **313**(8)**:** 1675-1686

Koga Y, Akita Y, Junko N, Yatsuga S, Povalko N, Fukiyama R, Ishii M, Matsuishi T (2006) Endothelial dysfunction in MELAS improved by l-arginine supplementation. *Neurology* **66**(11)**:** 1766-1769

Korinek WS, Bi E, Epp JA, Wang L, Ho J, Chant J (2000) Cyk3, a novel SH3-domain protein, affects cytokinesis in yeast. *Curr Biol* **10**(15)**:** 947-950

Korman SH, Yang SY (2007) HSD17B10 replaces HADH2 as the approved designation for the gene mutated in 2-methyl-3-hydroxybutyryl-CoA dehydrogenase deficiency. *Mol Genet Metab* **91**(1)**:** 115

Krammer PH (2000) CD95's deadly mission in the immune system. *Nature* **407**(6805)**:** 789-795

Kroemer G, Reed JC (2000) Mitochondrial control of cell death. *Nat Med* **6**(5)**:** 513-519

Krogan NJ, Cagney G, Yu H, Zhong G, Guo X, Ignatchenko A, Li J, Pu S, Datta N, Tikuisis AP, Punna T, Peregrin-Alvarez JM, Shales M, Zhang X, Davey M, Robinson MD, Paccanaro A, Bray JE, Sheung A, Beattie B, Richards DP, Canadien V, Lalev A, Mena F, Wong P, Starostine A, Canete MM, Vlasblom J, Wu S, Orsi C, Collins SR, Chandran S, Haw R, Rilstone JJ, Gandi K, Thompson NJ, Musso G, St Onge P, Ghanny S, Lam MH, Butland G, Altaf-Ul AM, Kanaya S, Shilatifard A, O'Shea E, Weissman JS, Ingles CJ, Hughes TR, Parkinson J, Gerstein M, Wodak SJ, Emili A, Greenblatt JF (2006) Global landscape of protein complexes in the yeast Saccharomyces cerevisiae. *Nature* **440**(7084)**:** 637-643

Laemmli UK (1970) Cleavage of structural proteins during the assembly of the head of bacteriophage T4. *Nature* **227**(5259)**:** 680-685

Lambert N, Grover L (1995) The mechanism of biphasic GABA responses. *Science* **269**(5226)**:** 928-929

Langston JW, Ballard P, Tetrud JW, Irwin I (1983) Chronic Parkinsonism in humans due to a product of meperidine-analog synthesis. *Science* **219**(4587)**:** 979-980

Lee MS, Kim JY, Park SY (2004) Resistance of rho(0) cells against apoptosis. *Ann N Y Acad Sci* **1011:** 146-153

Lenski C, Kooy RF, Reyniers E, Loessner D, Wanders RJ, Winnepenninckx B, Hellebrand H, Engert S, Schwartz CE, Meindl A, Ramser J (2007) The reduced expression of the HADH2 protein causes X-linked mental retardation, choreoathetosis, and abnormal behavior. *Am J Hum Genet* **80**(2)**:** 372-377

Levinger L, Jacobs O, James M (2001) In vitro 3'-end endonucleolytic processing defect in a human mitochondrial tRNA(Ser(UCN)) precursor with the U7445C substitution, which causes non-syndromic deafness. *Nucleic Acids Res* **29**(21)**:** 4334-4340

Levinger L, Morl M, Florentz C (2004) Mitochondrial tRNA 3' end metabolism and human disease. *Nucleic Acids Res* **32**(18)**:** 5430-5441

Li B, Pattenden SG, Lee D, Gutierrez J, Chen J, Seidel C, Gerton J, Workman JL (2005) Preferential occupancy of histone variant H2AZ at inactive promoters influences local histone modifications and chromatin remodeling. *Proc Natl Acad Sci U S A* **102**(51)**:** 18385-18390

Liu L, Amy V, Liu G, McKeehan WL (2002) Novel complex integrating mitochondria and the microtubular cytoskeleton with chromosome remodeling and tumor suppressor RASSF1 deduced by in silico homology analysis, interaction cloning in yeast, and colocalization in cultured cells. *In Vitro Cell Dev Biol Anim* **38**(10)**:** 582-594

Loeb DM (2006) WT1 influences apoptosis through transcriptional regulation of Bcl-2 family members. *Cell Cycle* **5**(12)**:** 1249-1253

Luo MJ, Mao LF, Schulz H (1995) Short-chain 3-hydroxy-2-methylacyl-CoA dehydrogenase from rat liver: purification and characterization of a novel enzyme of isoleucine metabolism. *Arch Biochem Biophys* **321**(1)**:** 214-220

Lustbader JW, Cirilli M, Lin C, Xu HW, Takuma K, Wang N, Caspersen C, Chen X, Pollak S, Chaney M, Trinchese F, Liu S, Gunn-Moore F, Lue LF, Walker DG, Kuppusamy P, Zewier ZL, Arancio O, Stern D, Yan SS, Wu H (2004) ABAD directly links Abeta to mitochondrial toxicity in Alzheimer's disease. *Science* **304**(5669)**:** 448-452

Lynch M, Chen L, Ravitz MJ, Mehtani S, Korenblat K, Pazin MJ, Schmidt EV (2005) hnRNP K binds a core polypyrimidine element in the eukaryotic translation initiation factor 4E (eIF4E) promoter, and its regulation of eIF4E contributes to neoplastic transformation. *Mol Cell Biol* **25**(15)**:** 6436-6453

MacKenzie EL, Ray PD, Tsuji Y (2008) Role and regulation of ferritin H in rotenone-mediated mitochondrial oxidative stress. *Free Radic Biol Med* **44**(9)**:** 1762-1771

Marelli M, Smith JJ, Jung S, Yi E, Nesvizhskii AI, Christmas RH, Saleem RA, Tam YY, Fagarasanu A, Goodlett DR, Aebersold R, Rachubinski RA, Aitchison JD (2004) Quantitative mass spectrometry reveals a role for the GTPase Rho1p in actin organization on the peroxisome membrane. *J Cell Biol* **167**(6)**:** 1099-1112

Markus SM, Taneja SS, Logan SK, Li W, Ha S, Hittelman AB, Rogatsky I, Garabedian MJ (2002) Identification and characterization of ART-27, a novel coactivator for the androgen receptor N terminus. *Mol Biol Cell* **13**(2)**:** 670-682

Matuszewska E, Kwiatkowska J, Kuczynska-Wisnik D, Laskowska E (2008) Escherichia coli heat-shock proteins IbpA/B are involved in resistance to oxidative stress induced by copper. *Microbiology* **154**(Pt 6)**:** 1739-1747

Maurer I, Zierz S, Moller HJ (2000) A selective defect of cytochrome c oxidase is present in brain of Alzheimer disease patients. *Neurobiol Aging* **21**(3)**:** 455-462

McGilvray R, Walker M, Bartholomew C (2007) UXT interacts with the transcriptional repressor protein EVI1 and suppresses cell transformation. *FEBS J* **274**(15)**:** 3960-3971

Montoya J, Ojala D, Attardi G (1981) Distinctive features of the 5'-terminal sequences of the human mitochondrial mRNAs. *Nature* **290**(5806)**:** 465-470

Moss TN, Vo A, McKeehan WL, Liu L (2007) UXT (Ubiquitously Expressed Transcript) causes mitochondrial aggregation. *In Vitro Cell Dev Biol Anim* **43**(3-4)**:** 139-146

Mutisya EM, Bowling AC, Beal MF (1994) Cortical cytochrome oxidase activity is reduced in Alzheimer's disease. *J Neurochem* **63**(6)**:** 2179-2184

Nass MM, Nass S (1963a) Intramitochondrial Fibers with DNA Characteristics. I. Fixation and Electron Staining Reactions. *J Cell Biol* **19:** 593-611

Nass S, Nass MM (1963b) Intramitochondrial Fibers with DNA Characteristics. Ii. Enzymatic and Other Hydrolytic Treatments. *J Cell Biol* **19:** 613-629

Nelson D, Cox M (2005) Lehninger Principles of Biochemistry. *W H Freeman* **4th edition**

Neupert W (1997) Protein import into mitochondria. *Annu Rev Biochem* **66:** 863-917

Nicklas WJ, Youngster SK, Kindt MV, Heikkila RE (1987) MPTP, MPP+ and mitochondrial function. *Life Sci* **40**(8)**:** 721-729

Nieuwkoop P, Faber J (1967) Normal table of *Xenopus laevis Amsterdam: North Holland Publishing, Co*

Nwachukwu JC, Mita P, Ruoff R, Ha S, Wang Q, Huang SJ, Taneja SS, Brown M, Gerald WL, Garabedian MJ, Logan SK (2009) Genome-wide impact of androgen receptor trapped clone-27 loss on androgen-regulated transcription in prostate cancer cells. *Cancer Res* **69**(7)**:** 3140-3147

Ofman R, Ruiter JP, Feenstra M, Duran M, Poll-The BT, Zschocke J, Ensenauer R, Lehnert W, Sass JO, Sperl W, Wanders RJ (2003) 2-Methyl-3-hydroxybutyryl-CoA dehydrogenase deficiency is caused by mutations in the HADH2 gene. *Am J Hum Genet* **72**(5)**:** 1300-1307

Ojala D, Merkel C, Gelfand R, Attardi G (1980) The tRNA genes punctuate the reading of genetic information in human mitochondrial DNA. *Cell* **22**(2 Pt 2)**:** 393-403

Ojala D, Montoya J, Attardi G (1981) tRNA punctuation model of RNA processing in human mitochondria. *Nature* **290**(5806)**:** 470-474

Okamoto K, Shaw JM (2005) Mitochondrial morphology and dynamics in yeast and multicellular eukaryotes. *Annu Rev Genet* **39:** 503-536

Olpin SE, Pollitt RJ, McMenamin J, Manning NJ, Besley G, Ruiter JP, Wanders RJ (2002) 2-methyl-3-hydroxybutyryl-CoA dehydrogenase deficiency in a 23-year-old man. *J Inherit Metab Dis* **25**(6)**:** 477-482

Oppermann UC, Salim S, Tjernberg LO, Terenius L, Jornvall H (1999) Binding of amyloid beta-peptide to mitochondrial hydroxyacyl-CoA dehydrogenase (ERAB): regulation of an SDR enzyme activity with implications for apoptosis in Alzheimer's disease. *FEBS Lett* **451**(3)**:** 238-242

Orrenius S (2004) Mitochondrial regulation of apoptotic cell death. *Toxicol Lett* **149**(1-3)**:** 19-23

Ozand PT, Rashed M, Gascon GG, al Odaib A, Shums A, Nester M, Brismar J (1994) 3-Ketothiolase deficiency: a review and four new patients with neurologic symptoms. *Brain Dev* **16 Suppl:** 38-45

Parker WD, Jr., Parks J, Filley CM, Kleinschmidt-DeMasters BK (1994) Electron transport chain defects in Alzheimer's disease brain. *Neurology* **44**(6)**:** 1090-1096

Perez-Cerda C, Garcia-Villoria J, Ofman R, Sala PR, Merinero B, Ramos J, Garcia-Silva MT, Beseler B, Dalmau J, Wanders RJ, Ugarte M, Ribes A (2005) 2-Methyl-3-hydroxybutyryl-CoA dehydrogenase (MHBD) deficiency: an X-linked inborn error of isoleucine metabolism that may mimic a mitochondrial disease. *Pediatr Res* **58**(3)**:** 488-491

Peter ME, Krammer PH (2003) The CD95(APO-1/Fas) DISC and beyond. *Cell Death Differ* **10**(1)**:** 26-35

Poll-The BT, Wanders RJ, Ruiter JP, Ofman R, Majoie CB, Barth PG, Duran M (2004) Spastic diplegia and periventricular white matter abnormalities in 2-methyl-3-hydroxybutyryl-CoA dehydrogenase deficiency, a defect of isoleucine metabolism: differential diagnosis with hypoxic-ischemic brain diseases. *Mol Genet Metab* **81**(4)**:** 295-299

Porat Z, Erez O, Kahana C (2006) Cellular localization and phosphorylation of Hrb1p is independent of Sky1p. *Biochim Biophys Acta* **1763**(2)**:** 207-213

Ptacek J, Devgan G, Michaud G, Zhu H, Zhu X, Fasolo J, Guo H, Jona G, Breitkreutz A, Sopko R, McCartney RR, Schmidt MC, Rachidi N, Lee SJ, Mah AS, Meng L, Stark MJ, Stern DF, De Virgilio C, Tyers M, Andrews B, Gerstein M, Schweitzer B, Predki PF, Snyder M (2005) Global analysis of protein phosphorylation in yeast. *Nature* **438**(7068)**:** 679-684

Raisner RM, Hartley PD, Meneghini MD, Bao MZ, Liu CL, Schreiber SL, Rando OJ, Madhani HD (2005) Histone variant H2A.Z marks the 5' ends of both active and inactive genes in euchromatin. *Cell* **123**(2)**:** 233-248

Rauschenberger K (2007) Funktion und Fehlfunktion der 17beta-Hydroxysteroid-dehydrogenase Typ 10 (HSD17B10) in der Entwicklung von *Xenopus laevis*.

Rauschenberger K, Scholer K, Sass JO, Sauer S, Djuric Z, Rumig C, Wolf NI, Okun JG, Kolker S, Schwarz H, Fischer C, Grziwa B, Runz H, Numann A, Shafqat N, Kavanagh KL, Hammerling G, Wanders RJ, Shield JP, Wendel U, Stern D, Nawroth P, Hoffmann GF, Bartram CR, Arnold B, Bierhaus A, Oppermann U, Steinbeisser H, Zschocke J (2010) A non-enzymatic function of 17beta-hydroxysteroid dehydrogenase type 10 is required for mitochondrial integrity and cell survival. *EMBO Mol Med* **2**(2)**:** 51-62

Ren Y (2008) Consequences of the interaction of amyloid beta with amyloid binding alcohol dehydrogenase and the receptor for advanced glycation end products.

Reyniers E, Van Bogaert P, Peeters N, Vits L, Pauly F, Fransen E, Van Regemorter N, Kooy RF (1999) A new neurological syndrome with mental retardation, choreoathetosis, and abnormal behavior maps to chromosome Xp11. *Am J Hum Genet* **65**(5)**:** 1406-1412

Rinaldo P, Matern D, Bennett MJ (2002) Fatty acid oxidation disorders. *Annu Rev Physiol* **64:** 477-502

Robertson HD, Altman S, Smith JD (1972) Purification and properties of a specific Escherichia coli ribonuclease which cleaves a tyrosine transfer ribonucleic acid presursor. *J Biol Chem* **247**(16)**:** 5243-5251

Rotinen M, Villar J, Celay J, Encio I (2010) Type 10 17beta-hydroxysteroid dehydrogenase expression is regulated by C/EBPbeta in HepG2 cells. *J Steroid Biochem Mol Biol* **122**(4)**:** 164-171

Rottensteiner H, Stein K, Sonnenhol E, Erdmann R (2003) Conserved function of pex11p and the novel pex25p and pex27p in peroxisome biogenesis. *Mol Biol Cell* **14**(10)**:** 4316-4328

Rumig C (2006) Etablierung konditionaler Knock-out Mäuse für ERAB (endoplasmic reticulum-associated amyloid β-peptide binding protein): Funktionelle Analysen zur Bedeutung für die T-Zellentwicklung und den Stoffwechsel.

Sakaguchi A, Tsuji G, Kubo Y (2010) A yeast STE11 homologue CoMEKK1 is essential for pathogenesis-related morphogenesis in Colletotrichum orbiculare. *Mol Plant Microbe Interact* **23**(12)**:** 1563-1572

Salas S, Jezequel P, Campion L, Deville JL, Chibon F, Bartoli C, Gentet JC, Charbonnel C, Gouraud W, Voutsinos-Porche B, Brouchet A, Duffaud F, Figarella-Branger D, Bouvier C

(2009) Molecular characterization of the response to chemotherapy in conventional osteosarcomas: predictive value of HSD17B10 and IFITM2. *Int J Cancer* **125**(4)**:** 851-860

Salim S, Filling C, Martensson E, Oppermann UC (2000) Lack of quinone reductase activity suggests that amyloid-beta peptide/ERAB induced lipid peroxidation is not directly related to production of reactive oxygen species by redoxcycling. *Toxicology* **144**(1-3)**:** 163-168

Sambamurti K, Lahiri DK (1998) ERAB contains a putative noncleavable signal peptide. *Biochem Biophys Res Commun* **249**(2)**:** 546-549

Sass JO, Forstner R, Sperl W (2004) 2-Methyl-3-hydroxybutyryl-CoA dehydrogenase deficiency: impaired catabolism of isoleucine presenting as neurodegenerative disease. *Brain Dev* **26**(1)**:** 12-14

Schroer A, Schneider S, Ropers H, Nothwang H (1999) Cloning and characterization of UXT, a novel gene in human Xp11, which is widely and abundantly expressed in tumor tissue. *Genomics* **56**(3)**:** 340-343

Schwarz H, Blanco FJ, von Kempis J, Valbracht J, Lotz M (1996) ILA, a member of the human nerve growth factor/tumor necrosis factor receptor family, regulates T-lymphocyte proliferation and survival. *Blood* **87**(7)**:** 2839-2845

Sell S (2008) Alpha-fetoprotein, stem cells and cancer: how study of the production of alpha-fetoprotein during chemical hepatocarcinogenesis led to reaffirmation of the stem cell theory of cancer. *Tumour Biol* **29**(3)**:** 161-180

Shafqat N, Marschall HU, Filling C, Nordling E, Wu XQ, Bjork L, Thyberg J, Martensson E, Salim S, Jornvall H, Oppermann U (2003) Expanded substrate screenings of human and Drosophila type 10 17beta-hydroxysteroid dehydrogenases (HSDs) reveal multiple specificities in bile acid and steroid hormone metabolism: characterization of multifunctional 3alpha/7alpha/7beta/17beta/20beta/21-HSD. *Biochem J* **376**(Pt 1)**:** 49-60

Shoffner JM (1995) Mitochondrial defects in basal ganglia diseases. *Curr Opin Neurol* **8**(6)**:** 474-479

Simon AK, Williams O, Mongkolsapaya J, Jin B, Xu XN, Walczak H, Screaton GR (2001) Tumor necrosis factor-related apoptosis-inducing ligand in T cell development: sensitivity of human thymocytes. *Proc Natl Acad Sci U S A* **98**(9)**:** 5158-5163

Smith CA, Farrah T, Goodwin RG (1994) The TNF receptor superfamily of cellular and viral proteins: activation, costimulation, and death. *Cell* **76**(6)**:** 959-962

Spagnolo M, Tomelleri G, Vattemi G, Filosto M, Rizzuto N, Tonin P (2001) A new mutation in the mitochondrial tRNA(Ala) gene in a patient with ophthalmoplegia and dysphagia. *Neuromuscul Disord* **11**(5)**:** 481-484

Sprinzl M, Horn C, Brown M, Ioudovitch A, Steinberg S (1998) Compilation of tRNA sequences and sequences of tRNA genes. *Nucleic Acids Res* **26**(1)**:** 148-153

Stock D, Leslie AG, Walker JE (1999) Molecular architecture of the rotary motor in ATP synthase. *Science* **286**(5445)**:** 1700-1705

Strasser A, Harris AW, Huang DC, Krammer PH, Cory S (1995) Bcl-2 and Fas/APO-1 regulate distinct pathways to lymphocyte apoptosis. *EMBO J* **14**(24)**:** 6136-6147

Sun S, Tang Y, Lou X, Zhu L, Yang K, Zhang B, Shi H, Wang C (2007) UXT is a novel and essential cofactor in the NF-kappaB transcriptional enhanceosome. *J Cell Biol* **178**(2)**:** 231-244

Susin SA, Lorenzo HK, Zamzami N, Marzo I, Snow BE, Brothers GM, Mangion J, Jacotot E, Costantini P, Loeffler M, Larochette N, Goodlett DR, Aebersold R, Siderovski DP, Penninger JM, Kroemer G (1999) Molecular characterization of mitochondrial apoptosis-inducing factor. *Nature* **397**(6718)**:** 441-446

Sutton VR, O'Brien WE, Clark GD, Kim J, Wanders RJ (2003) 3-Hydroxy-2-methylbutyryl-CoA dehydrogenase deficiency. *J Inherit Metab Dis* **26**(1)**:** 69-71

Swalwell H, Deschauer M, Hartl H, Strauss M, Turnbull DM, Zierz S, Taylor RW (2006) Pure myopathy associated with a novel mitochondrial tRNA gene mutation. *Neurology* **66**(3)**:** 447-449

Szewczyk A, Wojtczak L (2002) Mitochondria as a pharmacological target. *Pharmacol Rev* **54**(1)**:** 101-127

Takabe K, Paugh SW, Milstien S, Spiegel S (2008) "Inside-out" signaling of sphingosine-1-phosphate: therapeutic targets. *Pharmacol Rev* **60**(2)**:** 181-195

Takuma K, Yao J, Huang J, Xu H, Chen X, Luddy J, Trillat AC, Stern DM, Arancio O, Yan SS (2005) ABAD enhances Abeta-induced cell stress via mitochondrial dysfunction. *FASEB J* **19**(6)**:** 597-598

Taneja SS, Ha S, Swenson NK, Torra IP, Rome S, Walden PD, Huang HY, Shapiro E, Garabedian MJ, Logan SK (2004) ART-27, an androgen receptor coactivator regulated in prostate development and cancer. *J Biol Chem* **279**(14)**:** 13944-13952

Thomas JG, Baneyx F (1998) Roles of the Escherichia coli small heat shock proteins IbpA and IbpB in thermal stress management: comparison with ClpA, ClpB, and HtpG In vivo. *J Bacteriol* **180**(19)**:** 5165-5172

Tieu K, Perier C, Caspersen C, Teismann P, Wu DC, Yan SD, Naini A, Vila M, Jackson-Lewis V, Ramasamy R, Przedborski S (2003) D-beta-hydroxybutyrate rescues

mitochondrial respiration and mitigates features of Parkinson disease. *J Clin Invest* **112**(6)**:** 892-901

Tieu K, Perier C, Vila M, Caspersen C, Zhang HP, Teismann P, Jackson-Lewis V, Stern DM, Yan SD, Przedborski S (2004) L-3-hydroxyacyl-CoA dehydrogenase II protects in a model of Parkinson's disease. *Ann Neurol* **56**(1)**:** 51-60

Torroja L, Ortuno-Sahagun D, Ferrus A, Hammerle B, Barbas JA (1998) scully, an essential gene of Drosophila, is homologous to mammalian mitochondrial type II L-3-hydroxyacyl-CoA dehydrogenase/amyloid-beta peptide-binding protein. *J Cell Biol* **141**(4)**:** 1009-1017

Tzen CY, Thajeb P, Wu TY, Chen SC (2003) Melas with point mutations involving tRNALeu (A3243G) and tRNAGlu(A14693g). *Muscle Nerve* **28**(5)**:** 575-581

van der Vusse GJ (2009) Albumin as fatty acid transporter. *Drug Metab Pharmacokinet* **24**(4)**:** 300-307

van Roermund CW, Tabak HF, van Den Berg M, Wanders RJ, Hettema EH (2000) Pex11p plays a primary role in medium-chain fatty acid oxidation, a process that affects peroxisome number and size in Saccharomyces cerevisiae. *J Cell Biol* **150**(3)**:** 489-498

Venable JH, Coggeshall R (1965) A Simplified Lead Citrate Stain for Use in Electron Microscopy. *J Cell Biol* **25:** 407-408

Volkov A, Labady A, Thomas D, Shvetsova T (2001) Green Plants as Environmental Biosensors: Electrochemical Effects of Carbonyl Cyanide 3-Chlorophenylhydrazone on Soybean. *ANALYTICAL SCIENCES 2001,* **VOL.17 supplement**

Wallace DC (1982) Structure and evolution of organelle genomes. *Microbiol Rev* **46**(2)**:** 208-240

Wallace DC, Lott MT, Shoffner JM, Brown MD (1992) Diseases resulting from mitochondrial DNA point mutations. *J Inherit Metab Dis* **15**(4)**:** 472-479

Wanders RJ, Vreken P, den Boer ME, Wijburg FA, van Gennip AH, L IJ (1999) Disorders of mitochondrial fatty acyl-CoA beta-oxidation. *J Inherit Metab Dis* **22**(4)**:** 442-487

Wang CY, Mayo MW, Baldwin AS, Jr. (1996) TNF- and cancer therapy-induced apoptosis: potentiation by inhibition of NF-kappaB. *Science* **274**(5288)**:** 784-787

Wen L, Zhuang L, Luo X, Wei P (2003) TL1A-induced NF-kappaB activation and c-IAP2 production prevent DR3-mediated apoptosis in TF-1 cells. *J Biol Chem* **278**(40)**:** 39251-39258

White EJ, Cowan C, Cande WZ, Kaback DB (2004) In vivo analysis of synaptonemal complex formation during yeast meiosis. *Genetics* **167**(1)**:** 51-63

Wiesner RJ, Ruegg JC, Morano I (1992) Counting target molecules by exponential polymerase chain reaction: copy number of mitochondrial DNA in rat tissues. *Biochem Biophys Res Commun* **183**(2)**:** 553-559

Willkomm DK, Hartmann RK (2007) An important piece of the RNase P jigsaw solved. *Trends Biochem Sci* **32**(6)**:** 247-250

Yan SD, Fu J, Soto C, Chen X, Zhu H, Al-Mohanna F, Collison K, Zhu A, Stern E, Saido T, Tohyama M, Ogawa S, Roher A, Stern D (1997) An intracellular protein that binds amyloid-beta peptide and mediates neurotoxicity in Alzheimer's disease. *Nature* **389**(6652)**:** 689-695

Yan SD, Roher A, Chaney M, Zlokovic B, Schmidt AM, Stern D (2000a) Cellular cofactors potentiating induction of stress and cytotoxicity by amyloid beta-peptide. *Biochim Biophys Acta* **1502**(1)**:** 145-157

Yan SD, Shi Y, Zhu A, Fu J, Zhu H, Zhu Y, Gibson L, Stern E, Collison K, Al-Mohanna F, Ogawa S, Roher A, Clarke SG, Stern DM (1999) Role of ERAB/L-3-hydroxyacyl-coenzyme A dehydrogenase type II activity in Abeta-induced cytotoxicity. *J Biol Chem* **274**(4)**:** 2145-2156

Yan SD, Stern DM (2005) Mitochondrial dysfunction and Alzheimer's disease: role of amyloid-beta peptide alcohol dehydrogenase (ABAD). *Int J Exp Pathol* **86**(3)**:** 161-171

Yan SD, Zhu Y, Stern ED, Hwang YC, Hori O, Ogawa S, Frosch MP, Connolly ES, Jr., McTaggert R, Pinsky DJ, Clarke S, Stern DM, Ramasamy R (2000b) Amyloid beta - peptide-binding alcohol dehydrogenase is a component of the cellular response to nutritional stress. *J Biol Chem* **275**(35)**:** 27100-27109

Yang SY, He XY (2001) Role of type 10 17beta-hydroxysteroid dehydrogenase in the pathogenesis of Alzheimer's disease. *Adv Exp Med Biol* **487:** 101-110

Yang SY, He XY, Miller D (2007) HSD17B10: a gene involved in cognitive function through metabolism of isoleucine and neuroactive steroids. *Mol Genet Metab* **92**(1-2)**:** 36-42

Yang SY, He XY, Schulz H (2005a) 3-Hydroxyacyl-CoA dehydrogenase and short chain 3-hydroxyacyl-CoA dehydrogenase in human health and disease. *FEBS J* **272**(19)**:** 4874-4883

Yang SY, He XY, Schulz H (2005b) Multiple functions of type 10 17beta-hydroxysteroid dehydrogenase. *Trends Endocrinol Metab* **16**(4)**:** 167-175

Yao J, Irwin RW, Zhao L, Nilsen J, Hamilton RT, Brinton RD (2009) Mitochondrial bioenergetic deficit precedes Alzheimer's pathology in female mouse model of Alzheimer's disease. *Proc Natl Acad Sci U S A* **106**(34)**:** 14670-14675

Ye T, Elbing K, Hohmann S (2008) The pathway by which the yeast protein kinase Snf1p controls acquisition of sodium tolerance is different from that mediating glucose regulation. *Microbiology* **154**(Pt 9)**:** 2814-2826

Yu J, Tian S, Metheny-Barlow L, Chew LJ, Hayes AJ, Pan H, Yu GL, Li LY (2001) Modulation of endothelial cell growth arrest and apoptosis by vascular endothelial growth inhibitor. *Circ Res* **89**(12)**:** 1161-1167

Zeviani M, Tiranti V, Piantadosi C (1998) Mitochondrial disorders. *Medicine (Baltimore)* **77**(1)**:** 59-72

Zhang Y, McLaughlin R, Goodyer C, LeBlanc A (2002) Selective cytotoxicity of intracellular amyloid beta peptide1-42 through p53 and Bax in cultured primary human neurons. *J Cell Biol* **156**(3)**:** 519-529

Zhao H, Wang Q, Zhang H, Liu Q, Du X, Richter M, Greene MI (2005) UXT is a novel centrosomal protein essential for cell viability. *Mol Biol Cell* **16**(12)**:** 5857-5865

Zheng Y, Hart MJ, Shinjo K, Evans T, Bender A, Cerione RA (1993) Biochemical comparisons of the Saccharomyces cerevisiae Bem2 and Bem3 proteins. Delineation of a limit Cdc42 GTPase-activating protein domain. *J Biol Chem* **268**(33)**:** 24629-24634

Zoratti M, Szabo I (1995) The mitochondrial permeability transition. *Biochim Biophys Acta* **1241**(2)**:** 139-176

Zschocke J, Ruiter JP, Brand J, Lindner M, Hoffmann GF, Wanders RJ, Mayatepek E (2000) Progressive infantile neurodegeneration caused by 2-methyl-3-hydroxybutyryl-CoA dehydrogenase deficiency: a novel inborn error of branched-chain fatty acid and isoleucine metabolism. *Pediatr Res* **48**(6)**:** 852-855

9 APPENDIX

9.1. Abbreviations

17βHSD10	17β-hydroxysteroid dehydrogenase type 10
ABAD	amyloid β-binding alcohol dehydrogenase
ADPD	Alzheimer's disease and Parkinson's disease
AIF	apoptosis inducing factor
ANT	adenine nucleotide transporter
AP	alakaline phosphatase
BioGRID	Biological General Repository for Interaction Datasets
cDNA	copy DNA
CHOP	C/EBP homologous protein
CNS	central nervous system
COX	cytochrome c oxidase
CPEO	chronic progressive external ophtalmoplegia
CPM	counts per minute
ctr	control
CypD	cyclophilin D
DBH	dopamine β-hydroxylase
DICE	differentiation control element
DISC	death-inducing signalling complex
dNTP	2'-desoxy-nucleoside-5'-triphosphate
DSF	differential scanning fluorimetry
E.coli	*Escherichia coli*
eIF4E	eukaryotic translation initiation factor 4E
EMS	ethyl methanesulphonate
ER	endoplasmic reticulum
ERAB	endoplasmic reticulum-associated amyloid b-peptide binding protein
FADD	Fas associated death domain protein
FOX2	Multifunctional enzyme of the peroxisomal fatty acid β-oxidation pathway
Grp75	75 kDa glucose regulated protein
GST	glutathione S-transferase
h	hour(s)
HADH2	L-3-hydroxyacyl-CoA dehydrogenase type II
HRP	horse radish peroxidase
IAPs	inhibitors of apoptosis proteins
IMAC	immobilised metal ion affinity chromatography
kb	kilo bases
kD	kilo Dalton
LB medium	Luria Bertani medium
LC	locus coeruleus
LOF	loss-of-function
MELAS	mitochondrial encephalomyopathy, lactis acidose, stroke-

	like episodes
MHBD	2-Methyl-3-hydroxybutyryl-CoA dehydrogenase
min	minute(s)
MMP	mitochondrial membrane permeabilization
Mo	Morpholino antisense oligonucleotides
MPTP	1-methyl-4-phenyl-1,2,3,6-tetrahydropyridin
MPTP	mitochondrial permeability transition pore
mRNA	messenger RNA
MRPP1	Mitochondrial Ribonuclease P Protein 1
MS	mass spectrometry
mt	mitochondrial
n	number
NF	*Xenopus* stages according to Nieuwkoop and Faber
NFκB	nuclear factor κ-light-chain-enhancer of activated B cells
o/n	overnight
OAR1	Mitochondrial 3-oxoacyl-[acyl-carrier-protein] reductase
OD	optic density
ODC	Ornithine decarboxylase
p.f.	post fertilisation
PCBP1	PolyC binding protein 1
pH	pondus hydrogenii
PNS	peripheral nervous system
ROS	reactive oxygen species
RNaseP	ribonuclease P
rpm	rounds per minute
RT	room temperature
SCG	superior cervical ganglia
SCHAD	short chain 3-hydroxyacyl-CoA dehydrogenase
SCHMAD	short chain L-3-Hydroxy-2-Methylacyl-CoA Dehydrogenase
SDR	short chain dehydrogenases/reductases
Smac	second mitochondria-derived activator of caspase
SPINE	Strep-protein interaction experiment
TM	tunicamycin
TNFR	tumour necrosis factor receptor
TOMM20	translocase of outer mitochondrial membrane 20
TF, TL, TI and so on	tRNA coding different amino acids
tRNA	transfer RNA
TUNEL	Terminale deoxynucleotidyl transferase-mediated dUTP digoxygenin nick end labelling
U	Unit
UPR	unfolded protein response
UXT	ubiquitously expressed transcript
VDAC	voltage dependent anion channel
(v/v)	volume-volume ratio
WT	wildtype
(w/v)	weight-volume ratio

9.2. Figures

9.3. Tables

Acknowledgements

I am thankful to all those people who contributed to the completion of this dissertation and because of whom the last three years have been a wonderful time.

First of all, I would like to thank Prof. Dr. Herbert Steinbeisser for giving me the excellent chance to work in his group. He manages to combine a constant flow of new ideas with the liberty to pursue research on my own. His patience and support helped me finish this dissertation.

Likewise, I am grateful to Prof. Dr. Dr. Johannes Zschocke for the opportunity to work on an exciting project and the interesting meetings in Heidelberg, Innsbruck or Salzburg which always produced countless new ideas.

I owe my gratitude to many collaborators including Bernd Arnold from the DKFZ and Afsaneh Majdazari from the Max Planck Institute for Brain Research who helped me with the preparation of mouse tissue. I thank Heinz Schwarz and Ursula Müller for the kind collaboration on electron microscopy. Sven Sauer from the children's hospital in Heidelberg established the measurement of mitochondrial function for Xenopus material. For the kind reception during the weeks I spent at their lab I am grateful to Hans Mayr, Franz Zimmermann and Edith Müller from the children's hospital in Salzburg.

A big thank-you goes to the members of my group for the excellent working atmosphere, in particular to the "Steinbeisser sisters".

The support and care of my friends have helped me remain sane and overcome setbacks through these years. I greatly value their friendship and I deeply appreciate their belief in me.

Most importantly, I would like to thank my family with all my heart for their love, concern, support and advice.